PERFORMANCE ASSESSMENT OF MULTI-ARRAY PROCESSING WITH GROUND TRUTH FOR INFRASONIC, SEISMIC AND SEISMO-ACOUSTIC EVENTS

Brian W. Stump, et al.

Roy M. Huffington Department of Earth Science
Southern Methodist University
PO Box 750395
Dallas, TX 75275-0395

3 July 2012

Final Report

AIR FORCE RESEARCH LABORATORY
Space Vehicles Directorate
3550 Aberdeen Ave SE
AIR FORCE MATERIEL COMMAND
KIRTLAND AIR FORCE BASE, NM 87117-5776

DTIC COPY

NOTICE AND SIGNATURE PAGE

Using Government drawings, specifications, or other data included in this document for any purpose other than Government procurement does not in any way obligate the U.S. Government. The fact that the Government formulated or supplied the drawings, specifications, or other data does not license the holder or any other person or corporation; or convey any rights or permission to manufacture, use, or sell any patented invention that may relate to them.

This report was cleared for public release by the 377 ABW Public Affairs Office and is available to the general public, including foreign nationals. Copies may be obtained from the Defense Technical Information Center (DTIC) (http://www.dtic.mil).

AFRL-RV-PS-TR-2012-0123 HAS BEEN REVIEWED AND IS APPROVED FOR PUBLICATION IN ACCORDANCE WITH ASSIGNED DISTRIBUTION STATEMENT.

//SIGNED//   //SIGNED//

Robert Raistrick   Joel B. Mozer
Program Manager, RVBYE   Chief, AFRL/RVB

This report is published in the interest of scientific and technical information exchange, and its publication does not constitute the Government's approval or disapproval of its ideas or findings.

REPORT DOCUMENTATION PAGE

Form Approved
OMB No. 0704-0188

1. REPORT DATE (DD-MM-YYYY)	2. REPORT TYPE	3. DATES COVERED (From - To)
03-07-2012	Final Report	08-03-2008 to 07-03-2012

4. TITLE AND SUBTITLE
Performance Assessment of Multi-Array Processing with Ground Truth for Infrasonic, Seismic and Seismo-Acoustic Events

5a. CONTRACT NUMBER
FA8718-08-C-0008

5b. GRANT NUMBER

5c. PROGRAM ELEMENT NUMBER
62601F

6. AUTHOR(S)
Brian W. Stump, Junghyun Park, Chris Hayward, Stephen Arrowsmith and Il-Young Che

5d. PROJECT NUMBER
1010

5e. TASK NUMBER
PPM00004639

5f. WORK UNIT NUMBER
EF004018

7. PERFORMING ORGANIZATION NAME(S) AND ADDRESS(ES)
Roy M. Huffington Department of Earth Science
Southern Methodist University
PO Box 750395
Dallas, TX 75275-0395

8. PERFORMING ORGANIZATION REPORT NUMBER

9. SPONSORING / MONITORING AGENCY NAME(S) AND ADDRESS(ES)
Air Force Research Laboratory
Space Vehicles Directorate
3550 Aberdeen Ave SE
Kirtland AFB, NM 87117-5776

10. SPONSOR/MONITOR'S ACRONYM(S)
AFRL/RVBYE

11. SPONSOR/MONITOR'S REPORT NUMBER(S)
AFRL-RV-PS-TR-2012-0123

12. DISTRIBUTION / AVAILABILITY STATEMENT

APPROVED FOR PUBLIC RELEASE; DISTRIBUTION IS UNLIMITED. (377ABW-2012-0808 dtd 2 Jul 2012)

13. SUPPLEMENTARY NOTES

14. ABSTRACT
Natural and manmade sources at or near the solid earth – atmosphere boundary can generate waves in both the solid earth and atmosphere. The location and characterization of these sources can benefit from the analysis of both sets of waves. This report documents work first to investigate and develop new detection and location methods for infrasound signals (low frequency acoustic signals) that can be combined with seismic observations and thus applied to data recorded by regional seismo-acoustic arrays. Several empirical studies are reported that exercised these tools with complementary ground truth information in order to assess the adequacy of the new tools. Finally the automated procedures were tested and tuned for two regional seismo-acoustic networks in Korea and the western US. Automated bulletins were produced for these two networks and compared, providing constraints for additional work.

15. SUBJECT TERMS
infrasound, seismic, seismo-acoustic, array, regional network, automated location

16. SECURITY CLASSIFICATION OF: Fill in according to classification of report.			17. LIMITATION OF ABSTRACT	18. NUMBER OF PAGES	19a. NAME OF RESPONSIBLE PERSON Robert Raistrick
a. REPORT UNCLASSIFIED	**b. ABSTRACT** UNCLASSIFIED	**c. THIS PAGE** UNCLASSIFIED	Unlimited	84	19b. TELEPHONE NUMBER (include area code)

Standard Form 298 (Rev. 8-98)
Prescribed by ANSI Std. Z39.18

This page is intentionally left blank.

Table of Contents

List of Figures

List of Tables

1. INTRODUCTION AND SUMMARY OF RESEARCH

The work documented in this final report, a number of published reports, yearly papers at the Monitoring Research Review and quarterly progress reports has been a collaborative effort between Southern Methodist University funded by AFRL under contract number FA8718-08-C-0008 and Los Alamos National Laboratory by DOE under contract number DE-AC52-06NA25396. A portion of the Korean data used was made available as a result of Contract FA2521-09-C-8005 while a portion of the western US data was made available as a result of Contract DE-AC52-09NA293255.

The primary objective of this research was to develop an automatic, research system for processing seismic and infrasound data from multiple seismo-acoustic arrays and to apply the system to data from operating Korean seismo-acoustic arrays which numbered four at the outset of this work. The project led to the development of automated techniques for detecting, associating, and locating infrasound signals, at single and multiple arrays and then combining and comparing the processed results with seismic signals. The procedures developed and documented in this final as well as earlier reports were applied to all Korean seismo-acoustic arrays as well as two near-by IMS arrays and were additionally tested against a robust network of seismo-acoustic arrays in the western US for comparison.

This study has supported the design, production and testing of a new infrasound detection, association and location procedure by LANL, documented in Arrowsmith *et al.* 2008; Arrowsmith *et al.* 2009; and Modrak *et al* 2010.

A critical component of this study was the development of a catalog of ground truth events from which the detection and location procedures could be tested as well as used in assessment of existing atmospheric models. In order to assess the relative roles of seismic and infrasound signals in the location process and develop our understanding of source depth effects on the relative excitation of infrasound and seismic signals a large portion of this work was undertaken with the deployment of in-mine seismic and infrasound gauges at a working mine in Korea. Ground truth information from this study was delivered with quarterly reports. The data set was used to test location algorithms and compare and contrast the role of seismic and infrasound data in this process. The details were reported in Arrowsmith *et al* 2010. The work was extended and expanded in Che *et al* 2011.

Optimization of the tools developed during the course of this research have been the most recent focus followed by the systematic application of the procedures to seismo-acoustic data in Korea and the western US during the final phase. The optimization of the detector and its relationship to environmental conditions was reported at the 2011 MRR (Park *et al* 2011). This final technical report now documents in detail the relationship of environmental conditions on detection and location (Chapter 2), the comparison of the new adaptive F-detector to the well known infrasound detector PMCC (Chapter 3) and the production of event bulletins for the Korean Peninsula and the western US using the tools developed during this work (Chapter 4). This last contribution illustrates the importance of such studies in assessing both manmade and natural sources with seismo-acoustic data, in providing a mechanism to develop new ground truth data, in constraining depth of burial effects from near-surface events and possibly in

providing a path towards the use of time varying atmospheric models to reduce estimated location errors

2. MULTIPLE-ARRAY DETECTION ASSESSMENT AND RELATIONSHIP TO ENVIRONMENTAL CONDITIONS

2.1 Abstract

Detecting infrasonic arrivals is more complex than seismic arrivals since temporal variations in atmospheric conditions and local noise are substantial on the spatial scale of typical arrays. In order to produce the optimum signal detection, we assess detectors that distinguish the signal from both correlated and uncorrelated noise. One approach to this detection problem is implementation of the F-detector, which employs the F-statistic, and the cross-correlation technique separating correlated and uncorrelated signals and noise. A modified F-detector is tested which applies an adaptive procedure to identify variations in coherent noise, thus reducing false alarms. Using the modified F-detector, we investigate the temporal variation in the adaptation nature of the detector for a number of sites on the Korean Peninsula. In this study, six seismo-acoustic arrays in South Korea (BRDAR, CHNAR, KMPAR, KSGAR, TJIAR, and YPDAR), which are cooperatively operated by KIGAM and SMU, were used. We tested the sensitivity of the detection procedure to the adaptive window used to estimate the C parameter that characterizes the correlated noise and impacts the false alarms rate. The C values are found to be stable over long time periods for arrays within the peninsula, but show variations under high wind velocity conditions for adaptive windows as short as 1 hour at the arrays on islands or near the coast. The infrasound amplitudes on all channels increase as wind speed near the sensor increases. This result suggests that optimal detection processing requires careful characterization of background noise level and its relationship to environmental measures such as wind speed and azimuth at individual arrays. In order to further understand variations in background noise, the 10th, 50th, and 90th percentile noise spectral densities at all frequencies were estimated. The noise estimates show a strong wind speed effect on acoustic noise; for example, the spread between the 10th and 90th percentiles is about 40 dB at 0.1 Hz. For arrays on islands or near the coast the noise power densities are higher, indicative of higher wind speeds. Ultimately, this work will provide a basis for defining optimum detectors that will provide input for locating infrasound events using multiple arrays.

2.2 Objectives

This work is intended to support the development of an automated methodology for event detection and location of seismic and infrasound data from seismo-acoustic arrays and apply the methodology to regional networks with validation from ground truth information. The detection and location framework have been developed by Arrowsmith *et al*. (2009a and 2010). Additionally, the importance of ground truth data sets in refining atmospheric propagation path effects has been investigated. Work that is reported here focuses on the characteristics of the infrasound detectors that provide the input to the automated location procedures.

2.3 Motivation – Automated Detectors for Infrasound

Infrasound systems record two types of low frequency acoustic waves; Signals (*S*) from events, which will be coherent across an array and background noise (*N*) from a number of sources, which may or may not be coherent across an array of instruments depending on their spatial sampling. A detector is designed to identify the arrival of a signal from an event as separate from noise. Under the assumption that the signal and noise series are linear processes, the recorded data is written as:

$$D(t) = S(t) + N(t) . \tag{1}$$

This models the data as linearly filtered combinations of white noise vectors with square sumable coefficients and components with finite fourth order moments (Shumway *et al*., 1999). Here, the infrasonic signal contains the information that will be used for tasks such as event location and characterization while the noise is everything else that complicates signal detection and analysis. By improving the signal-to-noise ratio (SNR) through the processing of array data (closely spaced but individual sensors), detection of events that cannot be uniquely identified on a single station is possible. However, the problem is that parts of the noise field may be coherent across the array, such as seismic noise generated by trains or heavy industry. This type of noise can make data analysis and signal identification difficult. The detection of infrasonic signals is complicated by temporal variations in atmospheric conditions (Arrowsmith *et al*., 2008b) that impact both the signal as well as the noise.

Generally, regional infrasound signals are observed in the frequency range of 1-5 Hz (Arrowsmith and Hedlin, 2005). The ambient infrasound noise is typically characterized over a frequency band from 3 to above 7 Hz by high variability with respect to season, time, and stations, as discussed by Bowman *et al* (2005). The ambient infrasonic noise is affected at longer periods by microbaroms with long-range pressure fluctuations often generated over the oceans, eddies or winds resulting from the near-surface boundary layer, and at higher frequencies by short-range pressure fluctuations, including station dependent factors such as local weather, station location relative to oceans, local topography, local noise sources, and vegetation and snow cover at the sensor sites. The configurations of sensors with wind-noise reduction filters are used to control some aspects of this noise environment (Bowman *et al*., 2005). Studies link physical processes accompanying severe weather and the resulting high ocean surface waves to the generation of microbaroms (Daniels, 1962; Posmentier, 1967; Rind, 1980; Tabulevich, 1993). Le Pichon *et al.* (2004) also note that ocean waves that propagate from major storm centers to coastlines can generate surf-generated signals and that these signals along with the others are examples of common sources of infrasound noise that are linked to seasonal effects.

The dominant sources of noise such as weather systems, ocean waves, rivers, and cultural noise in some cases can produce either coherent or incoherent noise across an infrasound array that is time-dependent. Therefore, the understanding of these processes and how they vary among arrays is important work ultimately providing an approach and physical basis to distinguish signals from noise both correlated and uncorrelated. The data from these noise sources may also be important in characterizing environmental effects. Bowman *et al*. (2005) note that noise caused by wind and eddies is generated at frequencies higher than the microbarom band, which means wind-generated noise is a significant effect for signal detection in our observational

frequency band. Our interest is in assessing detectors that distinguish the signal from the correlated noise in order to obtain the optimum signal detection for subsequent processing including the location of impulsive events.

One recent approach to this detection problem has been incorporated into InfraMonitor (Arrowsmith and Whitaker, 2008) utilizes the F-statistic (Blandford, 1974) with cross-correlation estimates. Automatic detection is based on the F-statistic (F-detector) calculated as the power on the beam divided by the average over all channels of the power difference between the beam and the individual array channels (Blandford, 1974). For infrasound detection, previous methods such as the progressive multi-channel correlation (PMCC) algorithm (Cansi, 1995) and simple measures of correlation in InfraTool and MatSeis-1.7 (Hart and Young, 2002) have been based on the assumption of uncorrelated noise, resulting in false alarms under conditions of correlated noise. PMCC is based on progressive processing of the data recorded by different stations in an array using cross-correlation functions and reduces false alarms by starting with the processing of sub-arrays (Cansi, 1995). This method estimates trace velocities and azimuths from sub-arrays and then progressively increases the network aperture. InfraTool calculates an azimuth, trace velocity, correlation coefficient, and the conventional F-statistic for each segment using multiple overlapping windows that move through the data volume. The InfraTool detector performs well in cases where values of correlation and thus the F-statistic are high (Garcés and Hetzer, 2001).

The modified F-statistic as proposed by Arrowsmith *et al*. (2009b) accounts for temporal changes in noise by using an adaptive window to update the detection distribution as introduced later in this paper. An adaptive modification of this detection algorithm can be used to distinguish the signal from correlated noise, with the adaptation focusing on temporal variations in ambient noise rather than assuming that background noise is constant and uncorrelated as in InfraTool.

2.4 Stations

The Korea Institute of Geoscience and Mineral Resources (KIGAM) and Southern Methodist University (SMU) cooperatively operate the seismo-acoustic arrays, BRDAR, CHNAR, KMPAR, KSGAR, TJIAR, and YPDAR in South Korea as shown in Figure 1. BRDAR, CHNAR, KMPAR, KSGAR, and YPDAR are located near the border between North Korea and South Korea, whereas TJIAR is located in the center of the Korean peninsula, near Deajeon. The Baengnyeong island array (BRDAR) and the Yeonpyeong island array (YPDAR) are installed in the sea to the west next to the Korean Peninsula, and are surrounded by ocean as is KSGAR, on the east side of Korean Peninsula (Fig. 1). CHNAR, KMPAR, and TJIAR are located within the continent. KMPAR has sampling rate of 100 sample/s while the other arrays are sampled at 40 samples/s. At CHNAR and KSGAR, a four-element 1-km aperture seismo-acoustic array was installed with each element consisting of one GS-13 seismometer and a small (60~70 m) aperture infrasound subarray. Similar to CHNAR and KSGAR, BRDAR has one additional element.

There are a total of 11 microbarometers and 4 seismometers at CHNAR and KSGAR, and a total of 13 microbarometers and 5 seismometers at BRDAR. KMPAR, TJIAR, and YPDAR consist of 6, 5 and 4 infrasound gauges, respectively, configured with a small-aperture (~200 m). In the case of KMPAR, there is a three-component seismometer at the center of the array. YPDAR has

a three-component seismometer in the center of the array. TJIAR has no seismometer within the array but one near-by. All arrays have weather channels measuring wind velocity, wind azimuth, and temperature, except for the KMPAR. Each microbarometer is attached to ten porous hoses, each eight meters in length connected at the center in a star-like configuration for reducing the background noise from wind activity along the boundary layer. Sensor data is recorded by 24-bit digitizers and sent in real time via telemetry to KIGAM in South Korea and SMU in Texas.
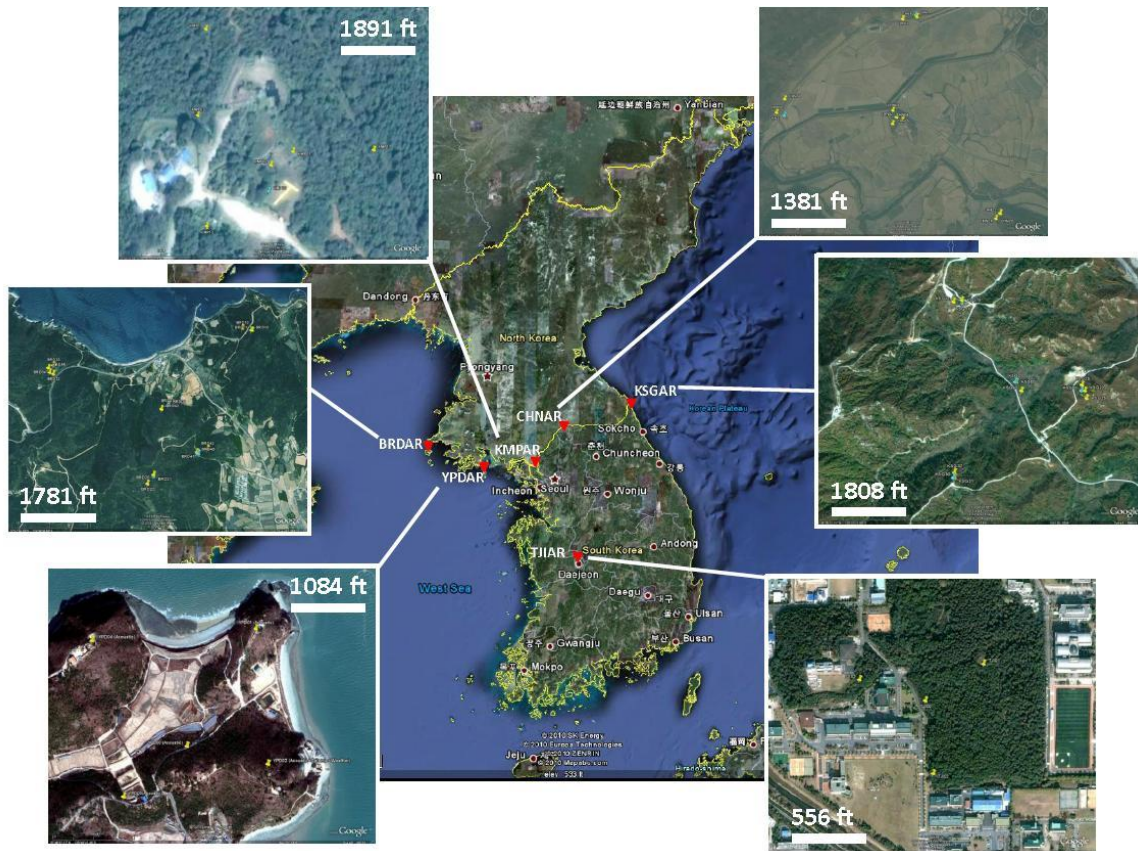
Figure 1: The Location of the Seismo-Acoustic Arrays in South Korea

In Figure 1, the yellow pushpins in each image designate the location of individual array elements.

2.5 Empirical Relationship between Wind Velocity and Infrasonic Noise

Fundamental to this work is the establishment of the relationship between infrasound noise characteristics and levels with environmental conditions such as wind velocity and direction and ocean atmosphere interactions. This section outlines work to establish these relationships using the robust data sets described previously in the Korean Peninsula. As documented in a later section there is an inverse relationship between the C value in the adaptive part of the detector and wind velocity further motivating this exploration of infrasound noise. This inverse relationship suggests two possible causes for the correlated noise under low wind conditions either surf or storm generated noise or local sources near the receivers that are only observed

under low noise conditions. In order to quantify the impact these correlated noise sources have on detection and event formation it is important to first assess the incoherent noise and in particular the relationship between absolute wind velocity and infrasound noise.

Absolute infrasound noise levels were estimated for each of the arrays for a total 7 days (days 079, 081, 082, 083, 084, 085, and 086) at BRDAR (BRD42), CHNAR (CHN05), KSGAR (KSG12), and TJIAR (TJI10) (Figs. 2, 3, 4, and 5). Wind velocity estimates were made by calculating the average wind value during 15 minutes intervals with moving windows and are plotted at the top of these figures. The middle and bottom plots in each of these figures represent the unfiltered and filtered (0.5-1 Hz, 1-2 Hz, 2-4 Hz, 4-8 Hz, and 8-16 Hz) maximum waveform amplitudes as a function of time. The maximum infrasound amplitudes were determined first for 1 second intervals and then averaged over 15 minutes duration with a moving window in a manner consistent with the wind velocity estimates.

Infrasound amplitudes on all channels increase as wind speed near the sensor increases in this study. Woodward *et al.* (2005) suggested that wind-induced noise for International Monitoring System (IMS) stations increases with increasing wind speed and that the absolute micro pressure amplitudes increase as wind velocity increases. It is well known that false signal detections can result from the wind-generated noise and, conversely, that these types of noise can mask detections by reducing the coherence between array elements (Woodward *et al*., 2005). The average maximum amplitude trend of both unfiltered and filtered waveforms in all arrays correlates with the wind velocity time history. The maximum noise levels of the unfiltered waveform are 9, 1.8, 1.2 and 1.5 Pa for BRDAR, CHNAR, KSGAR, and TJIAR, respectively. In addition, the order (BRDAR, KSGAR, CHNAR, and TJIAR) of the noise levels seems to reflect the background environment of each array.
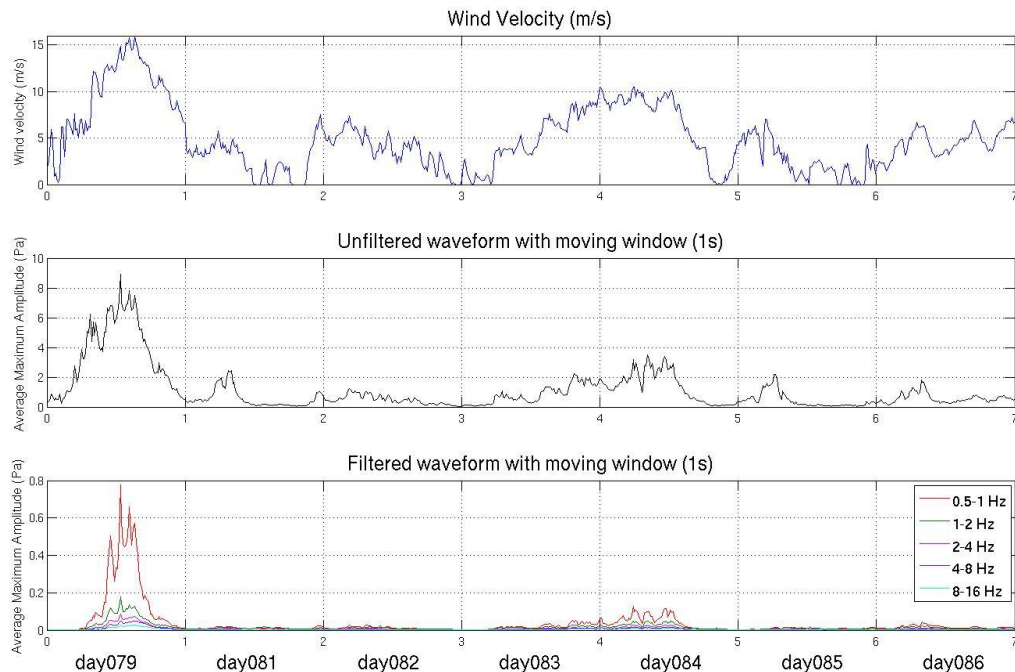
Figure 2: Relationship Between Wind Velocity and Noise Level During 7 Days (Julian Days 079, 081-086) at BRDAR
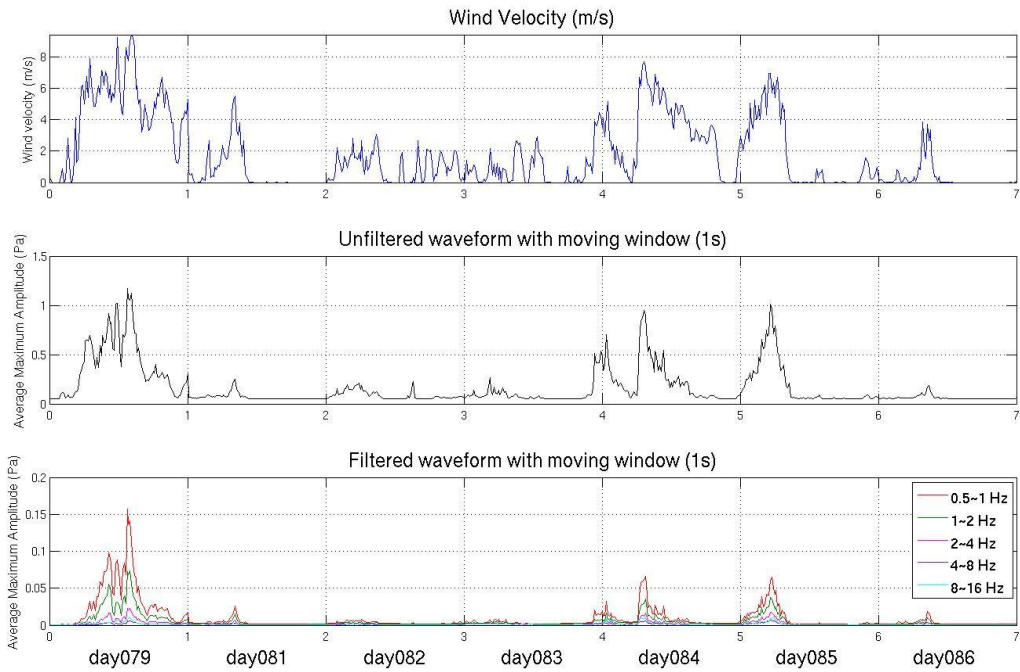
Figure 3: Relationship Between Wind Velocity and Noise Level During 7 Days (Julian Days 079, 081-086) at CHNAR
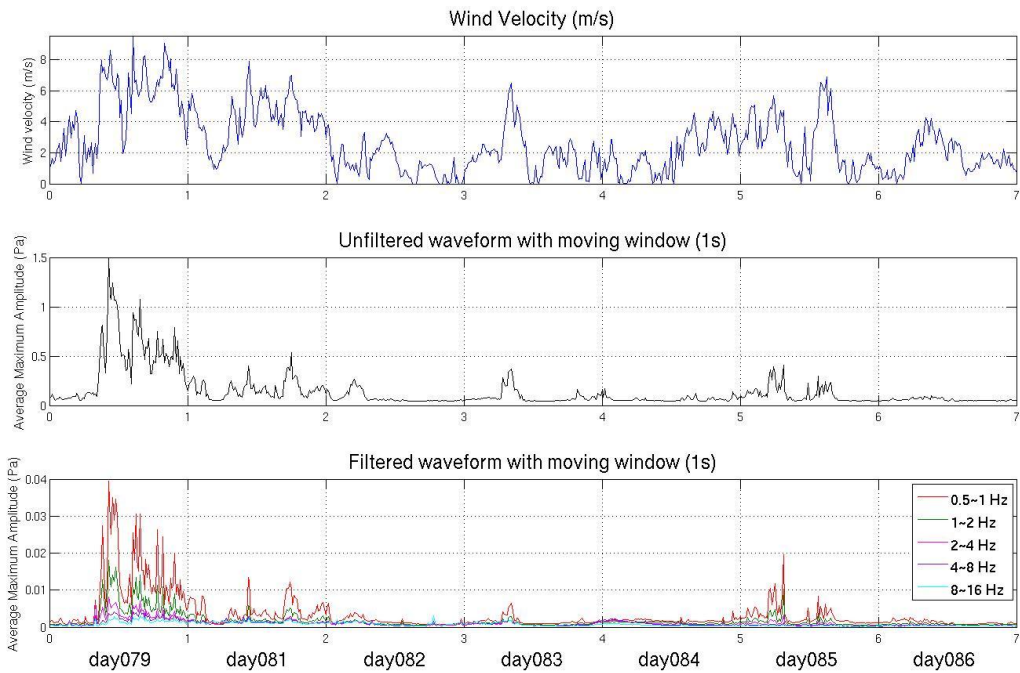
Figure 4: Relation Between Wind Velocity and Noise Level During 7 Days (Julian Days 079, 081-086) at KSGAR

7
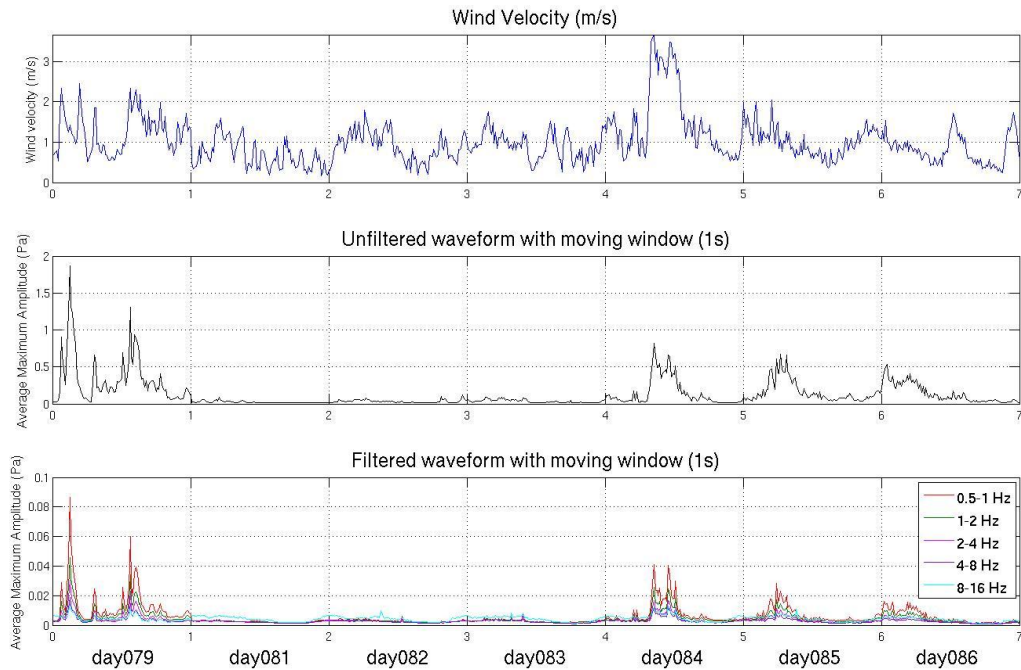
Figure 5: Relationship Between Wind Velocity and Noise Level During 7 Days (Julian Days 079, 081-086) at TJIAR

BRDAR as a result of its island location is also affected by ocean waves, wind and tides, so that background noise levels can reach higher values than at CHNAR where the primary nose source is wind. In the case of KSGAR, also affected by an ocean environment, the noise level is high, but less than that at BRDAR. KSGAR is not completely surrounded by ocean, thus mitigating the effect. The noise levels of the filtered waveforms have similar trends with the unfiltered one.

Figure 6 plots the average wind velocity against the average maximum amplitude of the filtered waveforms with respect to various frequency bands (0.5-1 Hz, 1-2 Hz, 2-4 Hz, 4-8 Hz, and 8-16 Hz). The range of wind velocities and noise levels is the greatest for BRDAR and smallest for CHNAR and TJIAR. The low wind velocities at TJIAR may reflect both its inland location as well as local topographic effects. Background noise at BRDAR, CHNAR, KSGAR, and TJIAR are all a function of wind velocity with ocean waves acting as a possible secondary source leading to higher noise levels at BRDAR and KSGAR.
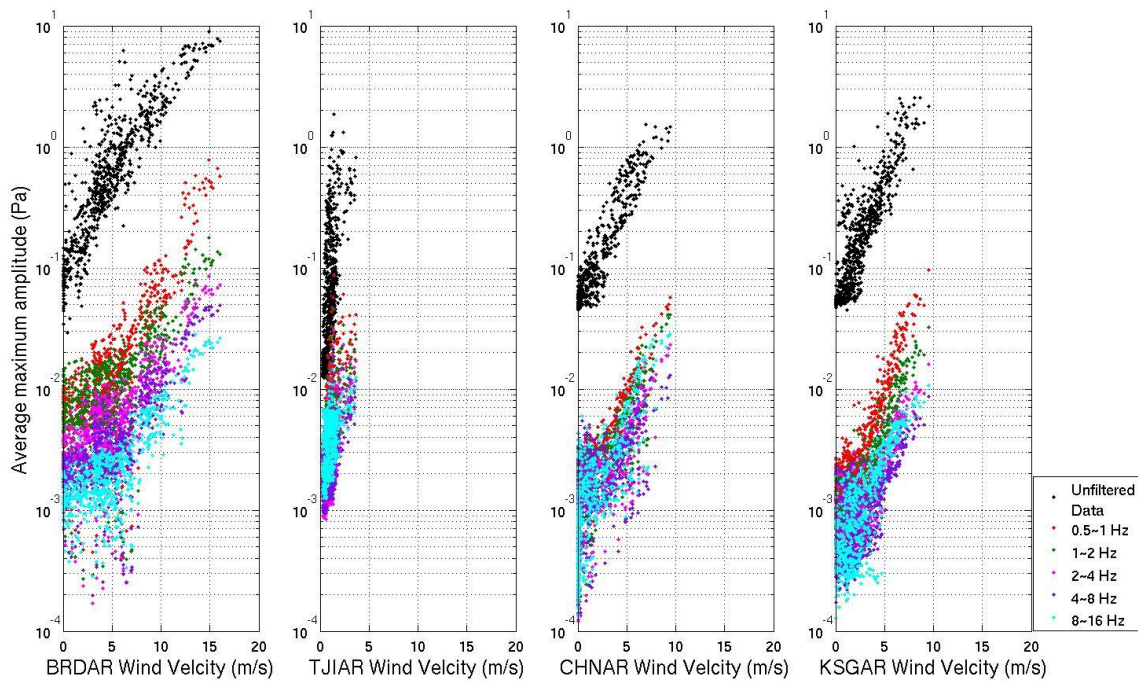
Figure 6: Relationship Between Wind Velocity and Average Maximum Amplitude of the Filtered Infrasound Waveforms (0.5-1 Hz, 1-2 Hz, 2-4 Hz, 4-8 Hz, and 8-16 Hz) During 7 Days (Julian Days 079, 081-086) at BRDAR, TJIAR, CHNAR, and KSGAR

To examine the spectral properties of the noise, the filtered waveform are analyzed using Welch's method (Welch, 1967) producing a single power spectral estimate from an average of spectra taken at regular intervals over a specific time period (Hedlin *et al.*, 2002). Four waveform segments each 204.8 s in length were extracted from the first 15 minutes of each hour, following the data processing steps of Hedlin *et al.* (2002). A 10 percent cosine taper was applied to the front and back of each time series and then zero-padded to avoid truncation effects. A single spectral estimate was derived from the average of four spectra. Using three weeks of data recorded in all arrays, a total of 454 power spectral density estimates were made for each site. Due to the recent installation of YPDAR, the analyzed data is from different time windows than those of the other data arrays, but used the same time procedure.

Estimates for BRD42, CHN05, KMP01, KSG12, TJI10 and YPD10 utilized Julian days 074-094 while YPDAR estimates were made for Julian days 260-262, 264-268, and 270-280. This analysis quantifies the range of noise conditions found at each of the arrays over the three-week time periods. Figure 7 displays 10th, 50th, and 90th percentile noise levels at frequencies from 0.0025 Hz to 20 Hz. The narrow band noise spikes spaced at 1 Hz intervals from 1 Hz and 20 Hz are a result of interaction of radios at the sites with the data acquisition system. The microbarom peak is centered at 0.2 Hz at all arrays. Hedlin *et al.* (2002) notes that the overall spectral shape is due to phenomena in the atmosphere that produces significant energy from 0.1 Hz to 0.001 Hz. The long-period noise spectra document the time dependence of the noise, for example the spread between the 10th and 90th percentiles noise spread at 0.1 Hz is about 40 dB. The 10th and 90th percentiles noise spread for 0.1 Hz at BRDAR and YPDAR are larger (>40 dB) than those

9

at other arrays (40 dB). In the high frequency band where many of our signals are observed (1-10 Hz), the spread in noise values between arrays tends to be similar. Thus the most significant difference between arrays located on the island and those on the continent is that there is more background noise at the island sites at the lower frequencies.
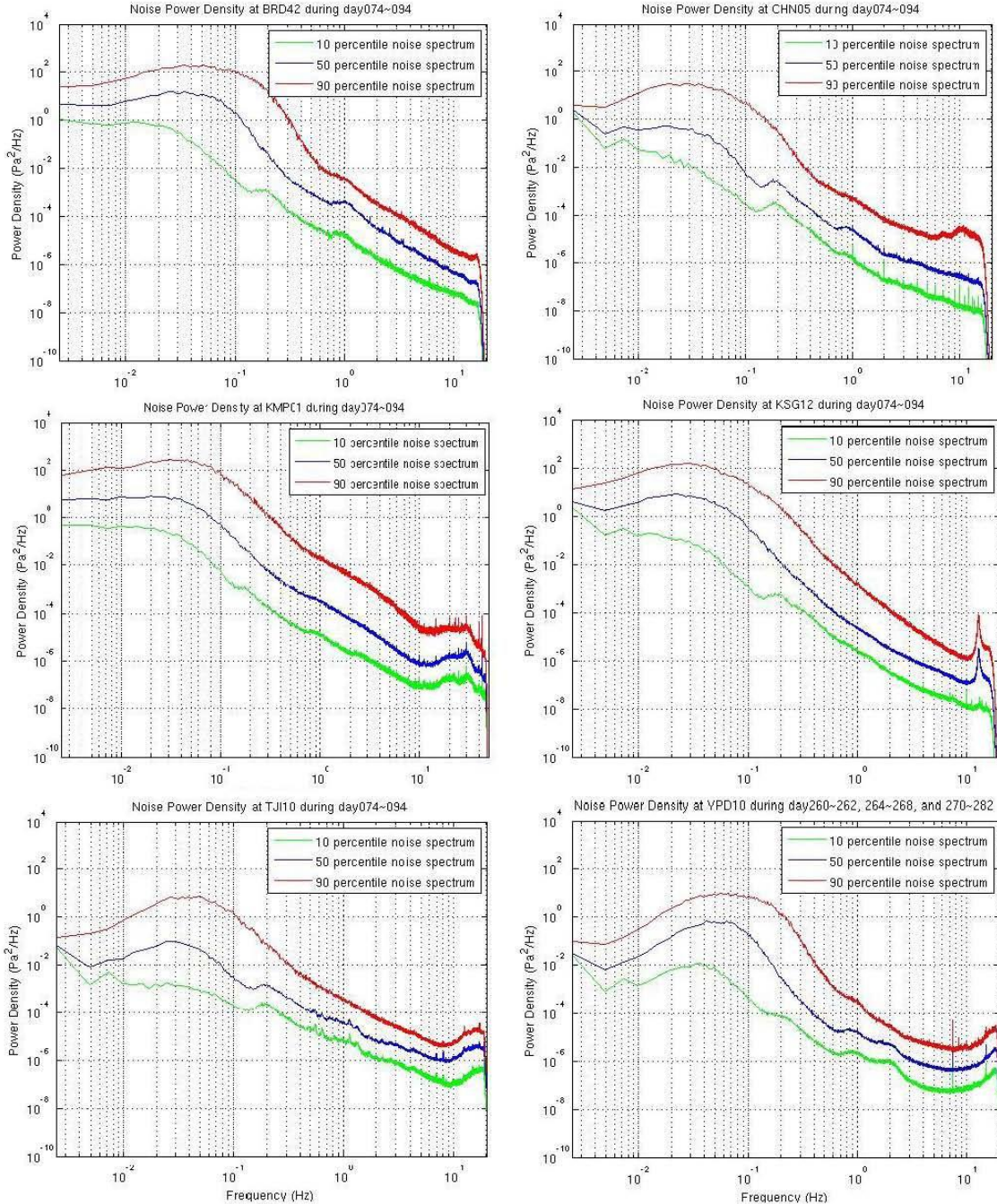
Figure 7: Infrasonic Noise Power Density at BRDAR(42), CHNAR(05), KMPAR(01), KSGAR(12), TJIAR(10) During Julian Days 074-094 (2010), and YPDAR(10) During Julian Days 260-262, 264-268, and 270-282 (2010)

Le Pichon *et al*. (2008) demonstrated the important role seasonal variations in atmospheric winds have on network detection capabilities for infrasound arrivals. Figs. 8 and 9 display the power spectral densities as a function of wind velocity centered at frequencies of 0.02 Hz, 0.05 Hz, 0.1 Hz, 0.25 Hz, 0.5 Hz, 1 Hz, 2.5 Hz, and 5 Hz for the four array sites during the spring (Julian days 074-094, 2010) and fall (Julian days 260-262, 264-268, and 270-282, 2010) and for three sites during the summer (Julian days 166-186, 2010) and winter (Julian days 357-365, 2009, and Julian days 001-012, 2010 for BRDAR and KSGAR, and Julian days 040-044 and 046-061, 2010 for TJIAR). YPDAR noise analysis is restricted to the fall season, due to the recent installation. CHNAR data from the winter time-period was not included in the analysis, due to a lack of weather data during this time period. Due to missing data, noise estimates for TJIAR could be obtained only for the spring and winter period.

Both the wind speed and noise ranges are dependent on both site and season. TJIAR and CHNAR located in the center of the peninsula have relatively low wind velocities compared to BRDAR, KMPAR, KSGAR and YPDAR. The range of wind velocities and noise power densities at TJIAR are the lowest. The highest wind speeds at CHNAR occur in the spring with significant reductions in peak winds and noise in the summer and fall. Since the noise power density increases with the wind velocity, BRDAR, YPDAR, and KSGAR, all of which are close to the ocean, have relatively higher wind speeds, up to 13 m/s, and higher noise power density than CHNAR. The strongest winds and noise at BRDAR and KSGAR occur in the winter and spring. This result indicates that all sites are strongly affected by wind speed, however, the background noise levels of CHNAR and TJIAR are less affected than those of BRDAR, KMPAR, YPDAR, and KSGAR. In addition, the distribution of the power density at BRDAR is somewhat more scattered than those at KSGAR. This additional result suggests that, in the case of BRDAR and possibly YPDAR the noise power density may be influenced by additional local site characteristics, such as the ocean environment.

The noise power density at BRDAR is higher, up to 1 Pa^2/Hz, in the 0.02-0.1 Hz band than the noise at CHNAR and KSGAR. Hedlin *et al*. (2002) demonstrated that sites located on islands are affected by the time-variant interaction of wind speed and azimuth with local topographic features producing a complex relationship between noise power and wind speed (Fig. 8). Additional time varying sources at BRDAR, YPDAR, and possibly KSGAR are atmospheric interaction of ocean waves and tides which depending on the generation mechanism can produce coherent noise and thus we plan to assess these additional noise sources for the island sites focusing on the coherent component of the noise field.

From top to bottom in each panel of Figure 8, noise power is shown at 0.02 Hz (purple); 0.05 Hz (red); 0.1 Hz (dark green); 0.25 Hz (light green); 0.5 Hz (yellow); 1 Hz (blue); 2.5 Hz (pink); and 5 Hz (black).
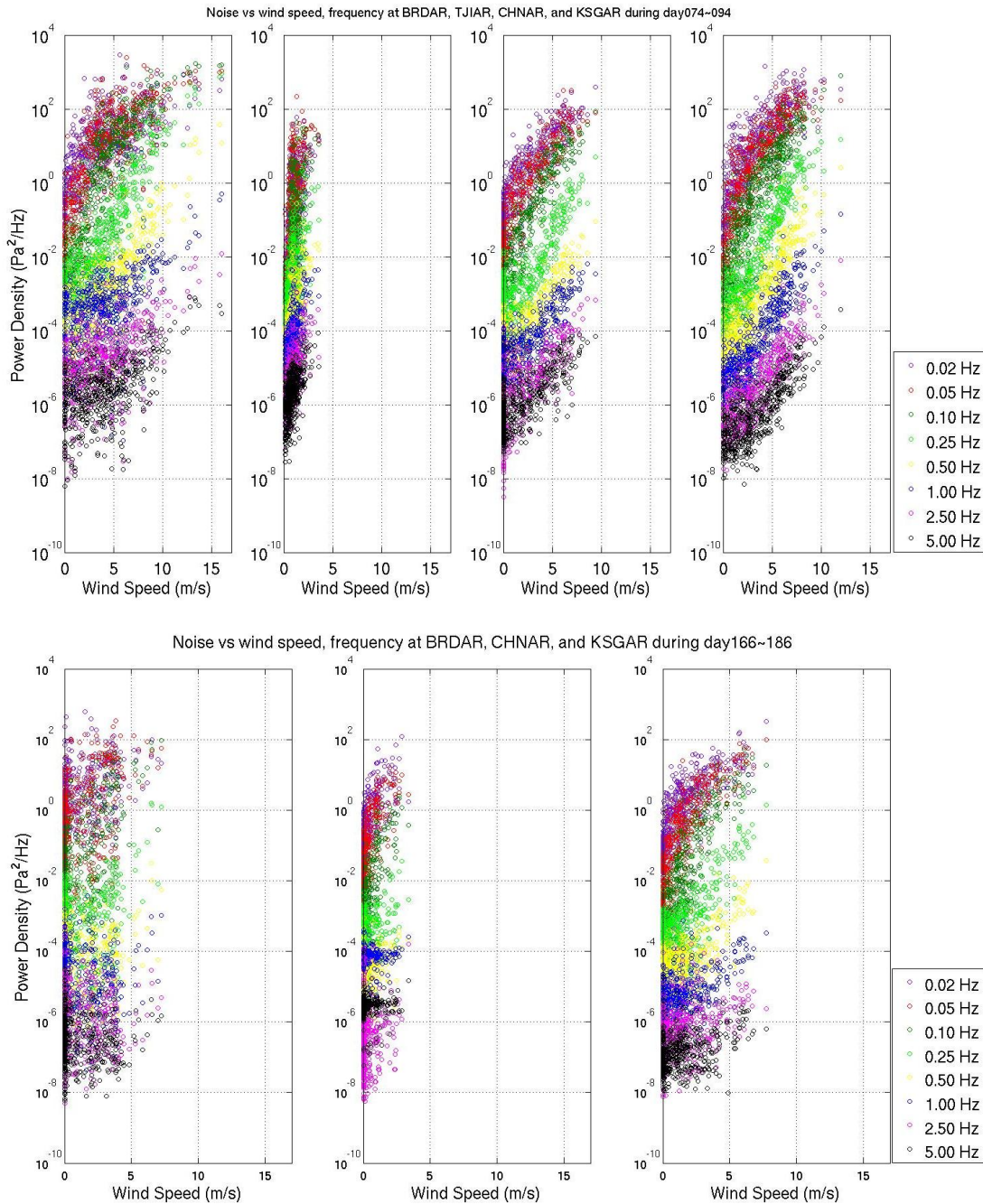
Figure 8: The Four Panels Document the Strong Dependence of Infrasonic Noise on Wind Speed and Frequency at the Four Sites in Korean Peninsula for Spring (Top) and at the Three Sites for Summer (Bottom)

Noise vs wind speed, frequency at BRDAR during day357~365 (2009) and day001~012 (2010),
TJIAR during day040~061 (2010), and KSGAR during day357~365 (2009) and day001~012 (2010)
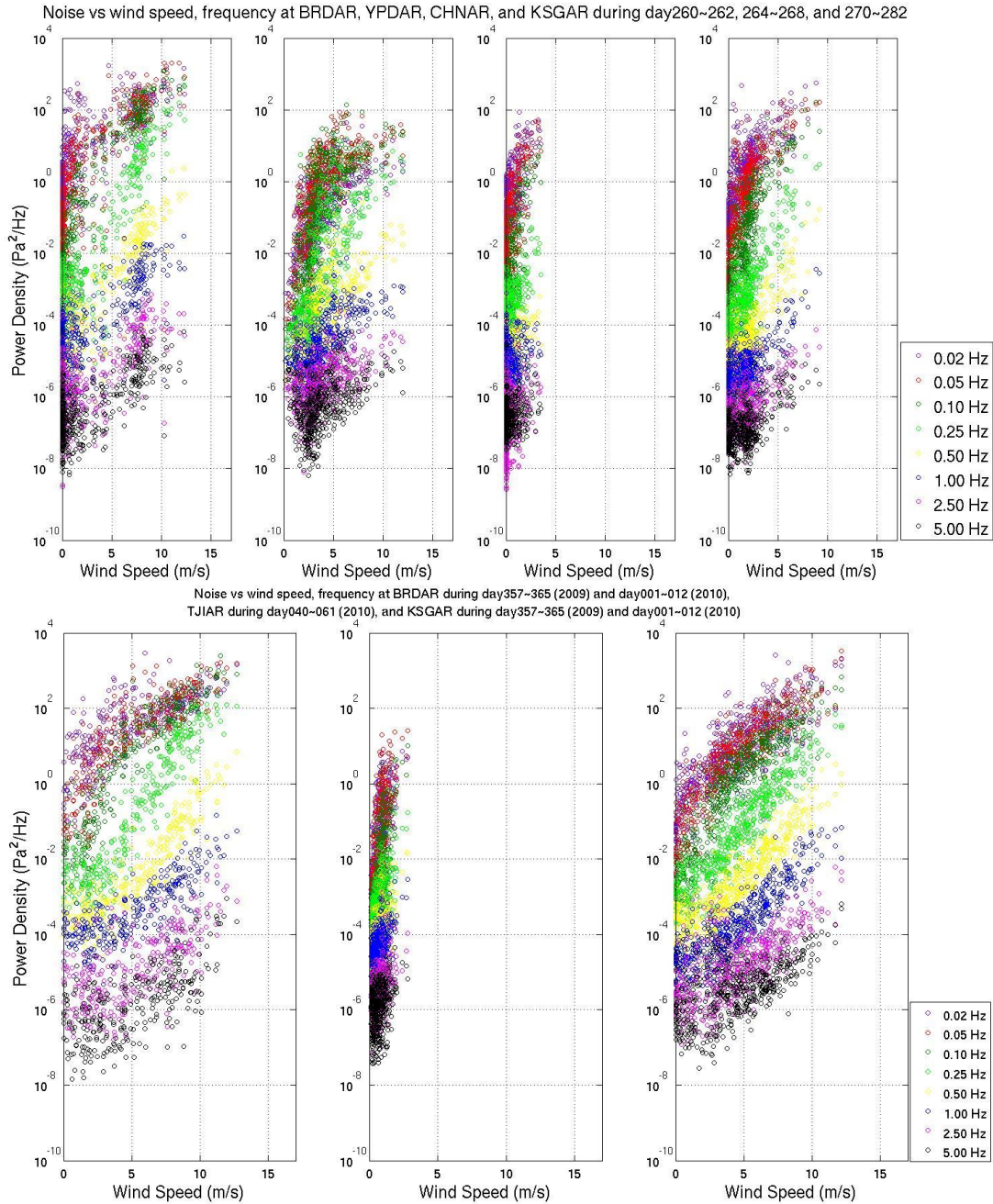
Figure 9: The Four Panels Document the Strong Dependence of Infrasonic Noise on Wind Speed and Frequency at the Four Sites in Korean Peninsula for Fall (Top) and at the Three Sites for Winter (Bottom)

From top to bottom in each panel of Figure 9, noise power is shown at 0.02 Hz (purple); 0.05 Hz (red); 0.1 Hz (dark green); 0.25 Hz (light green); 0.5 Hz (yellow); 1 Hz (blue); 2.5 Hz (pink); and 5 Hz (black).

Wind azimuth as well as speed can affect infrasonic noise, especially in cases where topographic interactions are important. The seasonal variation of wind azimuth for BRDAR, CHNAR, and KSGAR are documented in Figure 10. The wind azimuth data were processed in the same manner as the wind velocity data using a total of three weeks of data for spring (Julian days 074-094, 2010), summer (Julian days 166-186, 2010), fall (Julian days 260-262, 264-268, and 270-282, 2010), and winter (Julian days 357-365, 2010 and Julian days 001-012, 2011). The variation in wind azimuth is correlated with array location (Hedlin *et al.*, 2002). The data illustrates that the northwest and southeast wind directions are significant for all the arrays with slight shifts in the absolute direction in the NW winds for arrays that move from west to east across the peninsula, BRDAR to CHNAR to KSGAR. There are only small differences in azimuths between the array across the seasons illustrating that local wind directions are similar for the arrays and reflective of regional wind patterns. The most consistent wind directions occur in the winter and are from the northwest.
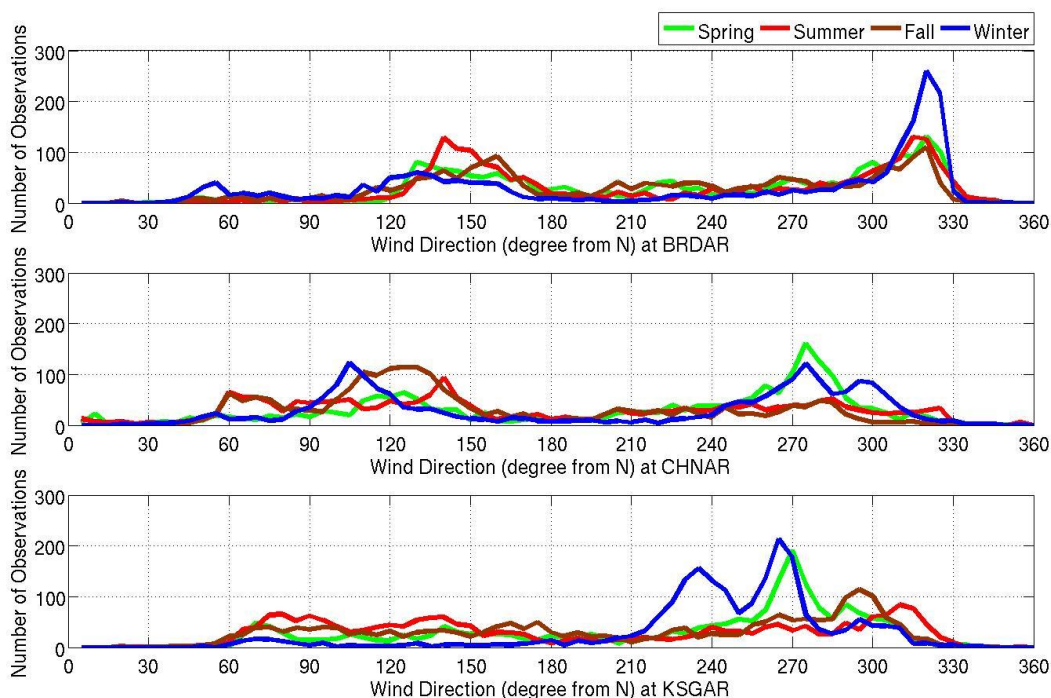
Figure 10: The Number of Observations as a Function of Wind Direction at BRDAR, CHNAR, and KSGAR in Korean Peninsula for Spring (Julian Days 074-094, 2010), Summer (Julian Days 166-186, 2010), Fall (Julian Days 260-262, 264-268, and 270-282, 2010), and Winter (Julian Days 357-365, 2009, and Julian Days 001-012, 2010)

Hedlin *et al*. (2002) have demonstrated that array site performance is better when wind azimuth and speed show little variation so the consistency of wind directions in the winter may contribute to improved triggers during this time period although wind velocities are generally higher during this time period. We will investigate seasonal variations in detections to further assess this issue. Arrowsmith and Hedlin (2005) indicate that the number of detections during the winter is larger than those in summer for their study area.

2.6 Implementation and Testing of Detector

Due to frequent and large uncorrelated bursts of wind noise that appear on elements of infrasound arrays as documented in the noise analysis section, the standard STA/LTA detectors conventionally used for seismic detection perform poorly, producing high false alarm rates (Blandford, 2002). Using a Box-Cox power transformation, a short-term average/long-term average (STA/LTA) can be calculated on the time series power and the distribution of STA/LTA transformed to a near-normal distribution (Arrowsmith *et al*., 2008a). An alternate approach is to design detectors that rely on the presence of the same signal on different channels of the array (Jacobson, 1957; Smart and Flinn, 1971; McKissic, 1996). In these detectors one must assess whether the corresponding estimates of backazimuth and phase velocity are representative of a signal.

One recent approach to these types of detectors in the presence of time varying background noise uses the F-statistic (e.g. Shumway, 1971; Smart, 1971; Smart and Flinn, 1971; Blandford, 1974; Evers and Haak, 2001) with the null hypothesis of perfectly uncorrelated noise as suggested by Blandford (2002). Automatic detection is based on the F-statistic calculated as the power on the beam from the array divided by the average over all channels of the power of the difference between the beam and the individual array channels:

$$
F = \left(\frac{J-1}{J} \right) \frac{ \sum\limits_{n=n_0}^{n_0+(N-1)} \left[\sum\limits_{j=1}^{J} x_j(n+l_j) \right]^2 }{ \sum\limits_{n=n_0}^{n_0+(N-1)} \left(\sum\limits_{j=1}^{J} \left\{ x_j(n+l_j) - \left[\frac{1}{J} \sum\limits_{m=1}^{J} x_m(n+l_m) \right] \right\}^2 \right) }, \tag{2}
$$

where J is the number of sensors, $x_j(n)$ is the waveform amplitude of the nth sample of the mean-free time series from sensor j, l_j is the time-alignment lag obtained from beamforming, n_0 is the starting sample index for the processing interval, and N is the number of samples in the processing window. The F-statistic is implemented using the maximum average cross correlation for beam formation, and associated *p*-value, which is the probability of obtaining an F-statistic at least as extreme as the calculated values under F-distribution: $p\{F(t)\}$, from all triplets of elements in an array for each time window. The detector relies on maximum correlation between sensors based on classical statistics. The power in the best beam becomes the numerator while the denominator is the power in the difference between the best beam at each time point and the average of the beam-aligned window.

When a signal is in a processing window, the F-statistic increases for two reasons. First, the numerator increases because the beam signal power is added to the beam noise power. Second, if the signal is correlated, then when the beam is subtracted from each individual channel, the residual noise is the same as before the signal arrived, and the numerator remains the same so that the ratio increases. In the case of a signal or noise burst that is incoherent across the array, the amplitude will increase with increasing beam's residual at the same time, and the ratio remains the same.

In the presence of correlated noise, the theoretical F-statistic is distributed as $CF_{2BT,2BT(N-1)}$, where B is the bandwidth of the filtered data and T is the length of the processing (detection) window over which the power is averaged, N is the number of array elements, and C is given by:

$$C = \left(1 + N\frac{Ps}{Pn}\right) \tag{3}$$

where Ps/Pn denotes the correlated-noise power to uncorrelated noise power power (Shumway *et al.*, 1999). The constant, C, is the scaling factor that aligns the peak of the distribution of the F-statistic in the time window with the peak of the theoretical central F-distribution with 2BT, 2BT(N-1) degrees of freedom. This constant is proportional to the number of sensors and the signal to noise ratio, and it becomes 1 when the signal power Ps=0.

The standard F detector can be modified so that it is adaptive in time, capturing changing noise characteristics with new extimates of C made for subsequent adaptive windows when the total time window duration is larger than the adaptive window. Using the output from a standard frequency-wavenumber (F-K) analysis (e.g. Rost & Thomas, 2002) and the original input parameters, the observed distribution of the F-statistic ($F_{2BT,2BT(N-1)}$) is adapted to the computed F-distribution ($CF_{2BT,2BT(N-1)}$) by estimating the maximum C-value which aligns the peaks of the two distributions. The fitted F-statistic is converted to *p*-value and a standard *p*-value threshold is applied to find detections with a specified statistical significance.

One of the purposes of this initial study is a quantification of the time period over which this adaptation is important to the detection process. The temporal variation in noise and signal characteristics at each of the arrays will be analyzed in order to physically interpret the adaptation process and identify an optimum detection strategy for each array. Finally, comparison of the calculated *p*-value and threshold significance level provides estimates of the start and end time for significant detections. Detection parameters are assembled retaining detection time, azimuth, slowness, and correlation coefficient and used subsequently for event location.

Data processing is composed of two steps – F-K analysis and detection. A flow chart of this process is reproduced in Figure 11. Generally, many infrasound signals are observed in the frequency band 1-5 Hz (Arrowsmith and Hedlin, 2005). Therefore, the data are bandpass filtered with a Butterworth filter in this band in order to increase SNR for regional infrasound signals and reduce the effects of the lower and higher frequency noise documented earlier. The free parameters for the detector are: analysis time window; window overlap; adaptive window length for noise assessment and C-value estimation; and *p*-value for signal identification (Figure 11).

The signal time window is set to the approximate duration of expected arrivals with overlap between subsequent processing windows. The window overlap provides the ability to better assess the continuous variation of slowness and backazimuth as a function of time and uses window overlap of 50 % (Arrowsmith and Whitaker, 2008). The *p*-value affects both the number of detections and signal-to-noise ratios of those detections. The adaptive window duration for noise characterization as illustrated earlier must be set long enough to obtain a sufficient sample distribution, but short enough to account for temporal variations in ambient noise and is related

to changes as a function of time in environmental parameters that affect the noise. One of the goals of this initial work is to characterize the variation of the adaptive window length at each of the arrays in Korea and understand the relationship between this window length and the noise characteristics at these arrays.
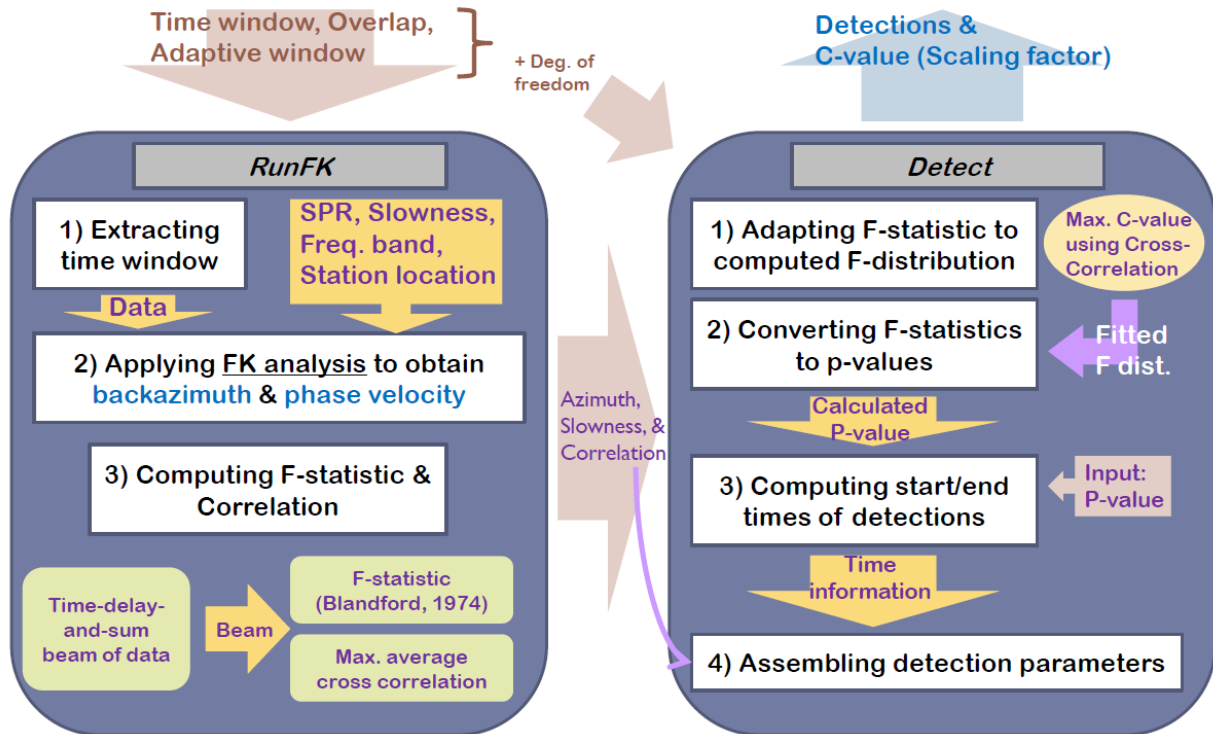
Figure 11: Flow Chart of Detection in InfraMonitor (Arrowsmith and Whitaker, 2008)

Data was initially processed with the following parameters: time window (20s); overlap (50%); *p*-value (0.01); and adaptive window of 1, 12 and 24 hours. Following the flow chart in Figure 11 first, the moving window is used to extract a time window from the array elements that is used to make the first frequency-wavenumber estimate (F-K analysis) from which an estimate backazimuth and phase velocity of signals is made (steps 1 and 2). These backazimuths and phase velocities are then used to compute the lag times (l_j in eq. 1), and the initial computation of the F-statistic (step 3 in Fig. 11). The limits for the backazimuth and phase velocity estimates are based on the following parameters in our study: sampling rate (40); slowness range (-400 to 400 sec/deg); and frequency band (1-5 Hz).

Time delay and sum beamforming is used as a linear array processing method in the next step based on a plane wave assumption. Delay and sum beamforming is simply the summing together of the signals from each element in the array after time shifts have been inserted to account for the slightly different arrival times for the signal arrival at each element of the array over a range of backazimuths and phase velocities. Using the beam calculated from the time delay and sum, we can obtain the F-statistic values in Equation (2) and the maximum average cross correlation value for each adaptive window segment. This process produces time varying estimates of horizontal slowness and backazimuth and these outputs can be used in the next step to detect signals at each array.

An important component of the detection step in the processing is the adjustment or adaptive remapping of the F-distribution. Firstly, each F-statistic value, having its own estimate of azimuth and slowness, is part of a distribution, which is the practical (empirical) F-distribution. This distribution is compared to the standard theoretical Central F-distribution. The C value in Equation 3 is used to remap the peak value of the empirical distribution to the peak of the theoretical distribution. Then, using the p-value based on a null hypothesis of uncorrelated noise, some portion of the area of the modified F-distribution can be selected as a detected signal. In this study, a p-value of 0.01 is used representative of approximately 1 percentage of the area under the curve and corresponds to a significant departure from the null hypothesis. Arrowsmith $et\ al.$ (2009b) analyzed hypothesis testing of the p-value thresholds with ranges from 0.01 to 0.05 and found that a p-value of 0.01 produced excellent performance as measured by a reduced false-alarm rate. Using this process, the starting and ending time of detection is computed for assembling detection parameters that include backazimuth and slowness to be used for event location.

2.7 Characterization of the Adaptive Nature of the F-Detector at Various Arrays

The first step in the detection process consists of the calculation of the F-statistics as introduced in the previous section. Figure 12 displays two examples illustrating the difference between the conventional and modified detectors for two different one-hour segments taken on Julian day 085 at BRDAR. The empirical F distribution (red) for the first hour, 00:00:00~01:00:00 (Figure 12a) is quite close to the theoretical distribution (black) and requires little remapping. The empirical F distribution (red) for the second hour, 20:00:00~21:00:00 (Figure 12b) departs significantly from the theoretical distribution (black) and requires significant remapping using the C parameter (Equation 3). In this example little or no remapping was necessary for the first window but without remapping the second window there would be a significant number of false alarms produced by the detector.

The departure of the empirical F-distribution from the theoretical one can be a result of changing coherent noise conditions as discussed in the earlier noise analysis and thus motivates the remapping of the distribution as proposed by Arrowsmith $et\ al.$ (2009b). Assuming the null hypothesis of uncorrelated noise, the calculated F-distributions (black solid distribution) and the limit of threshold (black vertical line) are plotted in Figure 12. To the left of the vertical line is the 99% threshold used in this test. The right side of the limit line represents the signals with a p-value of 1% representative of extreme departure from the null hypothesis and thus signal detection. By adaptively setting the p-values with respect to the characteristics and background noise level of individual arrays, the false alarm rate is reduced.

The right side of the limit line in the conventional F-distribution (the left figure in Fig. 12(a)) will have a higher probability of false detection than the modified F-distribution (the right figure in Fig. 12(a)), due to the temporal noise variation, as mentioned above. The percentage of detections using the conventional F-distribution is also higher than the modified one, which means more signals were detected as events in the case of the conventional method. The second example (Fig. 12(b)) illustrates how rapidly the distribution can change as a function of time. In this case, before remapping, a much larger portion of the empirical distribution is to the right of

the limit line and regarded as a 'detection' using the conventional F-statistics. These additional detections in all probability represent coherent noise during this time period. Arrowsmith *et al*. (2009b) introduced the adaptive remapping of the F-statistic to account for such situations. Figure 12b illustrates that the remapped observational distribution using equation 3 fits the theoretical F-distribution much better and the resulting detection percentage is significantly reduced.
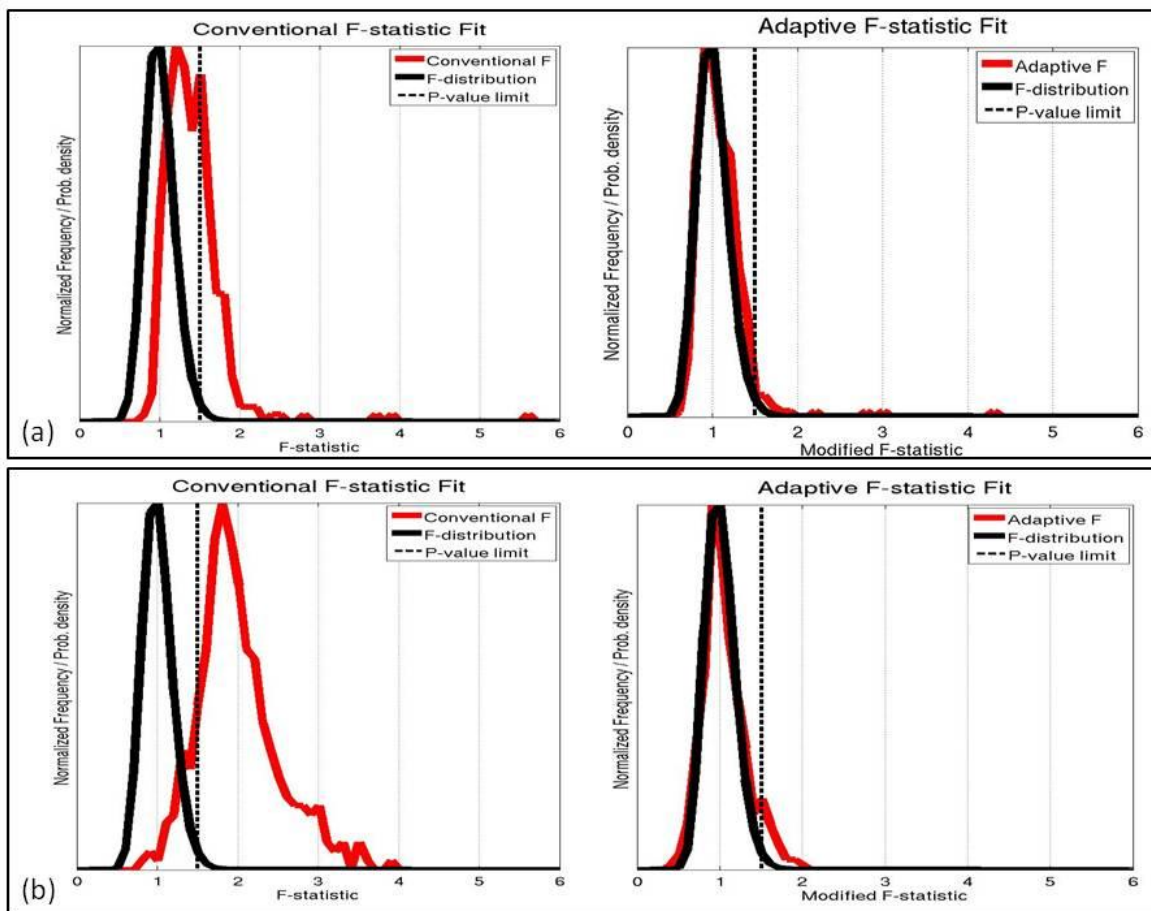
Figure 12: Example Illustrating the Difference Between a Conventional Detector (Left Two Panels), and the Modified Detector (Right Panels) Using an Adaptive Window

As seen in Figure 12, the theoretical (black) and empirical (red) F-distribution included in each panel is the 99% threshold. Data were analyzed for two different time windows: (a) BRDAR Julian day 085, 2010 (00:00:00~01:00:00) and (b) BRDAR Julian day 085, 2010 (20:00:00~21:00:00). Two panels are displayed for each hour of data, the left panel without applying adaptation and the right after adaptively remapping the empirical distribution using Equation 3.

The length of the adaptive window used in the processing is closely related to the time variations in the noise (possibly related to weather or other environmental conditions) as documented in the earlier noise analysis. In order to relate the time varying nature of the noise to the adaptive nature of the detector we document the sensitivity of the C estimates for different time windows. Figure

19

13 plots the C-value variations as a function of time estimated from the data at BRDAR, CHNAR, and KSGAR on day 085. Three different length adaptive noise windows (1, 12, and 24 hour) were independently applied to the data. The C-value for BRDAR (1.2) is higher than those from the other two arrays (1.1), using the 24-hour adaptive window. For the 1-hour adaptive window, BRDAR has C values as large as 1.6 with significant time variation, consistent with the results in Figure 12, possibly related to time variations in wind conditions on the island documented earlier. At CHNAR and KSGAR, the C-values using 1-hour windows are the same as those estimated using the 24 hour adaptive window suggesting little or no temporal variations at these two sites.

In an attempt to explore the link between the time varying nature of the adaptive remapping to physical noise processes, time varying C-values are contrasted against characterizations of shallow atmosphere environmental conditions over extended time periods. Calculated C-values using 1-hour adaptive windows are plotted against weather conditions (wind velocity, wind direction, and temperature) for 11 days of data (Julian days 085-095, 2010) at BRDAR, CHNAR, and KSGAR (Figures 14, 15, and 16). In these figures time was converted from UTC time to local time and included at the bottom of the figures. There is an unknown calibration constant for temperature at BRDAR, so we can only compare with the variation in temperature rather than its absolute value at this array. The weather data for these 11 days suggests that wind velocity at BRDAR and KSGAR vary randomly, but winds at CHNAR follow a more regular trend with higher winds from 12 to 24 hours. This temporal trend may be related to the location of sites on Korean Peninsula. BRDAR and KSGAR are located next to the West and East Sea, respectively. On the other hand, CHNAR is located in the center of the peninsula, so is less affected by the ocean. While the C-value at BRDAR is very low and consistent during time periods of high wind velocity, it is relatively high during time periods of low wind velocity. This pattern is somewhat similar to what is observed CHNAR (Fig. 15), although the change in C-value during low velocity winds is less.
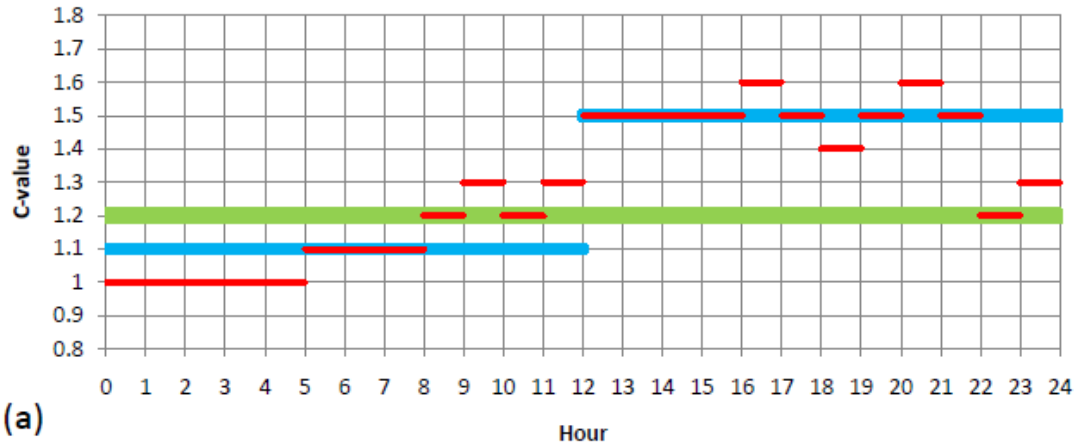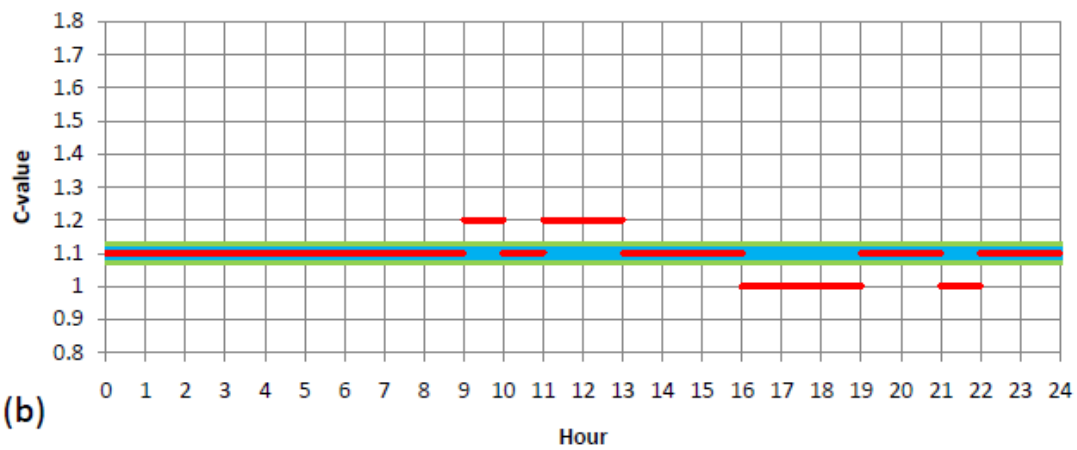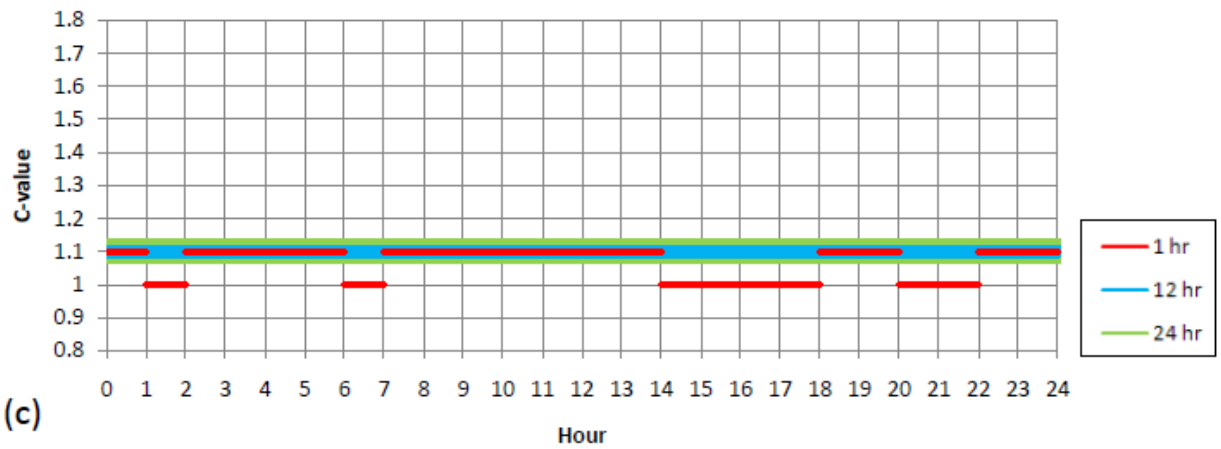
Figure 13: C-Value Variation with Time for (a) BRDAR, (b) CHNAR, and (c) KSGAR - Julian Day 085, 2010 (Hr in UTC)
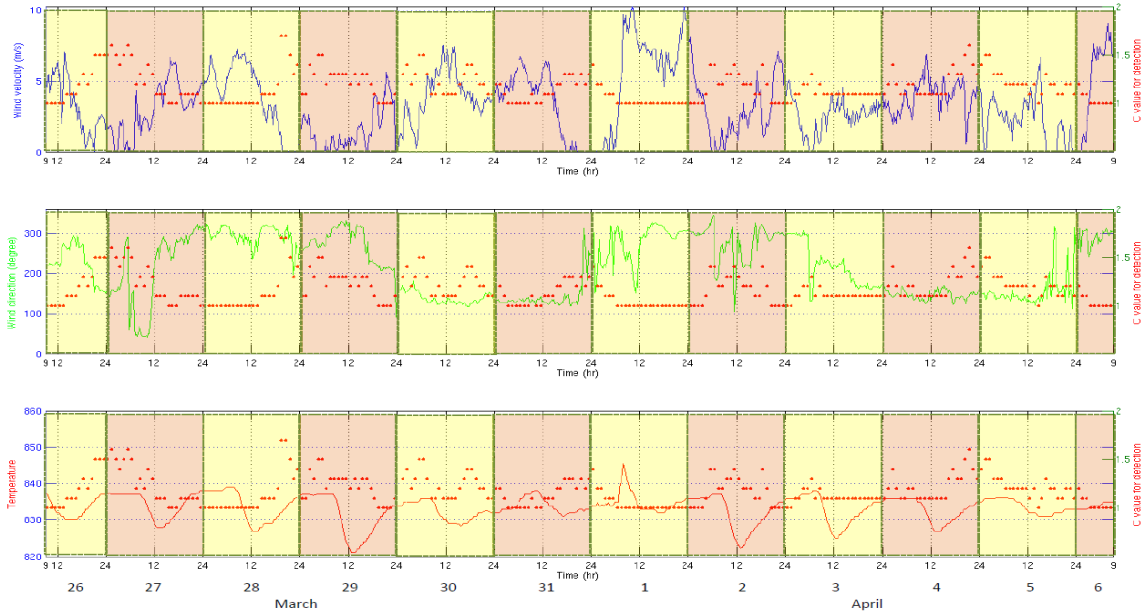
Figure 14: C-Value Variations with Weather Conditions (Wind Velocity, Wind Direction, and Temperature) for 11 Days of Data (Julian Days 085-095, 2010) at BRDAR
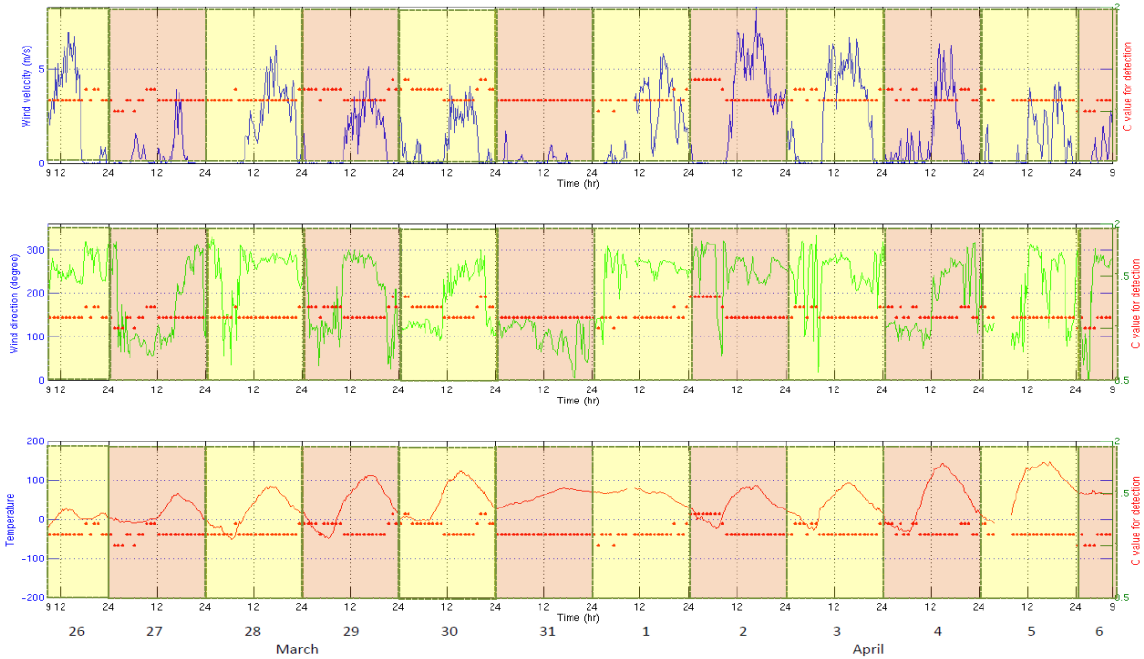
Figure 15: C-Value Variations with Weather Conditions (Wind Velocity, Wind Direction, and Temperature) for 11 Days of Data (Julian Days 085-095, 2010) at CHNAR
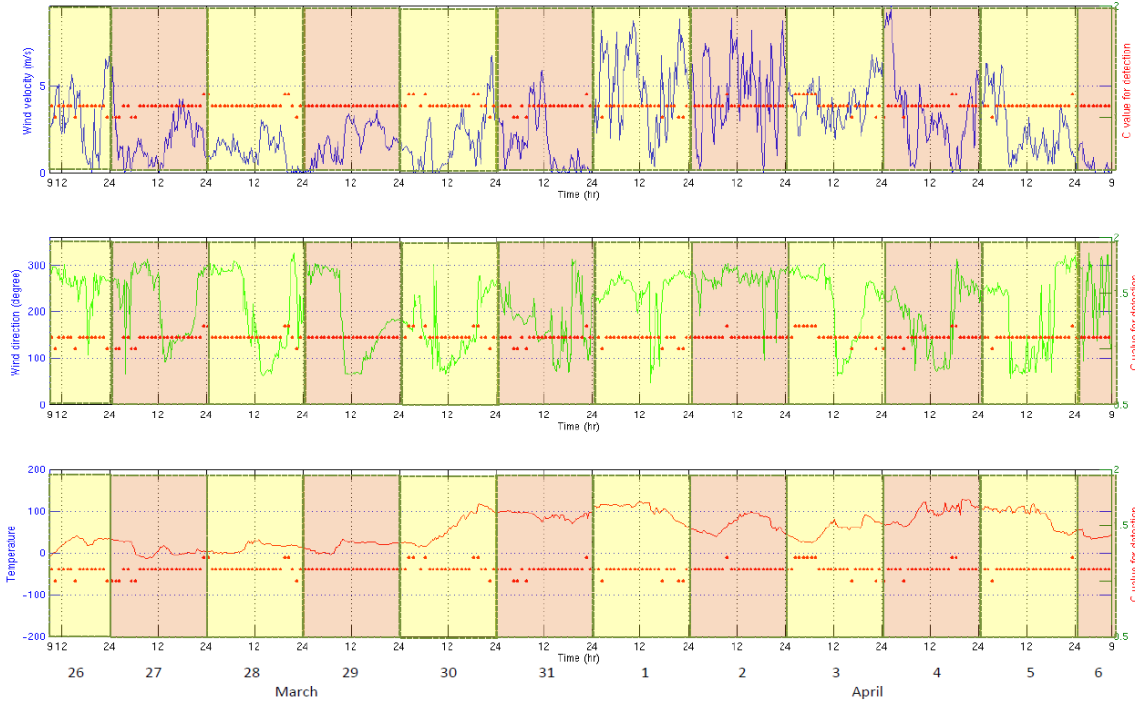
Figure 16: C-Value Variations with Weather Conditions (Wind Velocity, Wind Direction, and Temperature) for 11 Days of Data (Julian Days 085-095, 2010) at KSGAR

These results suggest that under conditions of low wind velocity that the infrasound sensors can be very sensitive to small local events such as movement of a tree or car, construction work or any of a variety of human activities if they are close to the array. For those arrays near the ocean this could include signals generated by ocean interactions. Under these conditions the coherent background noise level at low wind velocity is slightly higher than that observed for other arrays and the C-value increases due to this coherent noise source. On the other hand, the interpretation in case of high wind velocity needs additional consideration. Our next step is to study events at BRDAR under low noise conditions and will include careful frequency wave number analysis in order to characterize more fully the sources of coherent noise and relate them to physical processes.

Further noise analysis was undertaken for BRDAR in order to refine the relationship between wind velocity and C-value over a time period of 33 days (Julian days 085-117, 2010). Each C-value was calculated using a 1-hour adaptive window to assess the temporal variations, yielding a total 24x33 points in Figure 17. Wind directions of 120° to 180° and 300° to 360° dominate Baengnyeong island during the spring with the highest velocity associated with directions from 300° to 360°. As in the previous analysis, the C value increases with decreasing wind velocity, up to 2.3 in case of wind velocity less than 1 m/s. As mentioned above, high C-value under low wind speeds motivates the planned analysis of the signals under these conditions in order to identify the physical mechanism for the correlated noise.
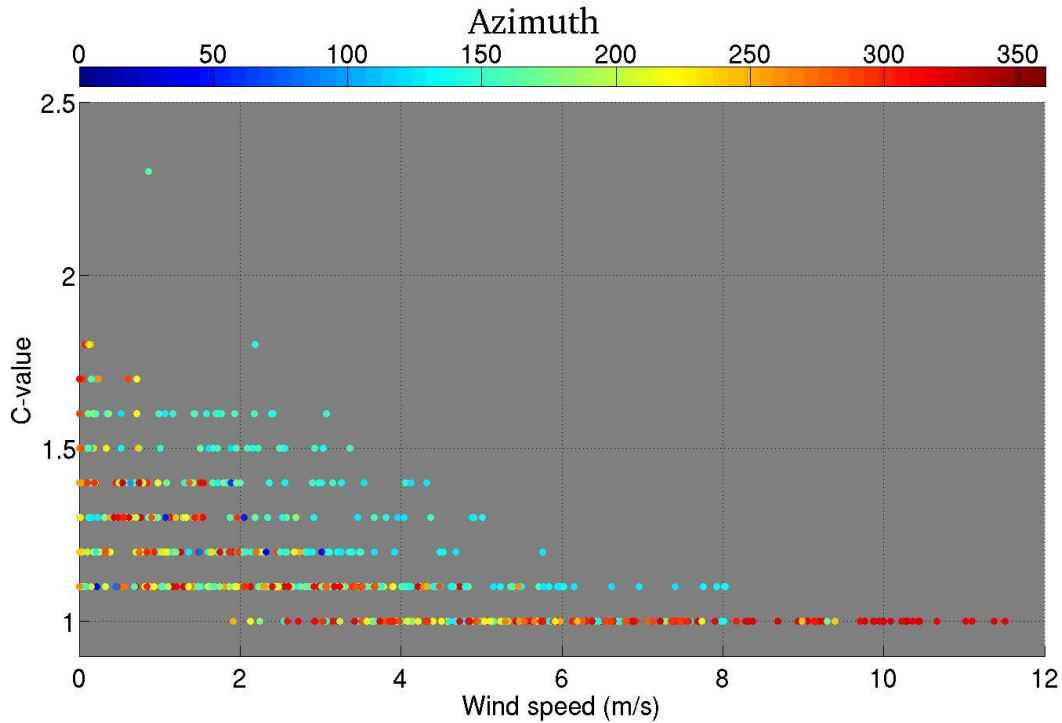
Figure 17: Relationship Between Wind Speed, Wind Direction and C-Value for 33 Days (Julian Days 085-117, 2010) at BRDAR

The final assessment in this study is to compare the actual number of detections produced by the adaptive F-detector to the environmental conditions. The number of detections (Figure 18, bars), calculated by InfraMonitor with 1-hour adaptive window, for BRDAR, CHNAR, and KSGAR during one day (Julian day 085, 2010) are compared to wind velocity (Figure 18, lines) averaged during the 1-hour segments. As discussed above, the C-values are dependent on wind velocity during each adaptive window. The trend in wind velocity varies on a diurnal basis as does the number of detections. Wind velocities from 0 to 9 hour in UTC (day time, from 9 am to 6 pm, in local time) for all arrays are generally high, up to 6 m/s, with low values during local night time, except for KSGAR. In the case of KSGAR, wind speed rises to over 6 m/s again during the night-time reducing the number of detections. This effect is likely related to the site characteristics since both mountains and ocean surround this site.
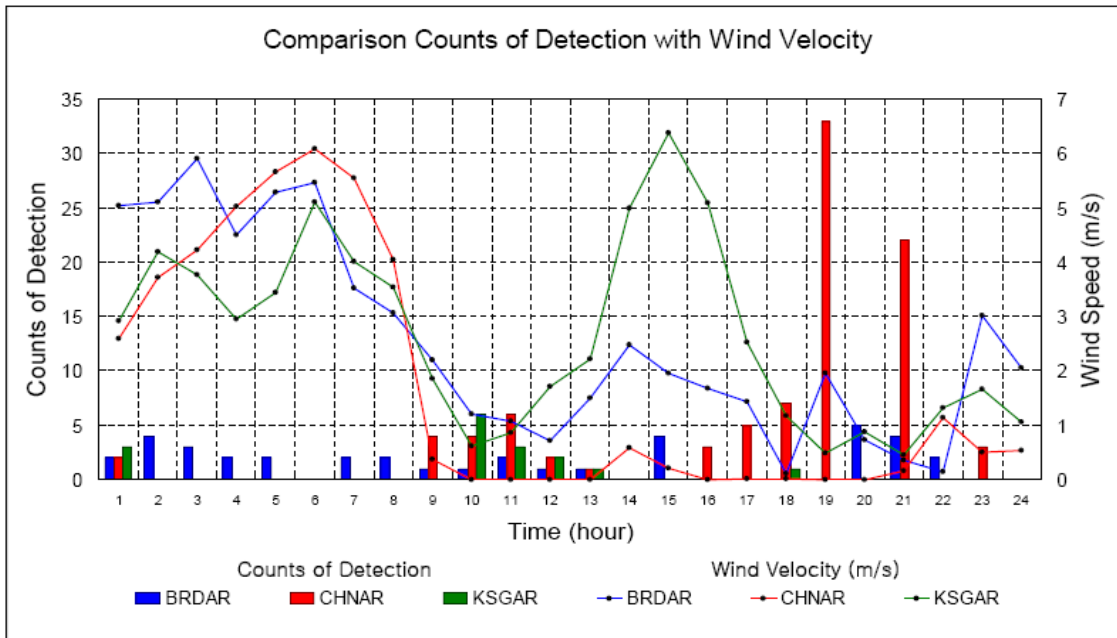
Figure 18: Relationship Between Numbers of Detections and Wind Velocity for One Day (Julian Day085, 2010) at BRDAR, CHNAR, and KSGAR

The number of detections increases when wind velocities are low values at all arrays, especially CHNAR, and is consistent with the International Data Centre (IDC) report that detections based on the PMCC algorithm (Cansi, 1995) increased under low wind velocity and low absolute micro pressure (Woodward *et al*., 2005). It was further shown that most of the detections during low wind velocity were false alarms (Woodward *et al*., 2005), caused by local events or other sources of coherent noise, further motivating the use of the adaptive F detector. During the day-time, there are few detections at CHNAR and KSGAR, but at BRDAR the number of detections can in some circumstances rise under increasing wind conditions. This result suggests that at BRDAR there is some other source of coherent noise such as that from ocean waves or local events.

2.8 Conclusion

Optimal estimation of infrasound detections is dependent upon an understanding and characterization of background noise levels and their relationship to environmental parameters such as wind speed, wind azimuth, surf noise, and local signals near each site. Separation of coherent and incoherent noise signals is also of importance. Data from a network of infrasound arrays in South Korea have been used to tackle these issues in order to provide a set of detections that can ultimately be used to produce a catalog of regional infrasound sources.

The noise analysis indicates that infrasound amplitudes increase as wind speed near the sensor increases. In order to fully characterize this background noise, the 10th, 50th, and 90th percentile noise spectral densities at all frequencies were calculated for each array. These noise spectra are found to be time dependent with the spread between the 10th and 90th percentiles large, about 40 dB at 0.1 Hz. This spread in noise power is largest for the arrays on the islands, with generally higher values correlated with higher wind speeds. All array sites in this study are impacted by noise associated with the wind, but the effect is reduced for the continental arrays thus

illustrating that both the wind speed distribution and noise levels are site dependent. In the case of arrays near the ocean, the noise power density is influenced by additional local site characteristics, possibly related to the ocean environment, that need further investigation. Finally, the data indicates that the most consistent wind directions occur in the winter and are from the northwest in South Korea. This result suggests that more reliable detection results might be expected during the winter and needs quantification.

An adaptive F-detector is applied to the observational data sets as implemented in InfraMonitor (Arrowsmith et al., 2009). This detector enables us to improve signal detection under noise conditions that change with time as quantified in this study. The procedure allows the empirical F distribution to be mapped to the theoretical distribution through a C-value estimated in the procedure. We report on an assessment of the time varying nature of this adaptive process at each of the arrays on the Korean Peninsula. There is only modest temporal adaptation for arrays within the continent, but strong time varying adaptation at the island arrays. The temporal variation in adaptation correlates with wind speed. In the unique case of the island site BRDAR, the C-value increases with decreasing wind velocity. This result suggests that local signals, regarded as correlated noise, might be affecting the detection process at this site. Additionally, it was shown that the number of detections increases as the wind velocity falls to low values at all arrays. Further work needs to be done to separate coherent noise at the arrays from source-generated signals of interest. These results now provide a set of preliminary array specific procedures that can be implemented in order to produce a network infrasound event bulletin. Such a bulletin will have to be validated against a set of analyst driven events in the final step of the assessment.

3. A COMPARATIVE STUDY OF AUTOMATED INFRASOUND DETECTORS – PMCC AND INFRAMONITOR WITH ANALYST REVIEW

3.1 Motivation

Signal detection is the first step in the production of regional infrasound bulletins. The large number of regional infrasound arrays in and near Korea and the surrounding region as well as a set of infrasound arrays distributed across the western U.S. provides an opportunity to explore the types and numbers of sources of infrasound observed at distances of 10's to 1000's km. The development of an automated event bulletin based on a robust set of automated detections provides a basis for more detailed source studies as well as the opportunity to quantify infrasound propagation effects across these distances. This report illustrates two such detectors and a testing procedure based on a limited data set. The results of the automated procedures are compared to multiple analysts as a step assessing the effectiveness of these procedures in terms of changing environmental conditions during the time period of the dataset.

There are several well-described infrasound detectors such as the PMCC algorithm (Cansi, 1995), InfraTool in MatSeism-1.7 (Hart and Young, 2002) and InfraMonitor (Arrowsmith and Whitaker, 2008). For comparison purposes in this investigation, PMCC and InfraMonitor are applied to the same data set, a four-hour sequence of infrasound data at the Korean infrasound

array, CHNAR. This data set is chosen as the array has both a short (< 100 m) and long (~1000 m) aperture and the four-hour time sequence has a number of easily identified signals as well as a transition from low wind and noise conditions to high wind and noise conditions half way through the time period. The detections estimated by the two automated procedures are compared to multiple sets of manual detections produced by a collection of five analysts individually reviewing the same data.

3.2 PMCC Background

This section describes PMCC testing including the development of optimal parameters for the Korean infrasound array, CHNAR. Like many other infrasound detectors, the PMCC algorithm (Cansi, 1995) assumes uncorrelated noise, resulting in false alarms in the presence of correlated noise. PMCC is based on progressive processing of data recorded by sub-arrays from a larger array using time domain cross-correlation estimates between individual stations (Cansi, 1995). The first step in PMCC is to use cross-correlation to measure the time delay Δt_{ij} between all pairs

of signals, $S_i(t)$ and $S_j(t)$ at station i and j, in each three-element sub-array, and in the case of a wave propagating without distortion, this delay is the same for all frequencies in the contributing signal (Cansi and Le Pichon, 2009):

$$\Delta t_{ij} = \frac{1}{2\pi f}(\varphi_j(f) - \varphi_i(f)), \tag{4}$$

where $\varphi_i(f)$ and $\varphi_j(f)$ represent the phase at station i and j. For each group of three sensors, the sum of the time delays for a plane wave signal obeys a closure relation, which can be used as an infrasound phase detector:

$$\Delta t_{ij} + \Delta t_{jk} + \Delta t_{ki} = 0, \tag{5}$$

The second step in PMCC is a progressive procedure that is designed to minimize interference from large but random signals and to the effects of spatial aliasing when sensors are far apart (Cansi and Le Pichon, 2009). The consistency of the set of delays is estimated with all the sensors of a sub-network, R_n, and is defined as the mean quadratic residual of the closure relations (Cansi and Le Pichon, 2009):

$$\left.\begin{array}{l} r_{ijk} = \Delta t_{ij} + \Delta t_{jk} + \Delta t_{ki} \\ \\ C_n = \sqrt{\dfrac{6}{n(n-1)(n-2)} \displaystyle\sum_{i>j>k} r_{ijk}^2} \end{array}\right\} i, j, k \in R_n. \tag{6}$$

When this consistency is below a threshold, a detection is declared on R_n and the procedure then determines the number of sensors in the final sub-network, the associated consistency, and the

detected wave velocities and azimuths by progressively increasing the network aperture in order to make robust estimates of these propagation parameters.

The progressive method used in the PMCC algorithm is represented pictorially in Figure 19. PMCC starts with a small subset of stations as a sub-network represented by the yellow circle in Figure 19 and then selectively adds stations until the final array is defined subject to the consistency threshold (Equation 6) and the wave propagation parameters are estimated. If additional elements or arrays (blue inverted triangle in Fig. 19) produce estimates consistent with the sub-network estimate then they are used in the final estimate of the wave parameters. Otherwise, if the added element of the array (red inverted triangle in Fig. 19) includes high background noise and has no consistency with the previous result this new element or sub-array is rejected.

Previous studies have documented the utility of PMCC, Garcés and Hetzer (2002) analyzed various infrasound signals including microbaroms, surf noise, volcanic arrivals, as well as signals from bolides, aircraft, and spacecraft, observed in Hawaii. These studies have illustrated that PMCC processing parameters must be chosen based on the infrasonic signal characteristics, array configuration, and background noise.
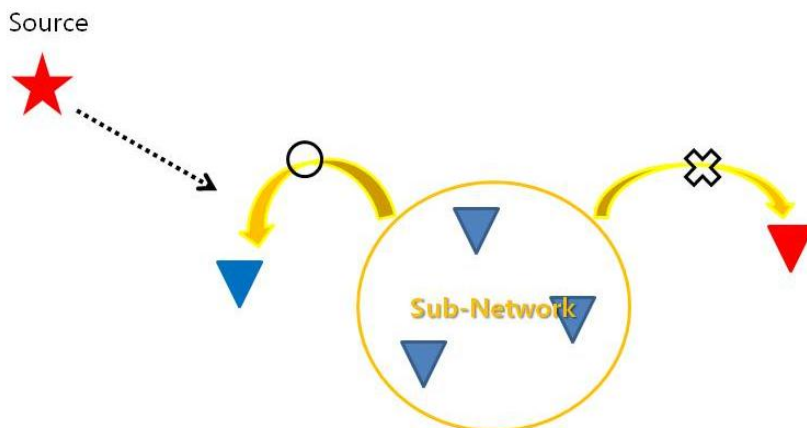
Figure 19: The Outline of the Progressive Method Used by the PMCC Algorithm

In Figure 19, under the assumption that the source (red star) is far from the arrays, PMCC starts coherence processing using the sub-network inside the yellow circle and selectively adds consistent data (blue inverted triangle) while ignoring additional data that are inconsistent or lack coherency (red inverted triangles). This process results in identifying signals and subsequent estimation of wave propagation parameters such as phase velocity and backazimuth.

In our regional applications, the signals of interest are 1-5 Hz from natural and man-made events, and so PMCC tuning parameters were initially set based on the experience documented by Garcés and Hetzer (2002) as well as previous work with InfraMonitor documented in the next section of this report. In this study, a window length of 20 s, overlap of 50%, and filtered band from 1 to 5 Hz were used. The threshold consistency defined as the maximum consistency threshold for declaring a detection is set to 0.1s. One advantage of PMCC is that the detections are assessed in both the time and frequency domain. Each frequency band within each time window represents a "pixel" of data, which is analyzed independently, followed by comparison

of adjacent pixels in time and frequency, where nearest-neighbor groups of pixels with similar characteristics are classified as "families" (Garcés and Hetzer, 2002). In this work, the standard deviation of 10° for azimuth and 20 m/s for phase velocity with a phase velocity range from 0.28 to 0.5 km/s were used for grouping into families. The distribution of backazimuths as well as phase velocities may be seasonally variable and depend on the specific infrasonic arrival but in this initial study these effects were not considered. Incorporation of this type of information is beyond the scope of this initial work and might require some kind of iterative procedure that is linked to phase identification.

3.3 InfraMonitor Background

In the presence of time varying background noise InfraMonitor (Arrowsmith and Whitaker, 2008) uses the F-statistic with the null hypothesis of perfectly uncorrelated noise as suggested by Blandford (2002). Automatic detection is based on the F-statistic calculated as the power on the beam from the array divided by the average over all channels of the power of the difference between the beam and the individual array channels:

$$F = \left(\frac{J-1}{J}\right) \frac{\sum_{n=n_0}^{n_0+(N-1)}\left[\sum_{j=1}^{J} x_j(n+l_j)\right]^2}{\sum_{n=n_0}^{n_0+(N-1)}\left(\sum_{j=1}^{J}\left\{x_j(n+l_j)-\left[\frac{1}{J}\sum_{m=1}^{J} x_m(n+l_m)\right]\right\}^2\right)}, \tag{7}$$

where J is the number of sensors, $x_j(n)$ is the waveform amplitude of the nth sample of the mean-free time series from sensor j, l_j is the time-alignment lag obtained from beamforming, n_0 is the starting sample index for the processing interval, and N is the number of samples in the processing window. The F-statistic is implemented using the maximum average cross correlation for beam formation, and associated p-value, which is the probability of obtaining a F-statistics at least as extreme as the calculated values under F-distribution: $p\{F(t)\}$, from all elements in an array for each time window.

In the presence of correlated noise, the theoretical F-statistic is distributed as $CF_{2BT,2BT(N-1)}$, where B is the bandwidth of the filtered data and T is the length of the processing (detection) window over which the power is averaged, N is the number of array elements, and C is given by:

$$C = \left(1+N\frac{Ps}{Pn}\right) \tag{8}$$

where Ps/Pn denotes the ratio of the correlated-noise power to uncorrelated noise power (Shumway *et al*., 1999). The constant, C, is the scaling factor that aligns the peak of the distribution of the F-statistic in the time window with the peak of the theoretical central F-distribution with 2BT, 2BT(N-1) degrees of freedom. This constant is proportional to the number of sensors and the signal to noise ratio, and becomes 1 when the signal power Ps=0.

The standard F detector can be modified so that it is adaptive in time capturing changing noise characteristics with new extimates of C made for subsequent adaptive windows when the total time window duration is larger than adaptive window. Using the output from a standard frequency-wavenumber (F-K) analysis (e.g. Rost & Thomas, 2002) and the original input parameters, the observed distribution of the F-statistic ($F_{2BT,2BT(N-1)}$) is adapted to the computed F-distribution ($CF_{2BT,2BT(N-1)}$) by estimating the maximum C-value which aligns the peaks of the two distributions. The fitted F-statistic is converted to a *p*-value and a standard *p*-value threshold is used to declare a detection with a specified statistical significance. Data was initially processed with the following parameters: time window (20s); overlap (50%); *p*-value (0.01); and an adaptive window of 1 hour. The estimation of these parameters and their relationship to environmental conditions that change as a function of time are discussed in another chapter 2 of this final report.

3.4 The Test Data Set

In this preliminary study, a 4-hour- dataset (02:00:00-06:00:00 in UTC, 11am-3pm in local time, Julian day 002, 2012) recorded at seismo-acoustic array, CHNAR, located within the continent in South Korea, were used for testing PMCC and InfraMonitor. As noted earlier, this array includes both a short aperture (< 100 m) and long aperture (~ 1000 m). The first two hours of data were recorded under low wind conditions and are thus low-noise while the wind velocity is increased for the second two hours producing a high-noise condition. The filtered (1-5 Hz) waveforms are shown in Figure 20, with four easily identified strong signals near 03:00:00 UTC along with initial output from PMCC discussed latter. Figure 21 illustrates the relationship between C values from InfraMonitor (Equation 8) estimated for this time window and wind conditions (wind velocity and azimuth) consistent with previous results (Park *et al.*, 2011) where the C-value decreases with increasing wind velocity. A one-hour adaptive window was used during the InfraMonitor processing based on the previous work. The associated wind velocities and azimuths are 5-minute averages from a weather station at the site. The first two-hours of data have relatively high C values of 2.4 and 2.3 associated with low wind velocities from the north and east, while the last two-hours of data have smaller C values of 1.8 and 1.5, with significantly higher wind velocities and azimuths from the northwest. The waveforms after 04:00:00 UTC have significantly higher background noise than those before 04:00:00 UTC (Fig. 2).

3.5 Test Procedures

The two detectors, PMCC and InfraMonitor, were applied to this common four-hour data set. As noted, this particular four-hour-time period has noise levels that increase after the first two hours producing data segments with two different background noise levels. CHNAR, like several of the Korean arrays, consists of a small infrasound array with an approximately 50 m aperture embedded in a larger approximate 1 km aperture array (Figure 22) with a second or sub-infrasound element approximately 50 m from the primary gauge in the larger array. PMCC was tested using four different starting configurations or sub-networks: a small aperture (<100m) array (CHN03/04/05)- PMCC (S); a large aperture (~1 km) array (CHN10/20/30)- PMCC (L); a hybrid of small and large aperture arrays- PMCC (S+L); and a combination of small, large, and sub-large (CHN12/22/32) aperture arrays- PMCC (All) (Fig. 22). Similarly, four array configurations were used in the accompanying detector tests of InfraMonitor: a small aperture

array (CHN03/04/05, <100 m) - IM (S), a large aperture array (CHN00/10/20/30, ~1 km)) - IM (L), a small and large array (CHN00/10/20/30/03/04/05) - IM (S+L), and all array elements (CHN00/10/20/30/03/04/05/12/22/32)-IM (All) (Fig. 22).
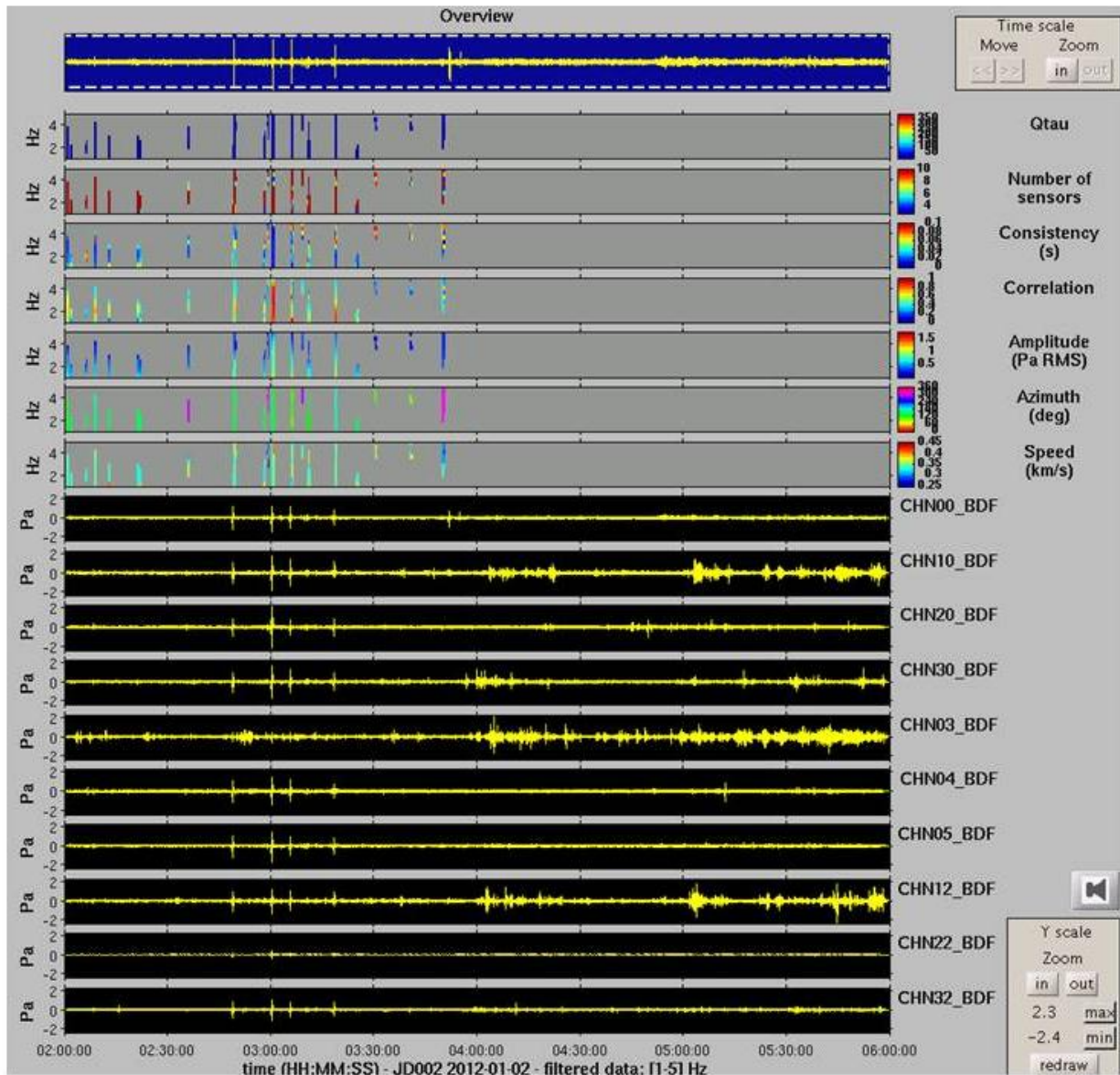
Figure 20: Summary of Detection Results from PMCC(S) (Q$_{tau}$, Number of Sensors, Consistency, Correlation, Amplitude, Azimuth, and Phase Velocity)

In Figure 20, the waveform beam is displayed at the top with the filtered waveforms below.
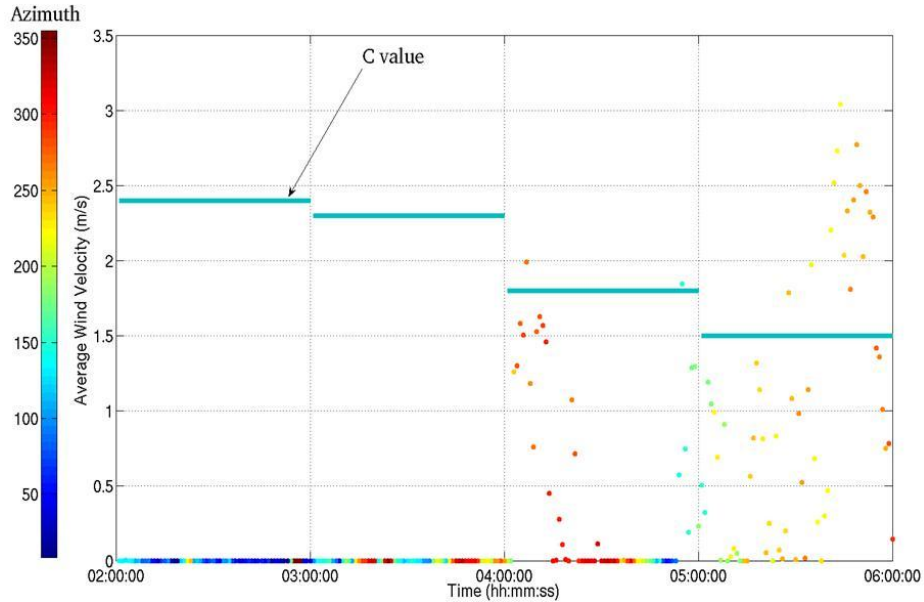
Figure 21: The Relationship Between C Value and Wind Conditions (Average Wind Velocity and Azimuth) During the 4-Hour-Dataset at CHNAR (02:00:00-06:00:00 in UTC, Julian Day 002, 2012)
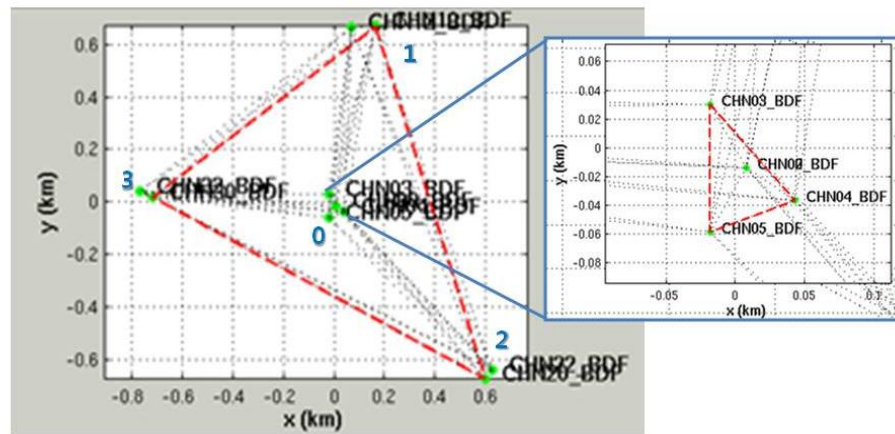
Figure 22: The Physical Configuration of CHNAR

As seen in Figure 22, the four-elements in the 1-km aperture seismo-acoustic array (00/10/20/30) are each composed of a GS-13 seismometer and infrasound gauge supplemented by a small aperture (< 100 m) infrasound subarray deployed around the center element. Each of three outer sites has an additional infrasound gauge offset by about 50 m from the primary.

An example detection output from PMCC (S) that includes the number of sensors, consistency, correlation, amplitude, azimuth, and phase velocity is included in Figure 20. Detections with small consistency values using all array elements in the final calculation were observed during the first two hours of data, while no detections under the consistency constraints were found in the last two hours of data when the background noise levels were higher.

Since automatic detections are dependent on background noise level and algorithmic tuning parameters, sensitivity tests for both detectors were conducted with respect to different values of consistency (0.1 s and 0.5 s) for PMCC and p-value (0.01 and 0.05) for InfraMonitor. The larger consistency values for PMCC provide the ability to include a larger number of automated detections although the quality of the signals across the array may be reduced. Similarly the use of a larger p-value in InfraMonitor, includes a larger number of detections that depart from the null hypothesis, although they may include correlated noise. Results from the sensitivity tests for the two detectors using all array configurations - PMCC (S), PMCC (L), PMCC (S+L), PMCC(All), IM (S), IM (L), IM (S+L), and IM (All) - are summarized in Figure 23. Hereafter, sensitivity tests with consistencies of 0.1 and 0.5 for PMCC are called PMCC1 and PMCC2, respectively, and sensitivity tests with p-values of 0.01 and 0.05 for InfraMonitor are called to IM1 and IM2, respectively. The numbers of detections are summarized in Table 1 and histograms from the tests are compared in Figure 24.

Table 1 The Numbers of Detections Estimated by InfraMonitor and PMCC

Configuration	The numbers of detections	Configuration	The numbers of detections
IM1 (S)	20	PMCC1 (S)	21
IM1 (L)	14	PMCC1 (L)	9
IM1 (S+L)	49	PMCC1 (S+L)	25
IM1 (All)	49	PMCC1 (All)	29
IM2 (S)	42	PMCC2 (S)	21
IM2 (L)	19	PMCC2 (L)	15
IM2 (S+L)	64	PMCC2 (S+L)	33
IM2 (All)	72	PMCC2 (All)	33

Both automatic detectors produce a larger number of detections when either the combined small and large aperture arrays or all array elements are used relative to the cases where the small or large aperture arrays are used alone. In some cases, the results using both the small and large aperture arrays for detection appear to combine individual detections found using the small aperture arrays and large aperture arrays separately. In addition, the number of detections estimated by InfraMonitor is almost twice that estimated by PMCC with many of the additional detections from InfraMonitor occurring in the last two-hour time period when the wind noise increases (Fig. 23). Moreover, the numbers of detections are significantly increased when the consistency for PMCC and the p-value for InfraMonitor are increased. The largest increase in detections occurs with the high p-value in InfraMonitor with a large number of detections identified during the high wind noise conditions. The strong signals around 03:00:00 UTC were detected with high correlation and consistent phase velocities of 0.3-0.38 km/s by both detectors. The azimuth distributions for the detections are primarily from the southeast with a secondary set of detections from the northwest (Fig. 23, right).
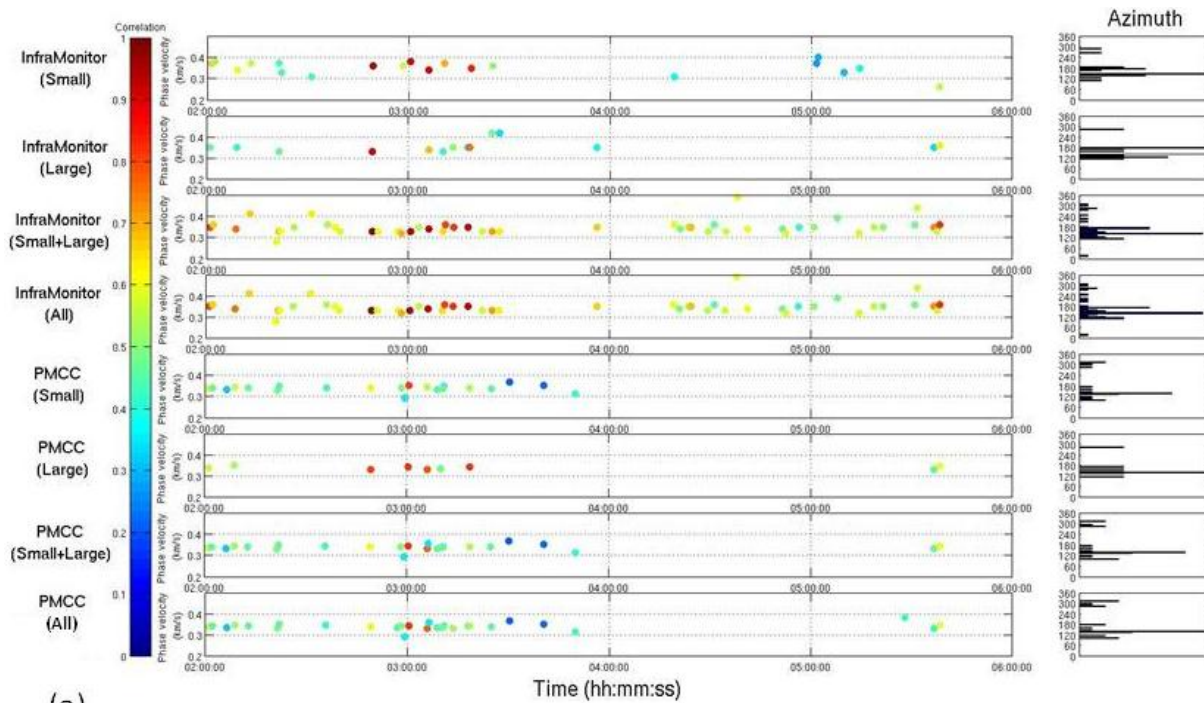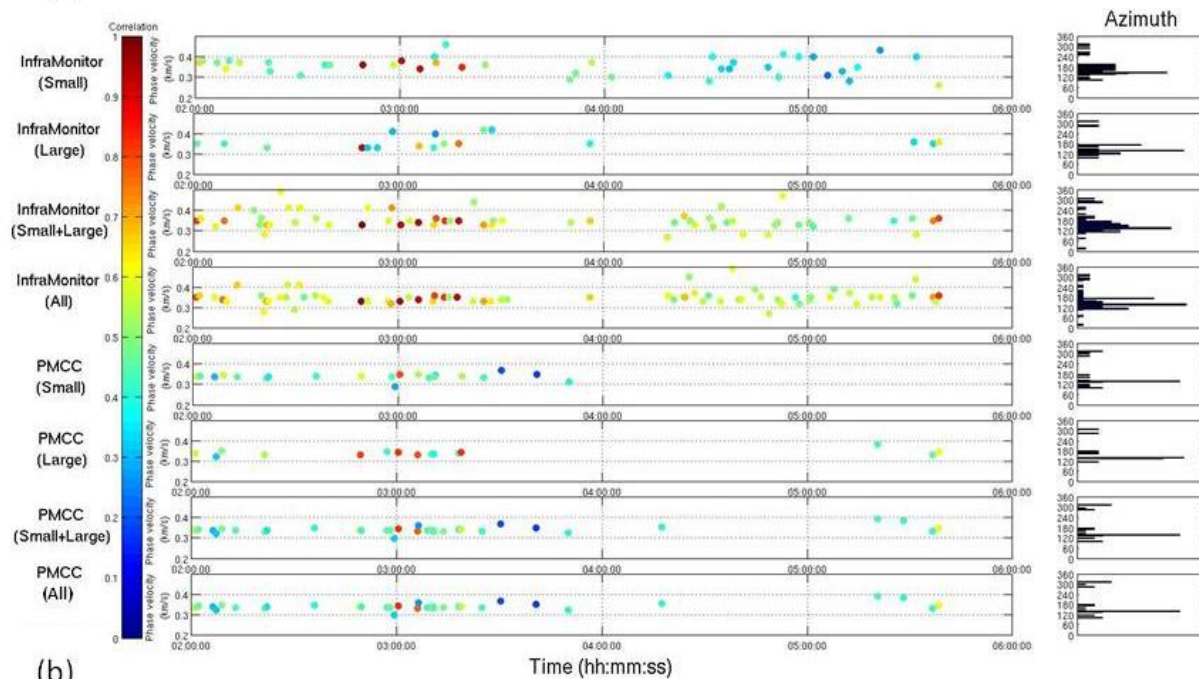
Figure 23: The Detection Results from Two Automatic Detectors (PMCC and InfraMonitor) Using the Different Sub-Arrays (PMCC (S-Small), PMCC (L-Large), PMCC (S+L), PMCC (All), IM (S), IM (L), IM (S+L), and IM (All))

In Figure 23, (a) is the result for the case with a maximum consistency of 0.1 s for PMCC and p-value of 0.01 for InfraMonitor; (b) is the result for the case with a maximum consistency of 0.5 s for PMCC and p-value of 0.05 for InfraMonitor. The correlation values for detection are

represented by the colors in the plot with the azimuthal distribution of detections plotted to the right.

3.6 Analyst Review

In order to assess the performance of the automated detectors, a series of tests using analysts to review the same data were undertaken as motivated by numerous previous studies, many focused on seismic observations. Freedman (1966) first studied estimates of picking errors from analyst reviewed seismograms using nine analysts and researchers. Sereno (1990) and Leonard (2000) assessed automatic picks comparing results with those produced by analysts and quantified the misclassification of seismic phases, mis-timing of seismic phases, and poor phase association (Sipkin *et al.,* 2000). Zeiler and Velasco (2009) focused on measurements by highly experienced analysts at a number of institutions. They concluded that main contributing factors to pick errors for analyst are ambient noise levels, distance from source to receiver, magnitude, source mechanisms, and propagation effects.

We have designed a set of analyst tests in order to address some of these same issues for infrasound data. As noted in the introduction, our goal is to determine an optimum set of automated procedures for infrasound detections suitable for input to an infrasound location algorithm and the production of a preliminary event bulletins. In the case of infrasound where the noise levels can be high and often time variable, it is important to assess the detected signals under various propagation conditions and quantify the effect of weather conditions or array environment on not only the detections but also the quality of the locations. Here we focus on only the first part of the assessment, the detection process.

Five analysts separately reviewed the same dataset used in the test of the automated systems and were free to define their own criteria for event identification (Table 2). All analysts used both time domain and f-k based tools in Geotool (Coyne and Henson, 1995) in order to identify signals. The number of detections produced by the five analysts are compared to the output of the automatic detectors using the two different consistency values, 0.1s and 0.5s, for PMCC and the two different p-values, 0.01 and 0.05, for InfraMonitor (Figure 24). In all cases the number of analyst detections is significantly higher than those determined by either automated detector.

Table 2: Analysts Defined Bandwidth for Data Review

	Analyst 1	Analyst 2	Analyst 3	Analyst 4	Analyst 5
Filter band (Hz)	1-5	1-5	0.5-4	1-5	4-8
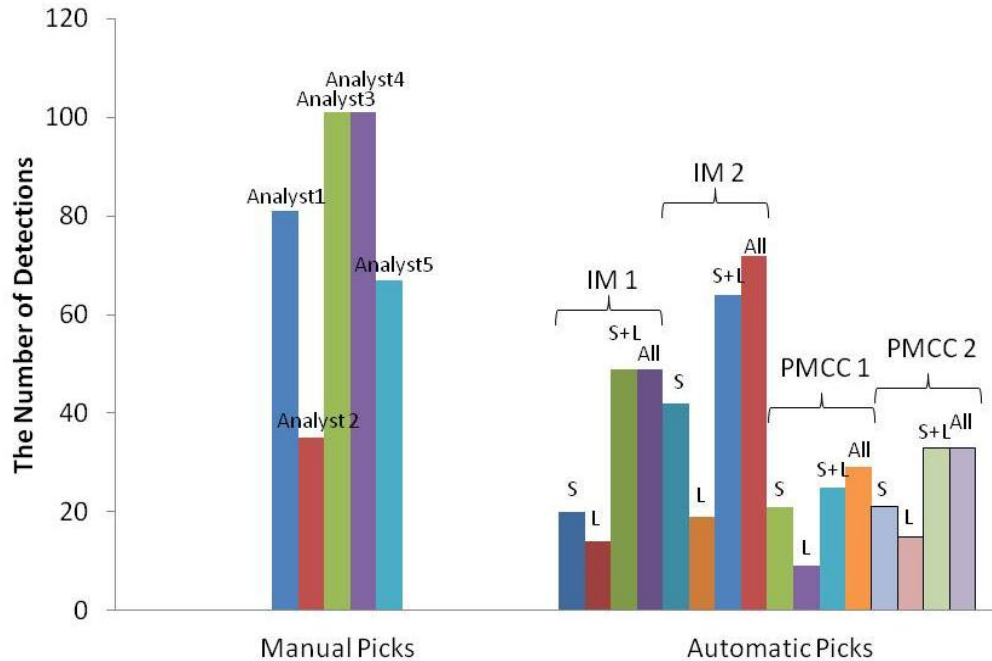
Figure 24: Comparison of the Total Number of Analyst and Automatic Picks (IM1: p-value, 0.01, IM2: p-value, 0.05, PMCC1: Consistency, 0.1 s, and PMCC2: Consistency, 0.5 s) for the Same Four-Hour Block of Infrasound Data Recorded at CHNAR

The times of the automatic detections estimated using different values of consistency and p-value are compared to those estimated by the analysts in Figure 25. In most all cases, the picks by the analysts included all the events identified by the two automatic detectors. The automatic detection using the larger values of consistency (0.5s) and p-value (0.05) included the automated detections using the lower values of consistency, 0.1 s, and p-value, 0.01. In the case of the last two hours of data where the noise levels are higher, there are fewer automated detections and a reduced number of detections identified by the analysts. Some picks by the analysts could be false alarms under these higher noise conditions. This result highlights that detection under high background noise conditions is difficult for both automatic and manual approaches.

Figure 25(b) compares the azimuth and phase velocity estimates for the signals identified by both the automatic detectors and analysts. In all cases, a large portion of the identified signals come from azimuths clustered around 150° and 300° before 04:00:00 UTC, the time period with low background noise levels. The azimuth estimates for signals after this time period are more scattered. Phase velocities range from 0.32 to 0.35 km/s with good match of automatic and manual detectors. Polar plots of azimuth and phase velocity for both the automated and human detection results are illustrated in Figure 8. In the first two hours of data most detections are distributed from 90° to 180° and from 270° to 330° clustering into the two groups. The source of these clusters may be local signals associated with human activities. In the last two hours of data (Figure 26), the automatic and human detections are more scattered although in the case of human detections there is a cluster from approximately 300° to 330°. This result implies that either infrasound signals from 90° to 180° stopped after the first two hours or they are difficult to detect due to high noise levels during this later time period.
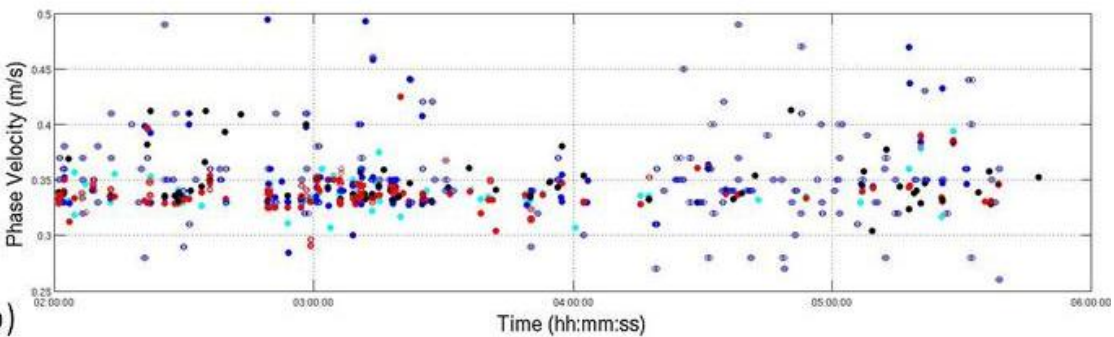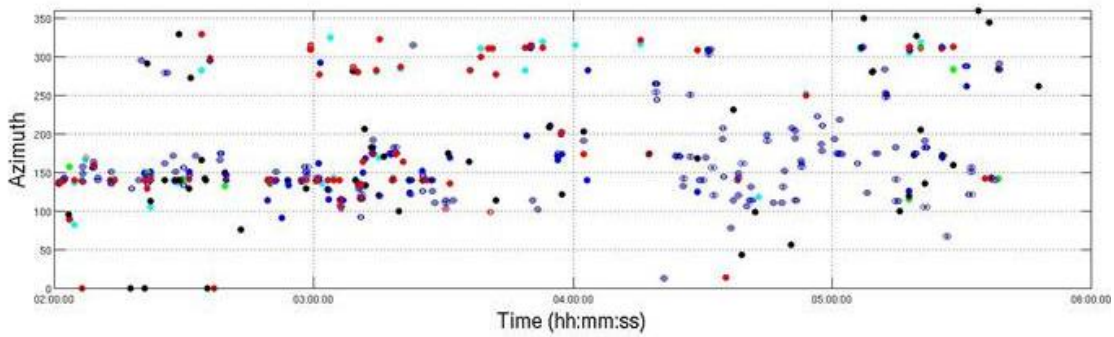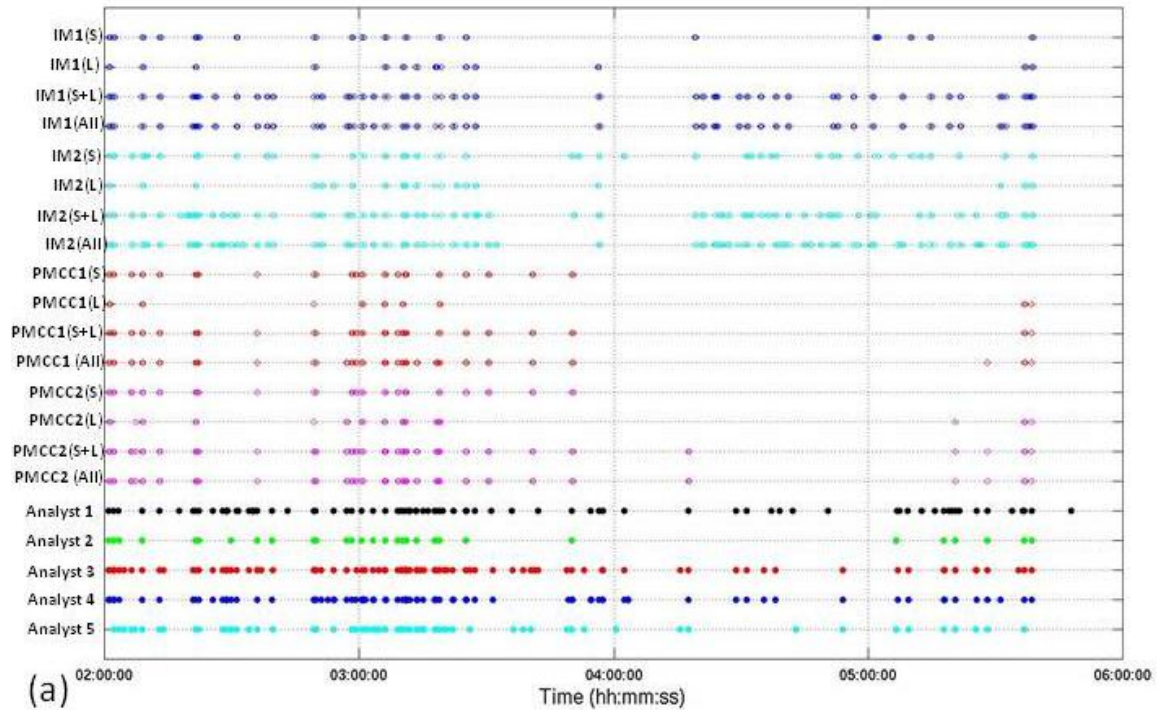
Figure 25: (a) Detection Times from the Automatic Detectors (PMCC: PMCC1 (Consistency, 0.1s) & PMCC2 (Consistency, 0.5s) and InfraMonitor: IM1 (p=0.01) & IM2 (p=0.05)) and Manual Detection by the Five Analysts; (b) The Azimuth and Phase Velocity Estimates from the Automatic Detectors (PMCC Results, Blue Open Circles and InfraMonitor Results, Red Open Circles) and the Analyst Review (Same Color Designation as in (a))

37
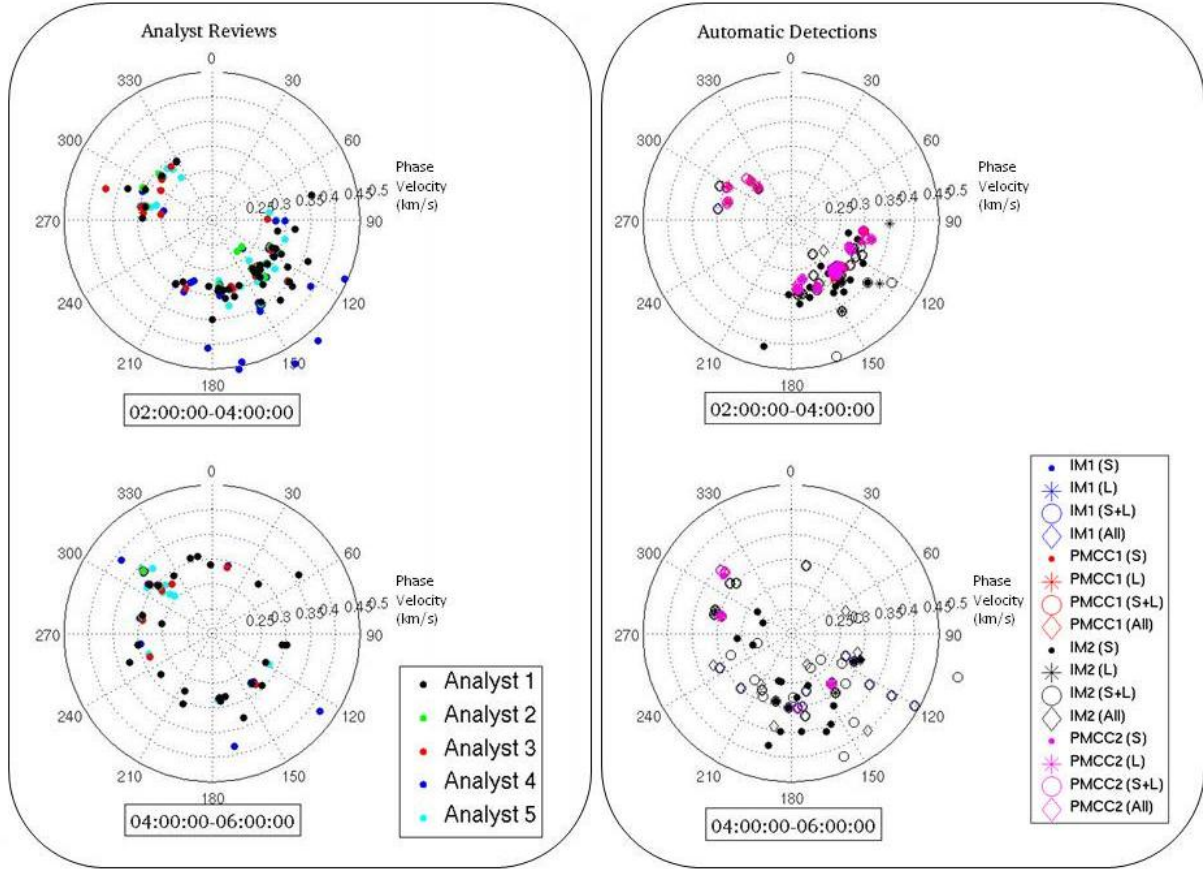
Figure 26: Polar Plot of Azimuth and Phase Velocity Estimates from the Analysts (Left) and the Automatic Detectors (Right) for the First Two Hour Data Set (Top) and the Last Two Hour Data Set (Bottom)

3.7 Estimated Receiver Operating Characteristic Curves

Garcés *et al.* (1998) demonstrated that the effects of spatially and temporally variable winds strongly influence infrasound propagation and directly affect event location. Our goal is to assess these effects on the performance of automated detectors, the first step in event location. In order to assess detector performance, Receiver Operating Characteristic (ROC) curves can be used to quantify the detection probability as well as the false alarm probability (Johnson and Dudgeon, 1993), providing a basis for optimizing the detector. This method has been applied to the performance of adaptive and conventional detectors and InfraMonitor in particular by Arrowsmith *et al*. (2009). ROC curves estimate the trade-off between the detection probability (P_D) and the false-alarm probability (P_F) for a range of detection thresholds as defined:

$$P_D = \frac{\text{number of detected signals}}{\text{total number of signals}}, \tag{9}$$

$$P_F = \frac{\text{number of noise detections}}{\text{total number of detection intervals during noise}}. \tag{10}$$

38

ROC analysis often relies on the insertion of known signals of varying size into realistic noise in order to provide a known number of signals within a collection of data. This approach is worth pursuing and should be done in the future. As an alternative, we introduce a modified data centric procedure that compares the results of the automated detectors against the detections identified by analysts. The total number of signals is defined by the analyst results in this case. In order to distinguish this approach with others, we call these curves the *Estimated* Receiver Operator Curves (EROC) to distinguish them from the more traditional approach.

There may be an implicit difference in the duration of the detected signals identified by the automatic detectors and the human analysts since each uses different criteria for picking arrival times. For example, some analyst might make several arrival picks during a 20 second window, the processing time used by both automatic detectors. There could be a number of detections in a single window estimated by the analyst while automatic detector would only identify a maximum of one detection during this time duration. In order to reduce this effect the 4-hour data set was evenly divided into consecutive 20-second window for evaluating detections in each window. Based on equations (9) and (10), a total of 720 tests were conducted in order to estimate detection and false alarm probability based on the review of all the analysts.

The EROC analysis is divided into the first two-hours of data (Fig. 27 (a)) and the last two-hours of data (Fig. 27 (b)) as result of the changing noise conditions. Depending on the reference values (analyst) used in estimating the EROC, the curve can change. For example if the analyst identifies a smaller number of signals it is possible that the EROC can be closer to the ideal detector.

During the first two-hours of data, cases using all array elements or small and large aperture arrays have higher detection probability than those using small or large aperture array only for both detectors (Fig. 27(a)). In the case of PMCC, all cases using consistency of 0.5 (PMCC2) tend to have high detection probability while the false-alarm probability is increased slightly. Especially, when using the large aperture arrays, the detection performance is significantly improved, up to twice. In the case of InfraMonitor, the detection probability when using p-value of 0.5 (IM2) is a little higher than that for a p-value of 0.1 (IM1) under low noise condition except for the case of Analyst 2. However, the false alarm rate is also increased when using the higher p-value. This result implies that InfraMonitor detects more of the signals identified by the analysts although some of these may represent correlated noise.

Under high noise conditions, both automatic detectors have low detection probability. Based on Analyst 1 and 4, InfraMonitor has slightly higher detection probability as well as a higher false-alarm probability except for the case of the large aperture arrays (Fig. 27(b)). Because PMCC produced few detections (conservative detection) in this time period, the false-alarm rate is very low. Since InfraMonitor applies the adaptive window based on background noise, the effect of the adaptive window length on these results merits further study. During the high noise levels, the analysts also reported difficulty in identifying signals with the possibility that a number of signals might have gone undetected or that some of the detections represent coherent noise across the array.
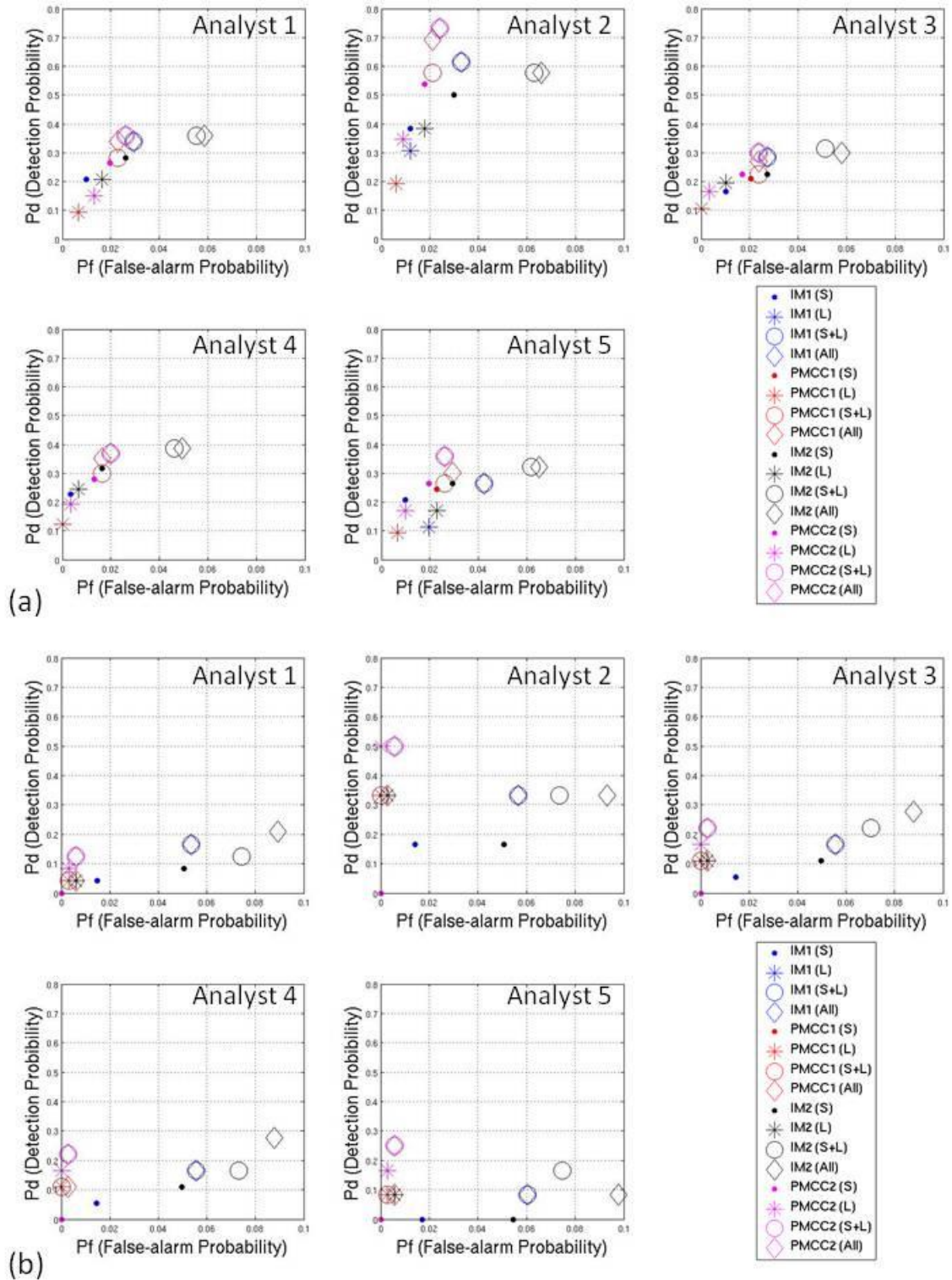
Figure 27: The Estimated Receiver Operating Characteristic (EROC) of All Automatic Detectors for the First Two-Hours (a) and the Last Two Hours of the Dataset (b)

In Figure 27, the x-axis, False-alarm Probability, is exaggerated by a factor of eight.

In order to quantify the impact of increasing wind velocity on the detection process, the average RMS amplitude and average wind velocity during 5 minutes windows for the complete data set was estimated. The average RMS amplitude, AA_{RMS} , was calculated using waveforms from all array elements as defined,

$$AA_{RMS} = \sqrt{\frac{\sum_{i=1}^{T}\left\{\left(\sum_{j=1}^{N}A^2\right)\Big/N\right\}}{\Delta T}} , \qquad (11)$$

where A is the amplitude of waveform, N is the number of infrasound array element, and T is the time and ΔT is the total time duration. These estimates are displayed in Figure 10 and document the strong correlation between RMS amplitude and wind velocity during this 4-hour time period. The amplitude and duration of the detected signals by Analyst 5 are also displayed in Figure 10, illustrating that relatively small amplitude signals can be detected under low noise conditions, while the detected signals which have small amplitudes are significantly reduced during high background noise. Using these same five-minute windows, the number of detections from both the automatic detectors and the analysts were counted and compared against the RMS amplitude and wind speed (Figure 11). Generally, the numbers of automatic and human detections are dependent on the RMS amplitude which is correlated with wind velocity. When InfraMonitor used the small and large aperture arrays together both IM1 and IM2 have a significantly higher number of detections during higher average RMS amplitudes.
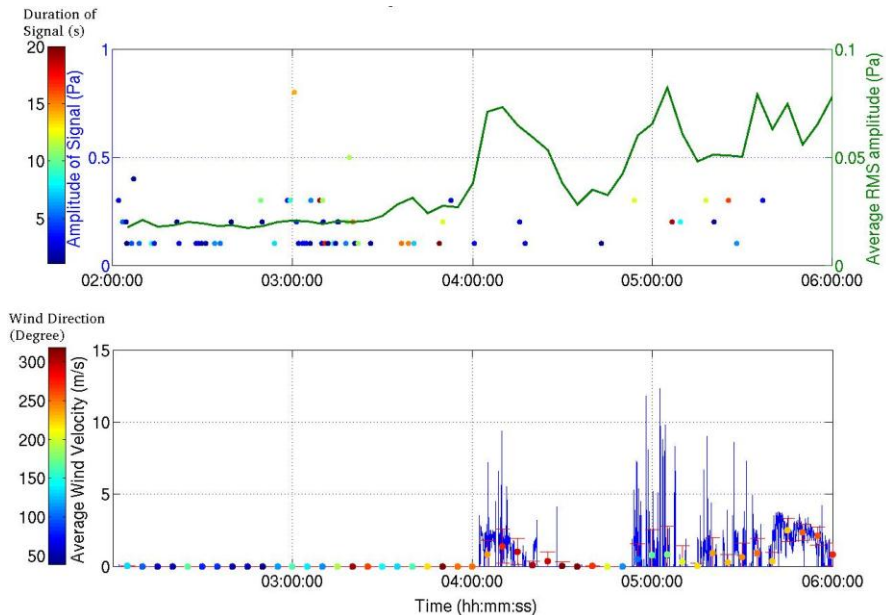
Figure 28: Top - The Average RMS Amplitude (Green Line) as a Function of Time Estimated Using All Waveforms Compared to the Amplitude (Top, Left Y-Axis) and Duration (Top, Colorbar) of the Detected Signals Identified by Analyst 5; Bottom - Wind Velocity Recorded at CHNAR During the Four Hour Time Period

As seen in Figure 28, the average wind velocity for 5-minute windows with standard deviation (red vertical bar) and average wind direction (colorbar) are plotted for comparison with amplitude data in the top plot.

Figure 30 compares the cumulative number of detections (automatic and analysts) to the average RMS amplitude and 1/(average RMS amplitude) for each 5-minute window. The number of detections in all cases significantly increases for average RMS amplitudes below 0.02 and includes most all the signals detected by the automated procedures. Most analysts identified signals under higher noise conditions although the largest number of detections identified by the analysts was identified during noise conditions with average RMS amplitudes below 0.02 as well. In the case of IM1 and IM2 with S+L and all array elements, a number of detections were identified under higher RMS noise conditions but comparison with analysts suggests that they may be false alarm. Since the 1/(average RMS amplitude) is proportional to the SNR, the higher SNR produces the largest number of detections (Figure 30 (b)) as expected.
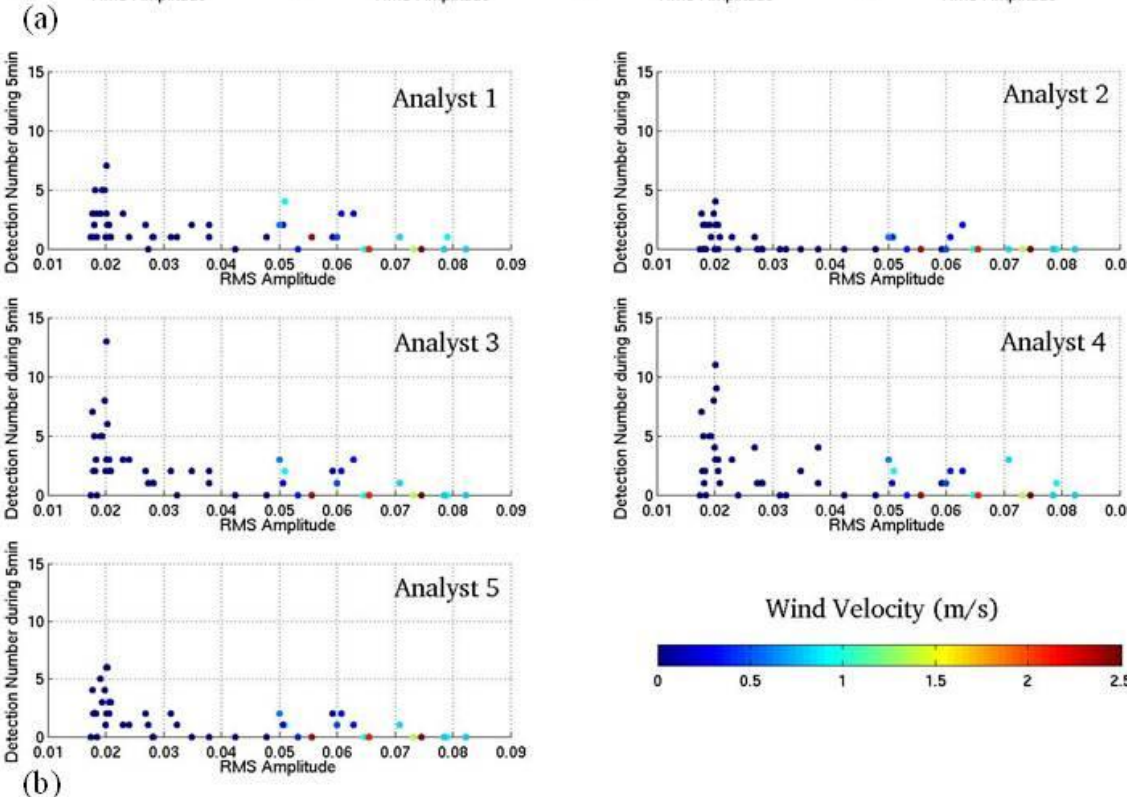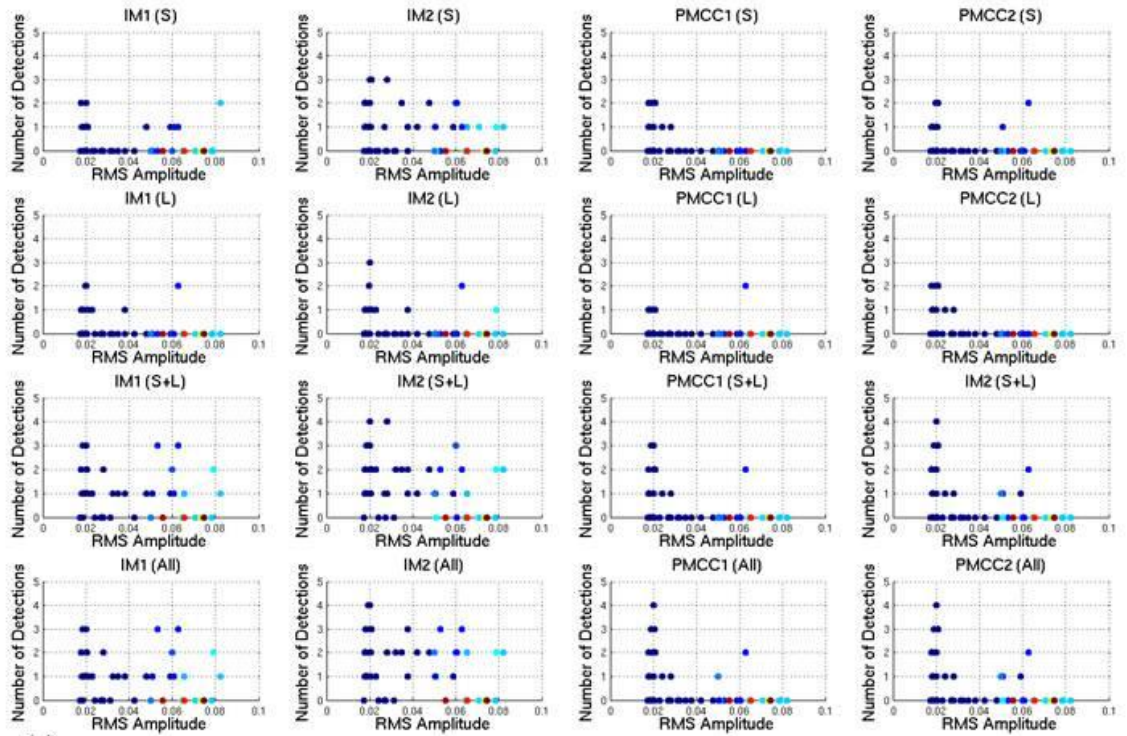
Figure 29: The Relationship Between the Number of Detections from Both the Automatic Analysis and the Analyst During 5-Minute Windows Compared to the Wind Velocity and Average RMS Amplitude During the Window
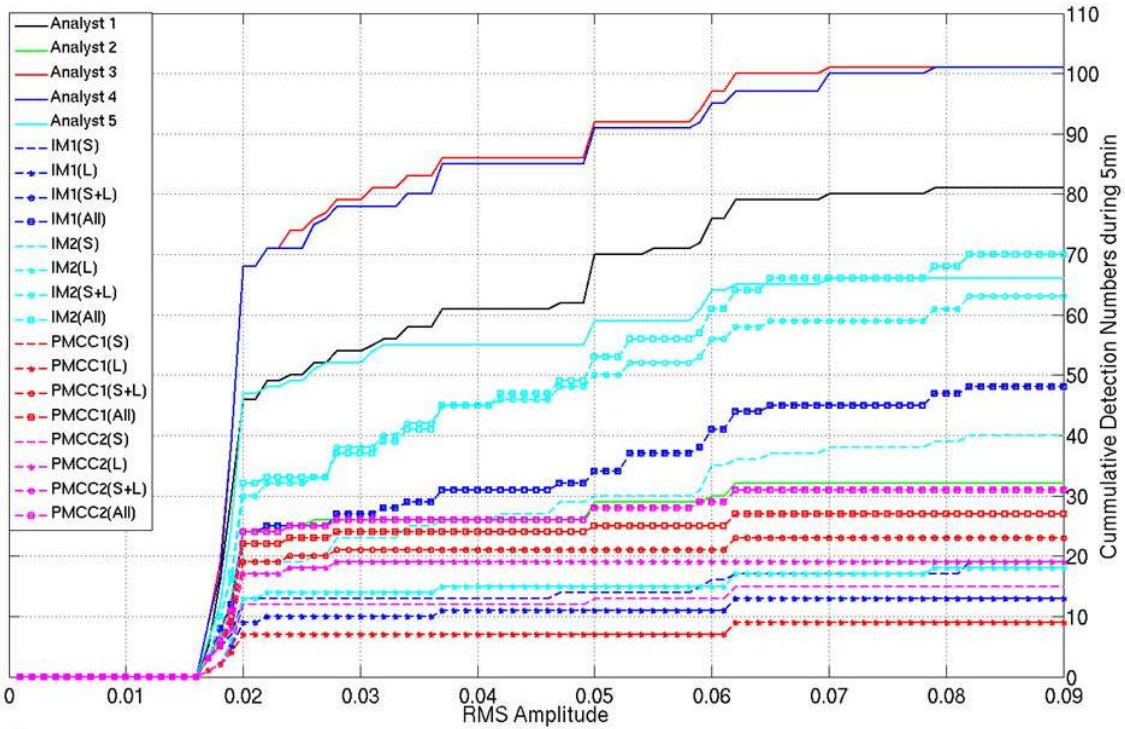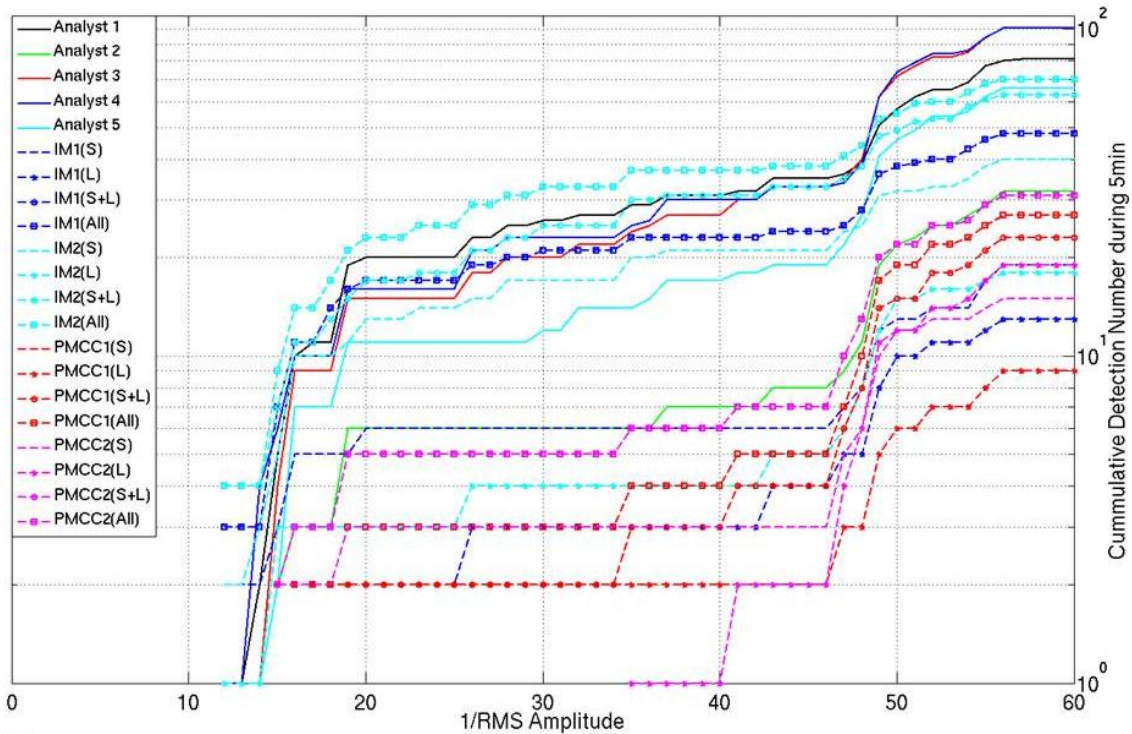
Figure 30: The Cumulative Number of Detections in All the 5 Minute Windows for Both the Automatic Detectors and the Analyst Plotted Against the Average RMS Amplitude in the Window (a) and Against 1/(Average RMS Amplitude) (B) Which Is Proportional to the Signal to Noise Ratio (SNR)

3.8 Conclusions and Discussion

In this preliminary study, a 4-hour- dataset (02:00:00-06:00:00 in UTC, 11am-3pm in local time, Julian day 002, 2012) recorded at CHNAR, located within the continent in South Korea, was used for testing the automated detectors PMCC and InfraMonitor. Automatic detections are dependent on tuning parameters specific to each procedure and background noise level. A number of the tuning parameters are common to the two approaches and reflect the character of the signals. A common window length of 20s, overlap of 50%, and filtered band from 1 to 5 Hz were used in this case since the focus was on regional infrasonic signals. In the case of PMCC, the standard deviation of 10° for azimuth and 20 m/s for phase velocity with a phase velocity range from 0.28 to 0.5 km/s were used for grouping into families. For InfraMonitor, the adaptive window of 1 hour was used and the range of phase velocity and azimuth were unconstrained. Sensitivity tests for both detectors were conducted with respect to different values of consistency (0.1s and 0.5s) for PMCC and p-value (0.01 and 0.05) for InfraMonitor.

Azimuth and phase velocity estimates for the signals identified by both the automatic detectors and analysts are consistent before 04:00:00 UTC (low noise condition), while the estimates are scattered after 04:00:00 UTC (high noise condition), with azimuthal variation increasing the most. EROC analysis is divided into the first two-hours of data and the last two-hours of data due to the changing noise conditions. During the first two-hours of data, both automated detectors using either all the array elements or the small and large aperture arrays have higher detection probability (0.3-0.75) than those using only the small or the large aperture arrays, and in the case of InfraMonitor the detection probability when using a p-value of 0.5 is twice that when using a p-value of 0.1. Both automatic detectors have low detection probability (0.1-0.5) under high noise conditions and InfraMonitor has a relatively high false-alarm probability, except for the case using large aperture arrays. This means that PMCC conservatively detects infrasound signals while InfraMonitor detects signals in a high noise environment, although these detections may be correlated noise sources. In all cases the analysts picked a higher number of signals than either automated process, including detections under the higher noise conditions.
The two detection methods both rely on signal correlation but the implementation of the two procedures are fundamentally different. InfraMonitor adapts to changing background noise conditions with the number of detections controlled by the p-value of F-statistics with increased false alarms for higher p-values (0.05) or many array elements that detect correlated local noise.

PMCC uses a cross-correlation technique with a progressive method of applying sub-networks in both time and frequency domain. By increasing the acceptable consistency value (0.5), the detection probability was increased under low noise conditions but these tests suggest that PMCC conservatively detects signals during high noise levels. Using small and large aperture arrays together as sub-network rather than using small or large aperture arrays separately for PMCC provided a higher detection probability.

Generally, the numbers of automatic and human detections are dependent on the RMS amplitude, strongly affected by wind velocity. The number of detections in all cases significantly increases for average RMS amplitudes below 0.02, which means high signal to noise ratio.

45

This study provides an initial investigation of the InfraMonitor and PMCC detectors for a four-hour time sequence at CHNAR in the Republic of Korea. This time period had approximately two hours of low wind velocity and noise and two hours of increased wind and noise. The array consists of a large (~1 km) and small aperture (< 100 m) component providing a variety of spatial scale lengths for detecting signals and separating noise. Based on the comparison of automated detections from InfraMonitor and analysts detections, the large aperture array is recommended in order to avoid the detection of local noise on the small array. For PMCC, a combination of both small and large aperture arrays for the sub-network improves the detection probability. This study should be expanded to other arrays in different noise and geographic environments including the arrays located in coastal and mountain areas. These tests need to be extended to the regional network of infrasound arrays in order to investigate how the detectors and environmental conditions impact signal association across the network and ultimately event location.

Finally a list of individual conclusions developed during this study are repeated:
1. Both automatic detectors produce a larger number of detections when either the combined small and large aperture arrays or all array elements are used relative to the cases where the small or large aperture arrays are used alone.
2. The results using both the small and large aperture arrays for detection appear to combine individual detections found using the small aperture arrays and large aperture arrays separately.
3. The number of detections estimated by InfraMonitor is almost twice that estimated by PMCC with many of the additional detections from InfraMonitor occurring in the last two-hour time period when the wind noise increases.
4. In all cases the number of analyst detections are significantly higher than those determined by either automated detector.
5. In most all cases, the picks by the analysts included all the events identified by the two automatic detectors.
6. In the case of the last two hours of data where the noise levels are higher, there are fewer automated detections and a reduced number of detections identified by the analysts.
7. During the first two-hours of data, cases using all array elements or small and large aperture arrays have higher detection probability than those using the small or large aperture array only for both detectors.
8. The false alarm rate is increased when using the higher p-value.
9. Generally, the number of automatic and human detections are dependent on the RMS amplitude which is correlated with wind velocity
10. The number of detections in all cases significantly increases for average RMS amplitudes below 0.02 and includes most all the signals detected by the automated procedures.

4. A COMPARATIVE STUDY OF AUTOMATIC INFRASOUND DETECTION AND LOCATION OF SOURCES IN KOREA AND WESTERN US UTILIZING REGIONAL ARRAYS

4.1 Motivation

The development of an automated infrasound event bulletin provides a means for quantifying the distribution of sources in time and space. Such a bulletin is the first step in not only studying the sources but also providing data that can be used to document the time varying nature of the atmosphere, especially in the case of repeated sources. Automated events can be used to trigger more detailed analyst review of events of particular interest.

Production of such a bulletin relies on data from stations distributed over a spatial area that is to be characterized. The focus of this report is on problems of regional scale where the receiving stations are spaced on the order of hundreds of kilometers spanning a total distance of one to two thousand kilometers. This scale is much smaller than say a global array of sensors as in the International Monitoring System. Although individual stations could consist of single gauges it is advantageous in infrasound to deploy small arrays at each site so that array processing techniques can be applied for signal detection and thus wavefield parameters such as backazimuth and phase velocity or celerity can be used in the location process.

The process of producing a bulletin relies first on signal detection followed by association of detections at different locations and finally the formal location procedure. This section of the final report builds upon the two previous sections where the details of the detection process have been discussed and interpreted in terms of time varying environmental conditions. Here we focus on the utilization of automated detections in the production of an infrasound bulletin in two regional settings, one in the western US and the second on the Korean Peninsula. The automated procedure we will illustrate has been developed in parallel with this project. InfraMonitor (Arrowsmith and Whitaker, 2008) utilizes the Bayesian Infrasonic Source Location (BISL) as described by Modrak *et al*. (2010).

4.2 Detection

Signal detection is the first step towards the production of an infrasound bulletin. Due to temporal variations in atmospheric conditions and thus noise, detecting infrasonic signals is more complex than detecting seismic signals. High winds lead to infrasonic noise on sensors deployed along the ground at the boundary layer with the atmosphere and thus can mask signals at single stations. If the noise has low spatial correlation then its effects can be mitigated by an array of stations spaced beyond the noise correlation length. Therefore, the seasonal variation of weather conditions must be considered in the detection. Seasonal variations in the atmosphere also have a major impact on the wave propagation and thus impact travel-times and wave characteristics and thus must be understood for both optimum detection as well as association and location. The relationship of environmental conditions and detector performance is discussed in some detail in earlier sections of this final report.

Additionally, some parts of the noise field may be coherent as they are generated by man-made sources such as trains or heavy industry. If the correlated noise is declared as a signal detection, it can increase the false alarm rate. In order to obtain the optimum signal detection for subsequent processing including the location of impulsive events, distinguishing the signal from the correlated noise is necessary. Based on the assumption of uncorrelated noise, algorithms such as the progressive multi-channel correlation (PMCC) (Cansi, 1995), InfraTool in MatSeis-1.7 (Hart and Young, 2002) or InfraMonitor (Arrowsmith and Whitaker, 2008) can be used for detection. Recently, Walker *et al*. (2011) used the method of reverse time migration (RTM) to detect and locate sources of infrasound. In section 3 of this report the details of PMCC and InfraMonitor are discussed and illustrated on a common set of regional infrasonic array data. Here, we briefly describe the two detectors for completeness.

PMCC is based on progressive processing of data recorded by sub-arrays from a larger array using time domain cross-correlation estimates between individual stations (Cansi, 1995). This method estimates trace velocities and azimuths starting with sub-arrays and then increasing the network aperture. When the consistency defined as the mean quadratic residual of the closure relations is below a threshold, detection is declared (Cansi and Le Pichon, 2009). Then, the procedure determines the number of sensors in the final sub-network, the associated consistency, and the detected wave velocities and azimuths by progressively increasing the network aperture for precise propagation parameters.

InfraTool calculates an azimuth, trace velocity, correlation coefficient, and the conventional F-statistic for each segment using multiple overlapping windows that move through the data volume. InfraMonitor (Arrowsmith and Whitaker, 2008) utilizes the F-statistic (Blandford, 1974) and cross-correlation techniques as the detection method. Automatic detection is based on the F-statistic calculated as the power on the beam from the array divided by the average over all channels of the power of the difference between the beam and the individual array channels. The standard F detector can be modified so that it is adaptive in time capturing changing noise characteristics with new estimates of C defined as the scaling factor between the theoretical and empirical central F-distribution made for subsequent adaptive windows. The difference between the conventional F-statistic and the modified F-statistic as proposed by Arrowsmith *et al.* (2009) is consideration of the temporal noise level through the use of an adaptive window. An adaptive modification can distinguish the signal from correlated noise, with the adaptation focusing on temporal variations in ambient noise rather than assuming that background noise is constant, as is done in InfraTool.

4.3 Location Procedure

Based on analysis of detection times, azimuth and phase velocities from the multiple arrays one can associate the signals and estimate the source location. Arrowsmith *et al.* (2007) pointed out that current atmospheric models for event location cannot capture the variation of weather conditions due to spatial and temporal variations in the atmosphere. Therefore, an event location procedure must be developed that takes the inability to quantify these changes into account (Arrowsmith *et al*., 2010). There are several approaches to determine the infrasound event location. Le Pichon *et al*. (2008) used a constant atmospheric velocity model and a least squares

method in Central Europe. Arrowsmith *et al*. (2008a) applied a grid search method using group velocity ranges for obtaining the region rather than point location in the western United States. Modrak *et al*. (2010) further developed their procedure called the Bayesian Infrasonic Source Location (BISL), which accounts for unknown source-to-array path effects by formulating infrasonic group velocity with a random component, for estimation of location and associated credibility regions in the current version of InfraMonitor. The BISL algorithm uses the likelihood function for backazimuth and traveltime constraints to assign a combined likelihood value to the location parameters when the predicted group velocities at each array are similar (Modrak *et al*., 2010).

4.4 Two Regional Infrasound Arrays for Comparison

This location study, as noted earlier, focuses on the detection and location of regional infrasonic signals with propagation distances focused on distances no greater than 2000 km and primarily less than 1000 km. It is comparative in that two different regional networks are analyzed. The first is in and around the Korean Peninsula with six seismo-acoustic arrays supplemented by two near-by IMS arrays. The second regional network extends from Nevada through Utah with a maximum of 12 infrasound arrays. These arrays were deployed for a variety of purposes from monitoring explosive activities in the west to a search for infrasound from earthquakes.

Infrasound Arrays In and Around the Korean Peninsula

The Korea Institute of Geoscience and Mineral Resources (KIGAM) and Southern Methodist University (SMU) cooperatively operate the seismo-acoustic arrays, BRDAR, CHNAR, KMPAR, KSGAR, TJIAR, and YPDAR in the Republic of Korea as shown in Figure 1. KMPAR has a sampling rate of 100 sample/s while the other arrays are sampled at 40 samples/s. These arrays are typically multi-scale with the largest offsets of approximately 1000 m consisting of both acoustc and seismic sensors, an imbedded secondary infrasound array with an aperture of 50 to 100 m, and finally a 50 m offset infrasound gauge from each of the 1000 m offsets. Sections 1 and 2 of this report detail the arrays and the effect of array geometry on signal detection. Two International Monitoring System (IMS) stations, operated by the Comprehensive Nuclear-Test -Ban Treaty Organization (CTBTO), I30JP in Japan and I45RU in Russia supplement the dataset to overcome the azimuthal bias of the arrays' distribution. These arrays are sampled at 20 samples/s. All arrays have weather channels measuring wind velocity, wind azimuth, and temperature, except for KMPAR.
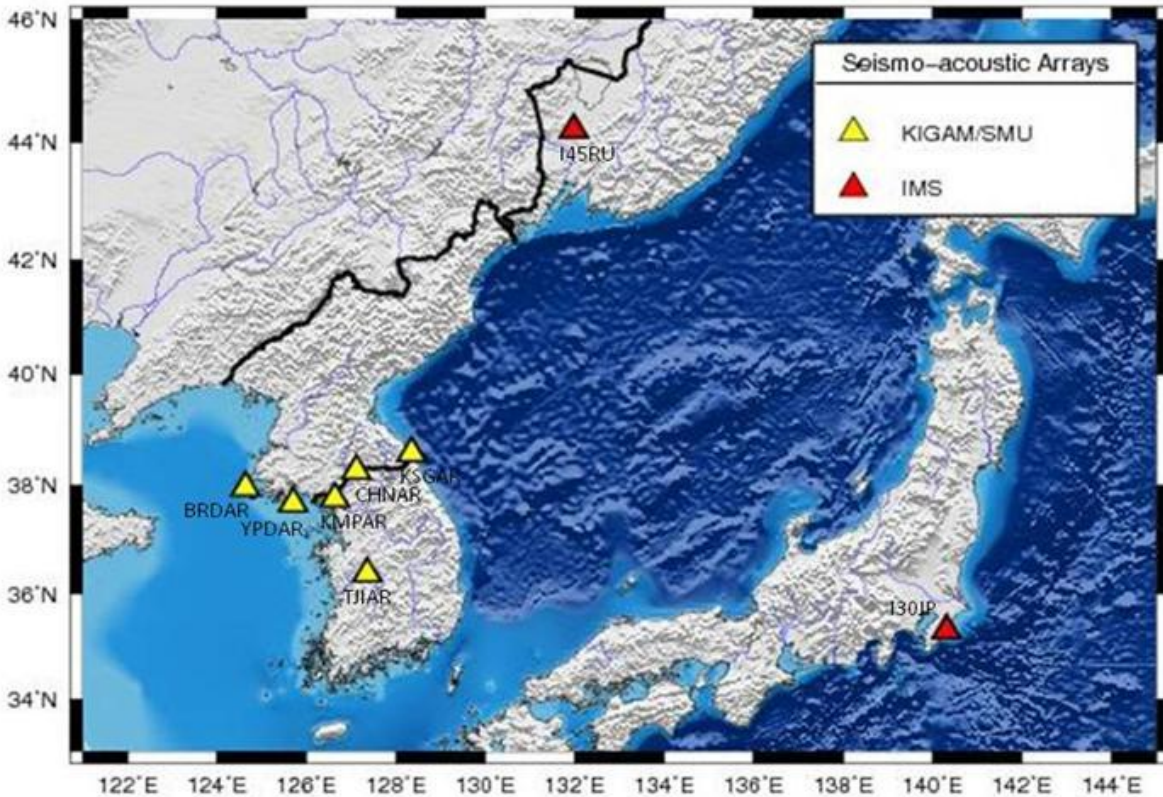
Figure 31: The Location of Seismo-Acoustic Arrays Near and in Korea Used in This Comparative Study of Automated Signal Detection and Event Location

Infrasound Arrays and Military/Mining Activity Near and in Utah and Nevada

The second data set used in this comparative study is from a regional infrasound network located near and in Utah (Fig. 2). The Utah network was deployed as part of a collaboration between the University of Utah, Southern Methodist University, and Los Alamos National Laboratory with a primary focus on assessing infrasound generation by shallow earthquakes (Arrowsmith *et al.* 2012). The infrasound network comprises twelve four-element arrays, with apertures of about 100 m, with infrasound gauges fitted with porous hoses for wind noise reduction (Arrowsmith *et al.*, 2008a). Data sampling is 100 per seconds. Infrasound arrays, DNIAR, FNIAR, and NVIAR are currently operated by SMU focusing on man-made sources in Nevada, including a repeated source where explosives are regularly destroyed, called New Bomb. These arrays are sampled at 100 samples/s and are comprised of four low-frequency microphones attached to microporous hoses for wind noise reduction (Walker and Hedlin, 2010). The data are sampled at 100 Hz. Locations of Bingham canyon mines, Dugway Testing Ground (DTG), New Bomb (NB), and Utah Test and Training Range (UTTR) that generate infrasound are plotted along with the network of regional infrasound arrays used in this study in Figure 2. The UTTR is the largest overland continuous block of supersonic-authorized restricted airspace and frequently is used to dispose of explosive ordinance in the western U.S., and the DTG supports military training exercises (Walker *et al.*, 2011). These repeated sources can be used to ground truth information for improving the automatic detection and location processing assuming that infrasound signals are regularly recorded from these sources.
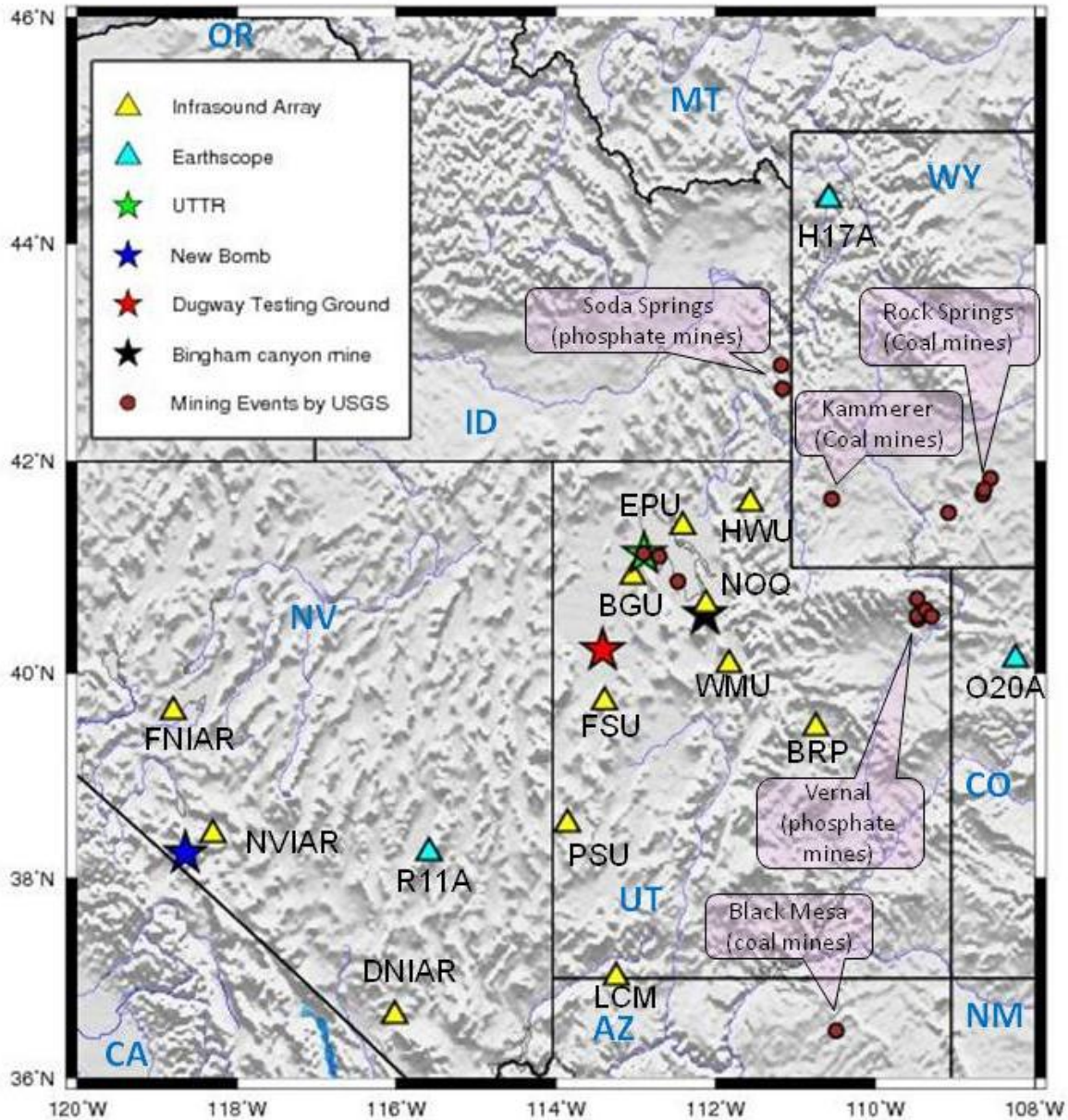
Figure 32: The Location of Regional Infrasound Arrays and Earthscope Infrasound Arrays with the Sites of the Utah Test and Training Range (UTTR), New Bomb, Dugway Testing Ground, Bingham Canyon Mines, and Mining Events (May 2011 - March 2012) Published by the USGS in the Study Area

The detection and analysis of the ground truth sources in this region provide the opportunity to study the time varying nature of the atmosphere, in particular the effects of seasonal variations in the atmosphere that will impact the resulting bulletins developed in this analysis. Although the bulletins reported here have not been extensively investigated for these effects they provide a basis for such further studies. Figure 3 illustrates a record section for a winter detonation at NB and a summer detonation at UTTR and illustrates the important effect of the atmosphere. The NB data illustrates a variety of arrivals with evidence of a tropospheric arrival to at least 400 km and

a stratospheric arrival that departs from a celerity of 300 m/s. The UTTR also shows a number of arrivals but there are stations arrays such as WMU, LCM and DNIAR where no arrivals are obvious as a result of the direction of atmospheric winds at the time of the detonation.
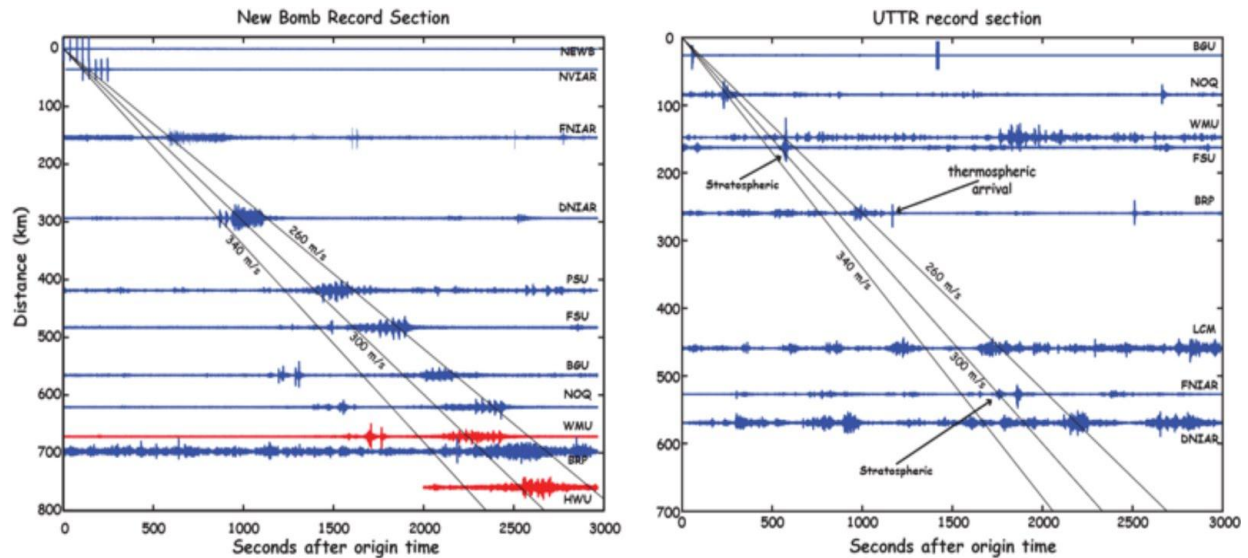
Figure 33: New Bomb (Left) and UTTR Record Sections Across the 700 Km Aperture Network (Figure Courtesy of Petru Negraru, SMU)

.

In Figure 33, the red waveforms have the position shifted by +50 km for better display. Lines corresponding to 340, 300 and 260 m/s celerity are also plotted.

An additional use of the automated bulletins will be to assess the degree to which mining explosions are detected and located by infrasound arrays (Arrowsmith *et al.* 2008b). A total of 16 mining events occurred in study area from May 2011 to March 2012 and were identified by the United States Geological Survey (USGS) (Figure 32). The local Richter magnitudes (M_L) range are from 1.9 to 3.1, and the origin times and locations of events are summarized in Table 3. These mining events are related with several different mining regions in Arizona, Idaho, Utah, and Wyoming based on the analysis of activity of routine mining seismic-event from May 1997 to March 2000 by the USGS. Large-scale coal-mines are located on the geomorphic feature named Black Mesa, south of Keyenta in Arizona (Keystone, 1997). Soda Springs in Idaho has explosions related to phosphate mining (USGS's mine blasts catalog) while the area also experiences a high level of seismicity that is unrelated to mining (Smith and Arabasz, 1991). The Bingham Canyon open-pit copper mine is near Copperton in Utah (Richins, 1979). Additional explosions associated with phosphate mining occur near Vernal in Utah (USGS's mine blasts catalog). There are two additional coal-mine regions, the Hams Fork Coalfield near Kammerer and the Green River Basin near Rock Springs, in Wyoming (Keystone, 1997).

Table 3: Origin Time and Location of Mining Events Published by USGS from May 2011 to March 2012

Region of Event	Date yyyy/mm/dd)	Origin time (hh:mm:ss)	Latitude (°)	Longitude (°)	Magnitude (M$_L$)
Vernal, UT	2011/07/14	23:28:13.0	40.512	-109.468	2.8
Vernal, UT	2011/08/04/	23:21:00.3	40.544	-109.468	3.0
UT	2011/09/12	20:28:45.5	41.442	-112.704	2.0
UT	2011/09/15	22:01:48.2	40.708	-109.471	2.9
Vernal, UT	2011/09/29	21:54:04.8	40.601	-109.362	3.0
UT	2011/11/02	17:13:20.0	41.137	-112.901	1.9
UT	2011/11/02	18:41:57.1	40.872	-112.472	3.1
Rock Springs, WY	2011/11/23	22:41:38.8	41.692	-108.646	2.7
Rock Springs, WY	2011/12/08	21:49:42.5	41.845	-108.551	2.5
Vernal, UT	2011/12/08	23:01:51.9	40.543	-109.292	2.6
Rock Springs, WY	2011/12/15	22:04:21.4	41.521	-109.078	2.6
Kemmerer, WY	2012/02/09	17:01:31.1	41.648	-110.542	2.0
Soda Springs, ID	2012/02/28	20:42:02.1	42.676	-111.160	3.1
Soda Springs, ID	2012/03/09	01:08:34.8	42.890	-111.174	2.8
Rock Springs, WY	2012/03/22	21:52:23.3	41.737	-108.632	2.9
Kayenta, AZ	2012/03/30	19:48:12.4	36.474	-110.488	2.6

4.5 Data Processing

Depending on signals of interest, parameters should be tuned well for detection, association, and location processing. The parameters used in InfraMonitor for automatic processing are summarized in Table 4 and are based on the analysis of regional signals discussed in sections 1 and 2 of this report. The same parameters were used in processing for both Korea and Utah data taking into account different aperture size of arrays, 1 km for Korean arrays and 100 m for Utah arrays.

The adaptive *F*-detector parameters that were used for detection focused on the 1-5 Hz frequency band typically the band with the best signal to noise ratio for regional signals. The time duration of the detector window was set at 30 s although additional work needs to be done to assess the impact of shorter windows, particularly in the association process. Window overlap was set at 50%. A number of adaptive window tests were undertaken and reported in section 1 of this report. This work led to the adoption of a 1 hour adaptive window in order to take into account the changing noise environment observed at the arrays. Finally in order to keep false alarms to a minimum a p-value of 0.01 was chosen as illustrated in Chapter 3 of this report.
Both detection association across the network and estimation of the location by the grid search process implemented in BISL relies on *a priori* estimates of the azimuthal variation and the range of acceptable group velocities. Considering to the wind effect to infrasound wave

propagation, the range of group velocities is to 0.28 - 0.38 km/s and azimuthal deviation is 8 °. Further analysis of ground truth data can help better constrain these values and incorporate models that change as function of time as demonstrated by the empirical work of Che *et al.* (2011). This initial work does not take these effects into account and thus the resulting associations are expected to be reduced and the location errors are expected to be large.

The input parameters for location are also included. The vector length in location means the number of origin-times and group velocities to search over. We assume that the plane is a spherical Earth, so value of flat earth in location is zero. The detail description of all parameters is summarized in the manual of InfraMonitor (Arrowsmith, 2012). These parameters are tuned for long duration signals generated from long distance source considering to the distance from two IMS stations for Korea data, so window length is large (30 s). In the case of Utah, there are several high frequency signals with short duration. Therefore, many short period signals within the designated time window for processing can be regarded as only one event even though several shots are existence. Arrowsmith *et al.* (2008a) have processed Utah data for a period of ~1 month (07/24/07-08/28/07) using window length of 10 s. Tuning the parameters of time window has to be adjusted to characteristics of signals recorded at local site.

Table 4: Parameters Used for Processing of Detection, Association and Location Using InfraMonitor for Korea and Western US Data

	Frequency band (Hz)	1-5
	Time window (s)	30
Detection	Overlap (%)	50
	Adaptive window (hr)	1
	p-value	0.01
	Azimuthal deviation	8
	Min. group velocity (m/s)	0.28
Association	Max. group velocity (m/s)	0.38
	Picking error (s)	20
	Azimuth standard deviation (°)	8
	Arrival time standard deviation (s)	100
Location	Vector length	1
	Flat earth	0

4.6 Detection, Association and Location Examples for Illustration

Several examples of detection and location using InfraMonitor are illustrated in this section. Unlike seismic events that propagated through the solid Earth, infrasound travels in the atmosphere where short term effects such as weather and seasonal variations result in changes in both propagation path and noise with respect to time and location. Here, we briefly summarize analyses of detection and weather conditions of Korea using the adaptive F-detector that accounts for background noise with time. The second example demonstrates the importance of array distribution in event location and in particular associated error estimates in the locations.

The array distribution in the Republic of Korea is almost linear across the demilitarized zone (DMZ), except for TJIAR located in the center of Peninsula. This distribution of arrays can

determine the event location using azimuth and phase velocity in the case of sources to the north or south, since each array produces backazimuth estimates. Sources from the east or west are more problematic as crossing angles from backazimuth estimates are small. In order to address this issue we have investigated the contributions of two IMS stations, I30JP and I45RU to the location process even though these sites are farther from the peninsula. The second example in this section illustrates this point for an infrasound event that occurred in Russia. The third and fourth examples illustrate the automatic detection and location using current Korea and Utah data, respectively. These examples illustrate the basis for producing the infrasound event bulletin.

Detection and Weather Analysis of Korea Data
The relationship between detections and local environmental conditions are discussed in detail in sections 1 and 2 of this report. Here we illustrate some of these effects briefly using, a one-week dataset (Julian day: 046-052, 2012) from BRD00/10/20/30/40, CHN00/10/20/30, KMP01/11/12/13, KSG00/10/20/30, TJI10/11/12/13, and YPD00/10/20/30/40 (Figure 1). The large aperture arrays were used to avoid locally correlated noise at the smaller scale offsets. A summary of the resulting detections (correlation, azimuth, and number of detections with respect to azimuth) over the one-week time period is reproduced in Figure 4. In cases of BRD and YPD, most of the detections are from the northwest with more detections at YPD.
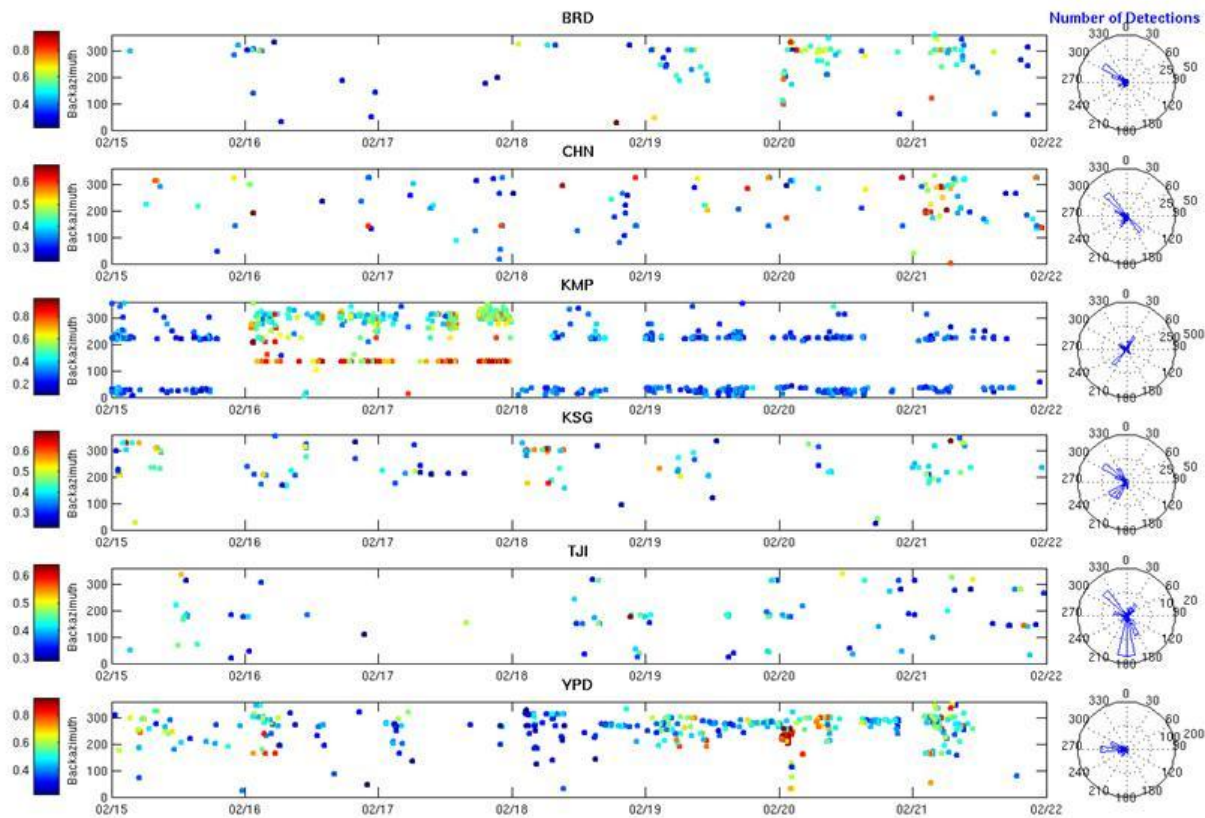

Figure 34: Detection Results Including Correlation Value (Color Bar), Azimuth (Y-Axis), and the Number of Detections with Respect to Azimuth (Rose Diagram) for BRD, CHN, KMP, KSG, TJI, and YPD from the One-Week Data Set (Julian Day: 046-052, 2012)

Many detections with high correlation were found at KMP and are associated with noise sources. The continental arrays, CHN and TJI, and the mountain-surrounded array, KSG, have a relatively smaller number of detections distributed across a number of azimuths. The temporal trend in the detections follows a diurnal pattern with many high correlation signals during local daytime. This diurnal change of detections can be compared to weather conditions (wind velocity and azimuth, and temperature) and the adaptive C-value used in the F-detector with the1-hour adaptive window (Figure 5). KMP has no weather measurement and the temperature measurement of BRD is currently not operating correctly.

The C-values estimated follow the diurnal changes already noted. There is some hint that arrays near the ocean produce greater variation in C-values as well as being associated with higher wind velocities that during this time period are from the northwest. Where either the continent or mountains surround the arrays there are more moderate temporal variations in the estimated C-values. This analysis suggests that array dependent noise environments can impact C-value estimates and need to be taken into account, possibly including longer period seasonal variations. This result suggests that assessing local environmental effects and tuning detectors at individual arrays may be necessary for optimum detection across a broad region with multiple arrays.
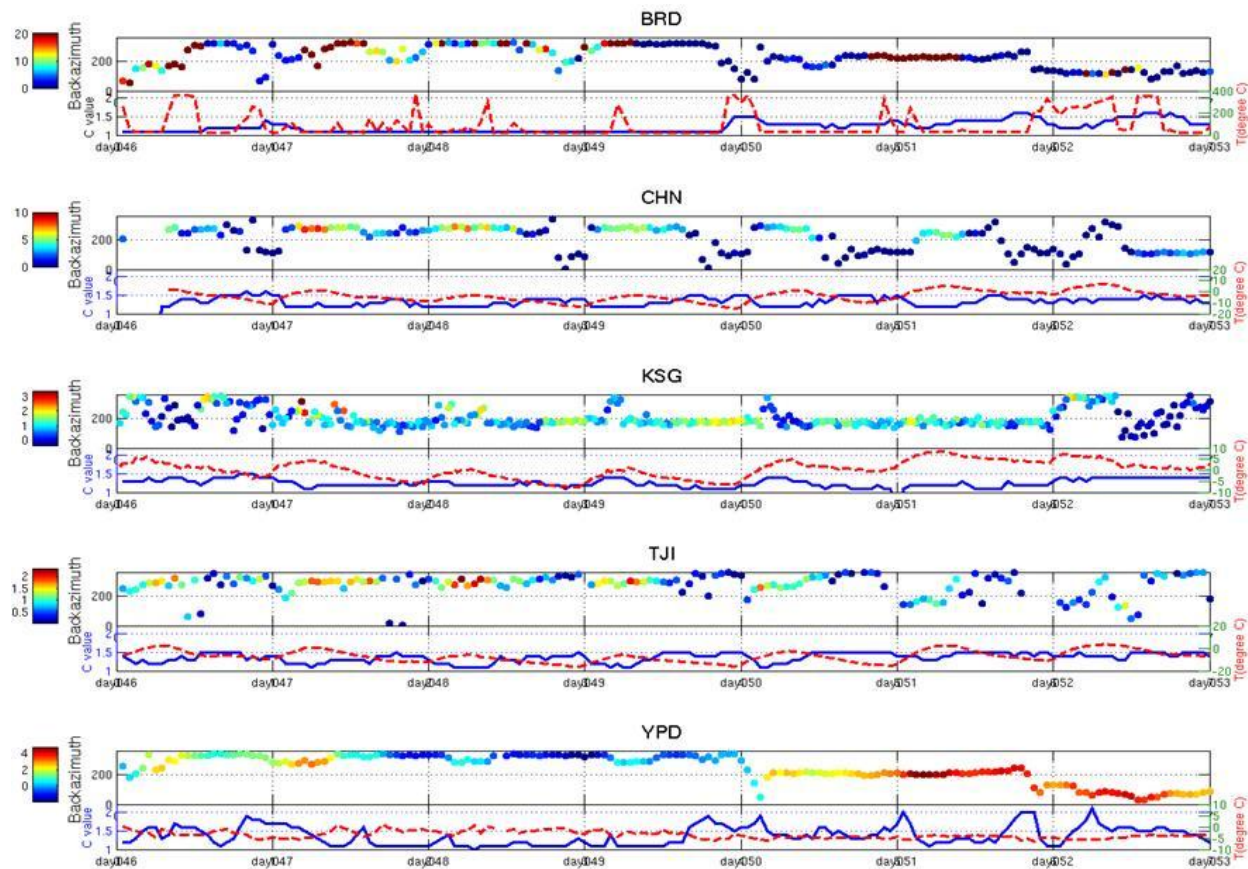

Figure 35: The Weather Conditions Including Wind Velocity (Color Bar), Azimuth (Y-Axis), and Temperature (Red Line) from the Five Arrays (BRD, CHN, KSG, TJI and YPD) with C-Value Variations (Blue Line), Estimated by InfraMonitor Using a 1-Hour Adaptive Window

Effect of Station Distribution on Location Estimates - Infrasound Event from Russia
In this section, we document a location example that illustrates the importance of station distribution on both the location and its accompanying error estimates. A 2-hour dataset (12:00:00-14:00:00 in UTC, Julian day 059, 2012) from the Korean seismo-acoustic arrays, BRD, CHN, KMP, KSG, TJI, and YPD supplemented by data from the two IMS stations, I30JP in Japan and I45RU in Russia were used to produce detections followed by association and location (Figure 6). Two additional arrays ULD, located on an island in the East sea of Korea, and YAG, located between CHN and KSG, operated by KIGAM, were added bringing the total number of arrays used for location purposes to 10. Strong signals (between 9-11 pm local time) were observed at all arrays except I45U and were automatically detected by InfraMonitor using the detection parameters discussed earlier and summarized in Table 4. This source is similar to some events that occurred during the summer of 2011 reported by Arrowsmith (personal communication, 2012) and may represent a repeated source of large infrasound signals in the region. The lack of a clear signal at I45RU might be because this station is in the zone of silence (Negraru *et al.*, 2010).
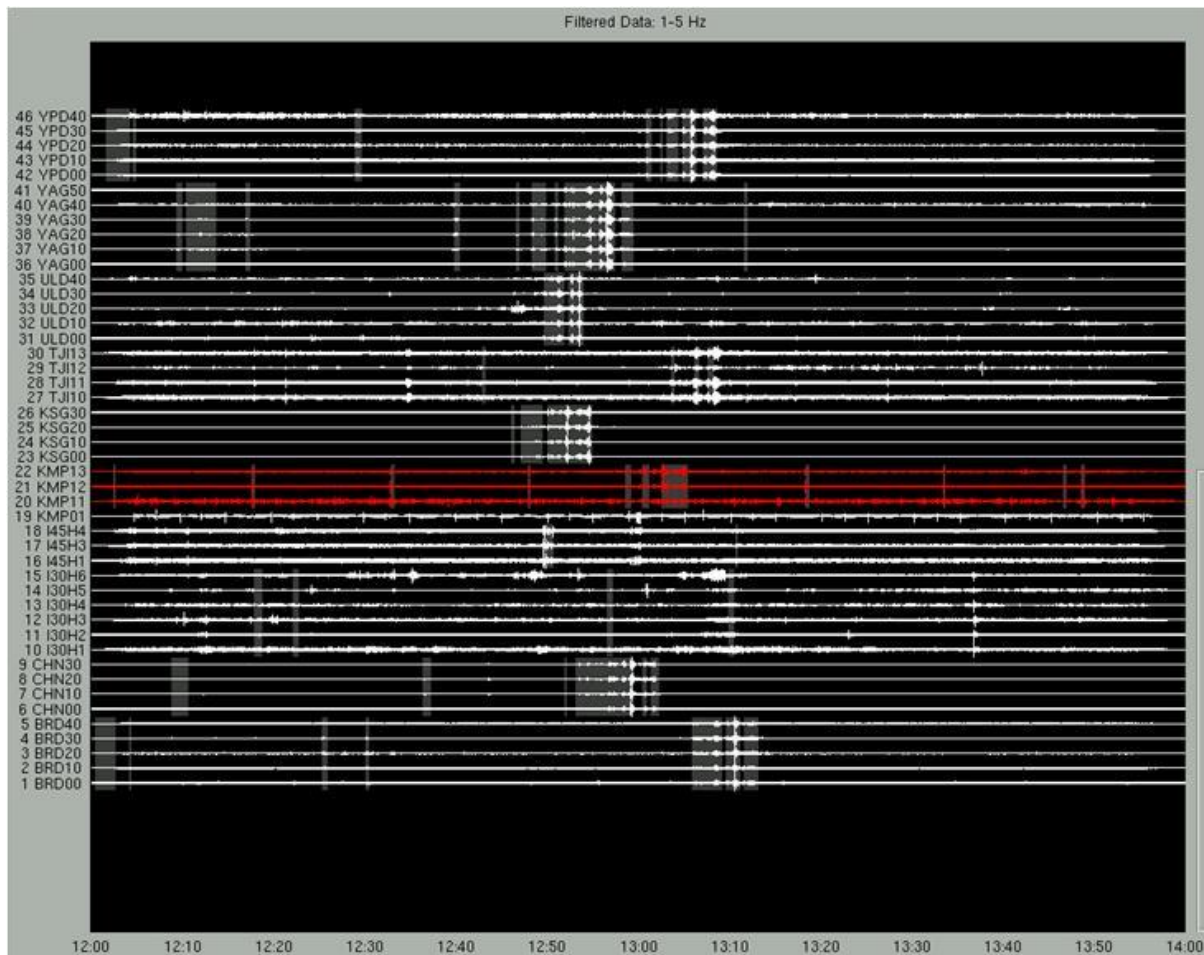
Figure 36: The Filtered (1-5 Hz) Waveforms from the Seismo-Acoustic Arrays, BRD, CHN, KMP, KSG, TJI, ULD, YAG, and YPD in South Korea Used in Detection, Association, and Location Processing of InfraMonitor; Additionally, the Waveforms Recorded at Two IMS Stations, I30JP and I45RU, Are Plotted

In Figure 36, the gray intervals indicate the detected signals and red-colored waveforms represent the selected three channels in KMPAR

An example detection result at ULD is illustrated in Figure 7 with a high F-statistic and correlation value accompanied by a consistent azimuth and phase velocity. As noted earlier, group velocity ranges from 0.28 to 0.38 km/s were used in the event location procedure. Two location estimates are presented in Figure 8, the first using all arrays except the IMS stations and the second adding in the IMS arrays although the only one that contributed was I30JP. In the location example using I30JP, the uncertainty range is significantly reduced as the backazimtuh is nearly at right angles to those of the other stations. This result illustrates the importance of good azimuthal array coverage for estimating event location.
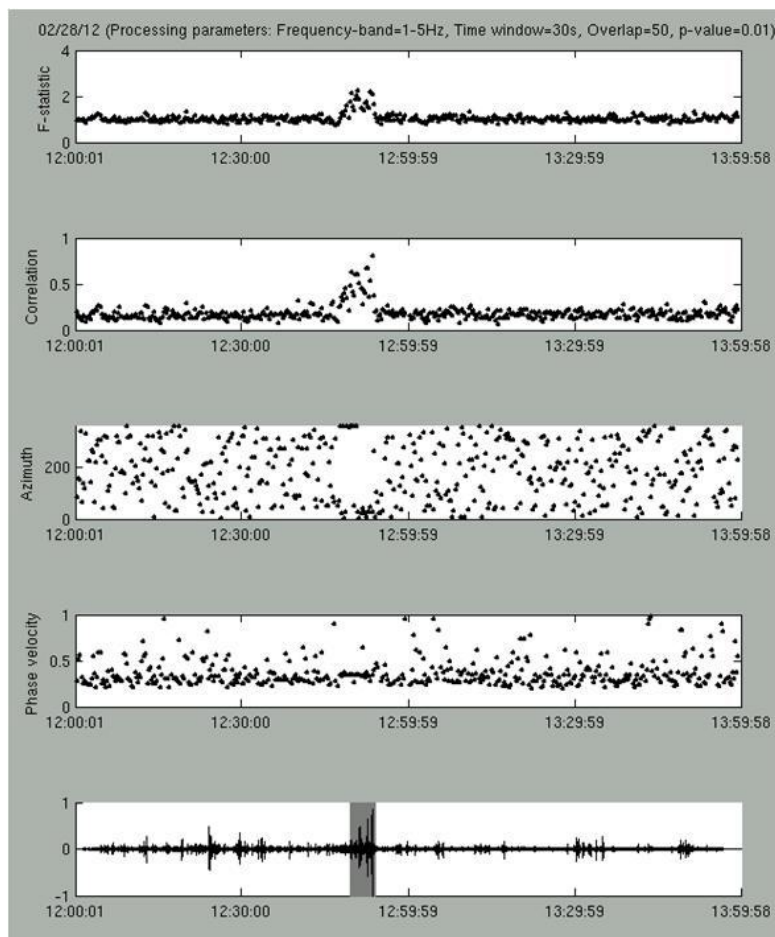
Figure 37: Example Detection Results (F-Statistic, Correlation Value, Azimuth, and Phase Velocity) from ULD Filtered 1- 5 Hz. Waveform Is from ULD10
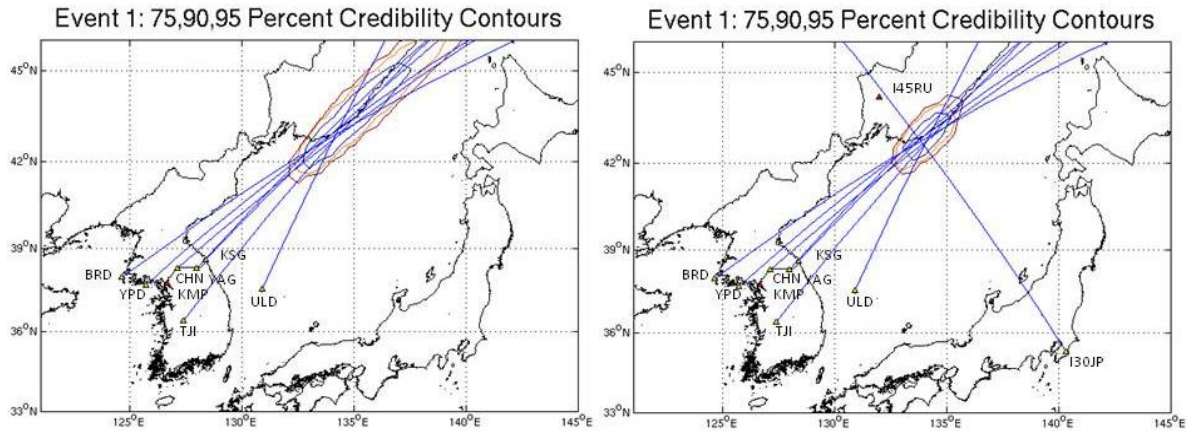
Figure 38: Comparison of the Two Location Estimates Using Multiple-Arrays, the One to the Left Does Not Including I30JP and the Location to the Right Includes This Station with a Backazimuth Nearly Perpendicular to the Other Station Estimates

In Figure 38, the yellow and red triangles indicate the arrays used and the blue line from each array represents the azimuth estimate from each. The three contours indicate the 75, 90, and 95 percent credibility contours for each event location.

4.7 Automatic Detection and Location Using Data from Korea

A four-month-dataset (01/01/2012-05/01/2012) from the Korean seismo-acoustic arrays, BRD, CHN, I30JP, I45RU, KMP, KSG, TJI, and YPD, were used to produce automatic detections (Fig. 9). The large aperture arrays (~1 km) were used for processing. Detection results from I30JP and I45RU are shown from the middle of March, when the data from the two IMS arrays are made available. Currently, KMP has some electronic noise as illustrated by the detections with high correlation and a consistent azimuth (≈140°). BRD, TJI, and YPD have many detections from the northwest, north, and, west, respectively. BRD and YPD are affected by the ocean environment and possibly local human activity. Similarly, human activity may affect TJI, which is located in the city of Taejon.

Figure 39: Automatic Detection Results – Correlation Value (Color Bar), Azimuth (Y-Axis), Number of Detections with Respect to Azimuth (Rose Diagrams) for BRD, CHN, KMP, KSG, I30JP, I45RU, TJI, and YPD from the Four-Month Data Set (01/01/12-05/01/12)

The automatic event locations of Korea data during this time period are shown in Figure 40. A total of 366 infrasound events were determined using InfraMonitor. Since Korean arrays are located inside of the Peninsula, many event locations with high uncertainty are plotted on the west side of the map which is reflective of poor station coverage, as illustrated with the earlier Russian example. Two events occurred inside of the Peninsula in January and can be associated with a limestone quarry in Danyang. Some of events occurred in Russia in March, as shown in the previous section. Several infrasound signals are generated near the capital of North Korea, Pyungyang, in February and March.
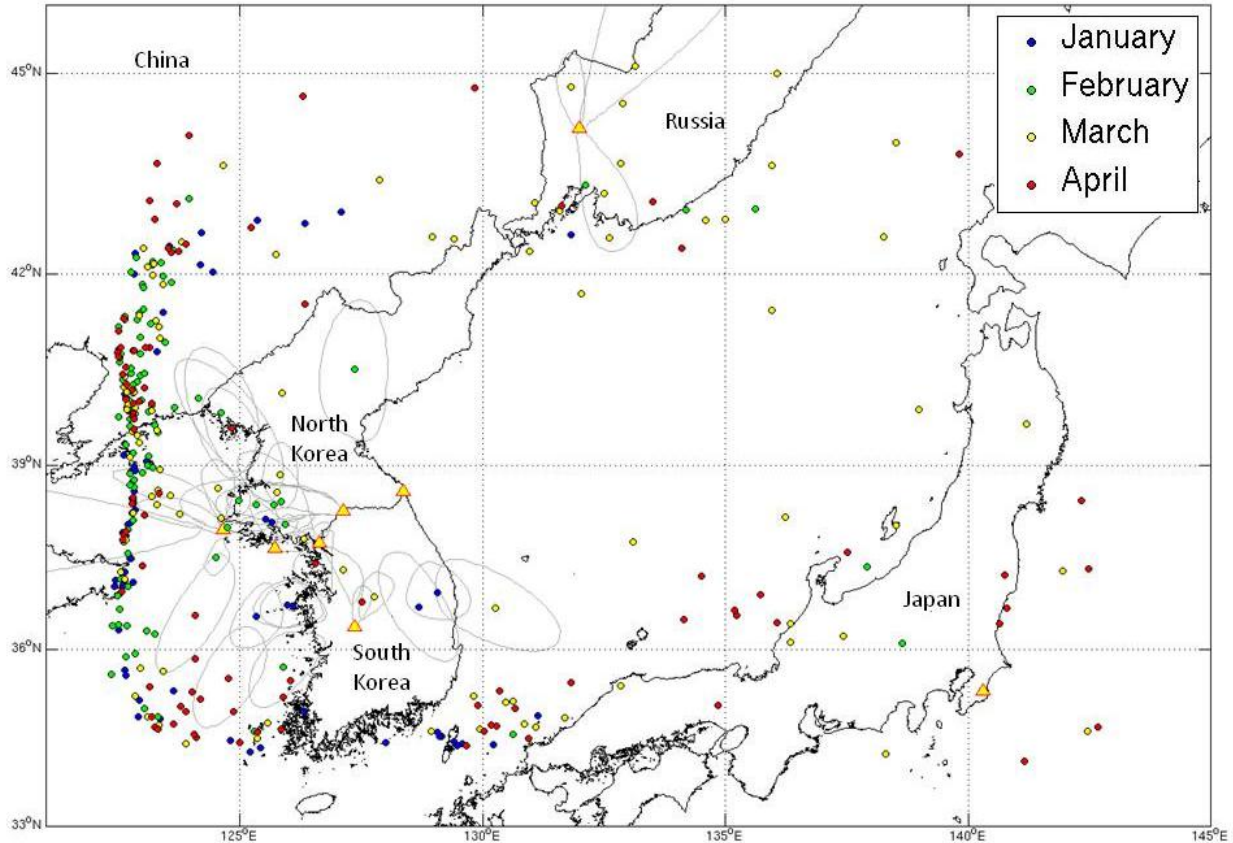
Figure 40: Automatic Event Locations in Korea from 01/01/2012 to 05/01/2012

In Figure 40, the events are color-coded by time. The events with uncertainties less than 25,000 km^2 are emphasized by light grey error contours.

4.8 Automatic Detection and Locations Using Data from Utah and Nevada

The one-year-dataset (04/01/2011-04/03/2012) from the infrasound arrays, BGU, BRP, DSR (DNIAR), EPU, FAL (FBIAR), FSU, HWU, NOQ, and WMU (Figure 32) were used to produce automatic detections (Fig. 41). The small aperture arrays were used for processing of detection and location. Generally, detection results for all arrays during the winter time have high correlation compared to those during summer. This result implies that infrasound detections are affected by seasonal variations in either noise levels and/or atmospheric path changes. Walker *et al*. (2011) demonstrated that the detected events in this area mostly occurred during the day-time and work week. This indicates that infrasound generated from man-made activity is time-variant, which means that infrasound detections have temporal distribution, daily, weekly, and seasonally.

EPU has a relatively small numbers of detection and DSR and FAL have missing data during the winter time. BGU, FSU, NOQ, and WMU located in the northern part of the network, have many detections with high correlation from the southeast and west. BRP has detections from azimuths to the northwest and southwest. There are many detections from southwest of FAL and DSR, and FAL has additional detections from the north.
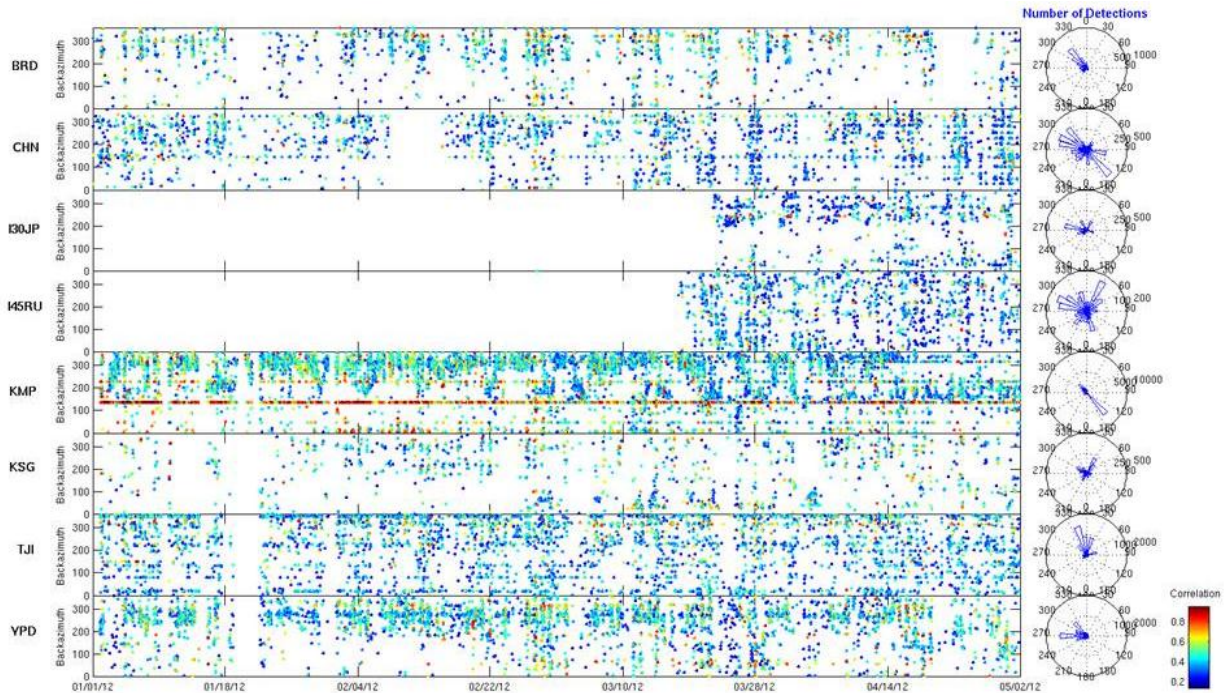
Figure 41: Automatic Detection Results - Correlation Value (Color Bar), Azimuth (Y-Axis), Number of Detections with Respect to Azimuth (Rose Diagrams) for BGU, BRP, DSR, EPU, FAL, FSU, HWU, NOQ, and WMU from the One-Year-Dataset (04/01/2011-04/03/2012)

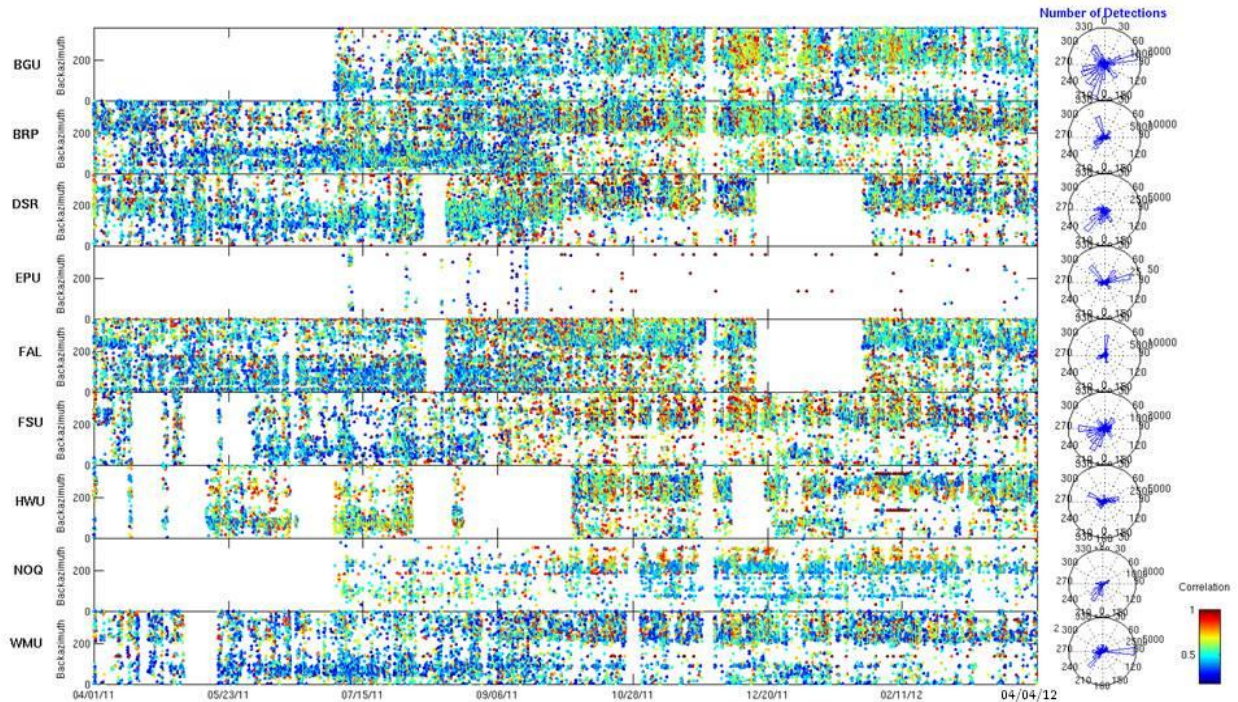The automatic event locations for the western US during the one-year time period are shown in Figure 42. A total of 963 infrasound events were estimated using InfraMonitor. Comparison of this map with a similar map of infrasound sources from 2007 through 2008 by Walker *et al*. (2011) illustrates that there are common areas from which multiple sources are identified. Walker used all the USArray stations that were deployed across the region during 2007 and 2008 along with reverse time migration at acoustic velocities in order to make his maps. Since individual seismic stations were used the method relies on good infrasound to seismic coupling at each instrument location. Stations had an approximate 70 km spacing across the western US during this time period. The fact that the ten arrays used in this study produce similar results suggests that a modest number of arrays with the opportunity to estimate phase velocity and backazimuth as well as reduce incoherent noise can be very valuable in assessing regional events. Walker determined 910 events over the two-year time period with this analysis producing a similar number of events in a single year. There are common concentrations of events associated with New Bomb, UTTR, and Dugway as well as areas in central Nevada and southwest Idaho.

There are many infrasound events in the southwest part of the study area (Figure 12), mostly occurring from October 2011to March 2012 during the winter. Infrasound event distribution in this area is strongly similar to the infrasound hot spot identified by Walker and associated with military activities (Walker *et al*. 2011). A number of infrasound events occurred near the site of New Bomb from July 2011 to March 2012 and reflect the regular demolition of explosives at this site (Figure 43(a)). Infrasound event clusters April to June 2011 north of FNIAR may also

represent human activity based on the analysis by Walker *et al*. (2011). Events in Utah between BGU and EPU may be associated with UTTR (Figure 43(b)). Many infrasound events occurred near the Dugway Testing Ground between BGU and FSU and mostly occurred during two time periods, July - September 2011 and January - March 2012 (Figure 43(b)). These events have significantly high credibility and seem to form a linear cluster.
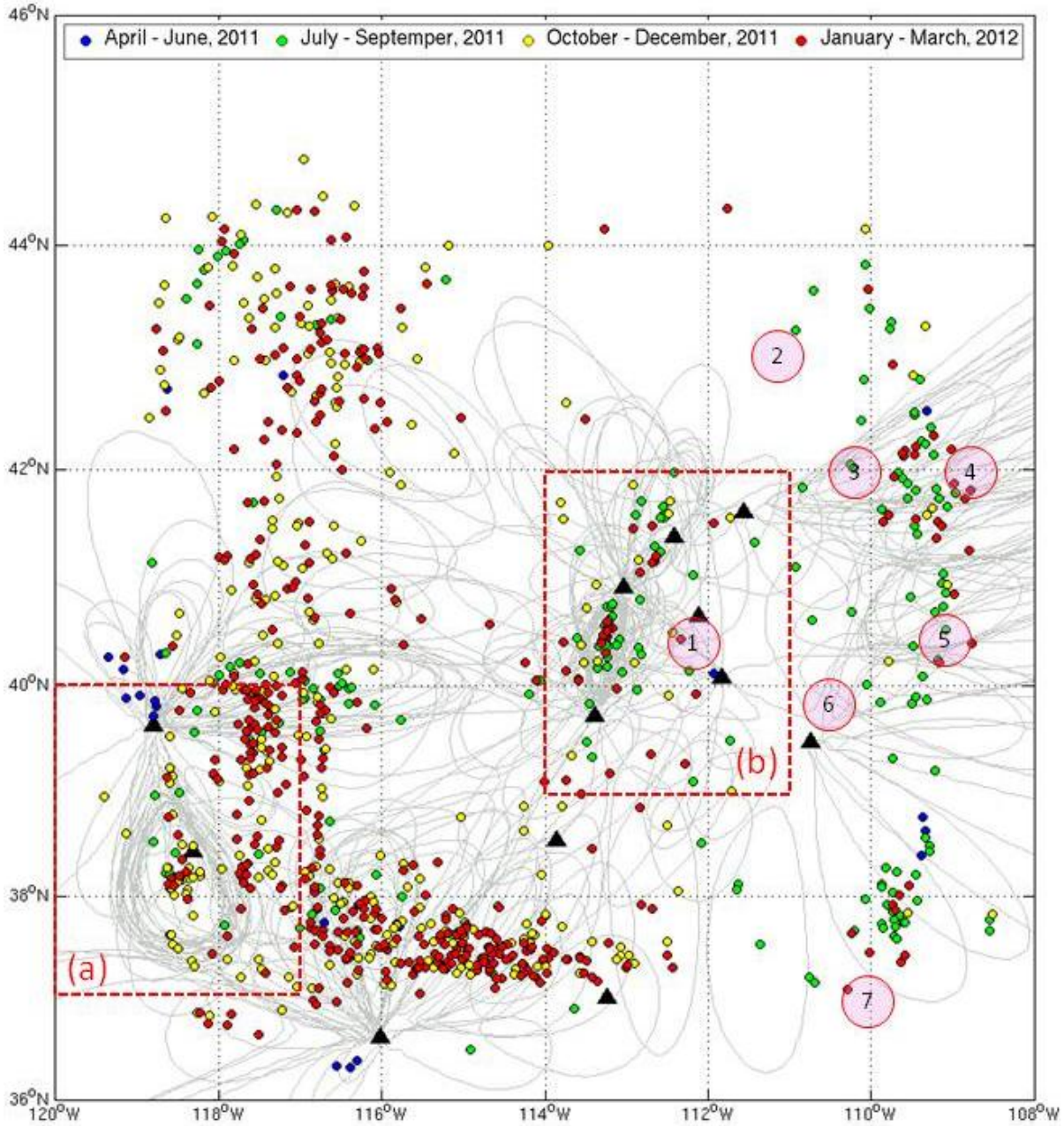
Figure 42: Automatic Event Locations Near and in the Western US from April 2011 to March 2012

In Figure 42, the events are color-coded by time. Events with uncertainties less than 25,000 km^2 are emphasized by light grey error contours. Mining regions denoted by the USGS are presented

by pink circles (1: Copperton, 2: Soda Springs, 3: Kemmerer, 4: Rock Springs, 5: Vernal, 6: Price, and 7: Kayenta). Regions inside red boxes (a) and (b) are expanded in Figure 43.
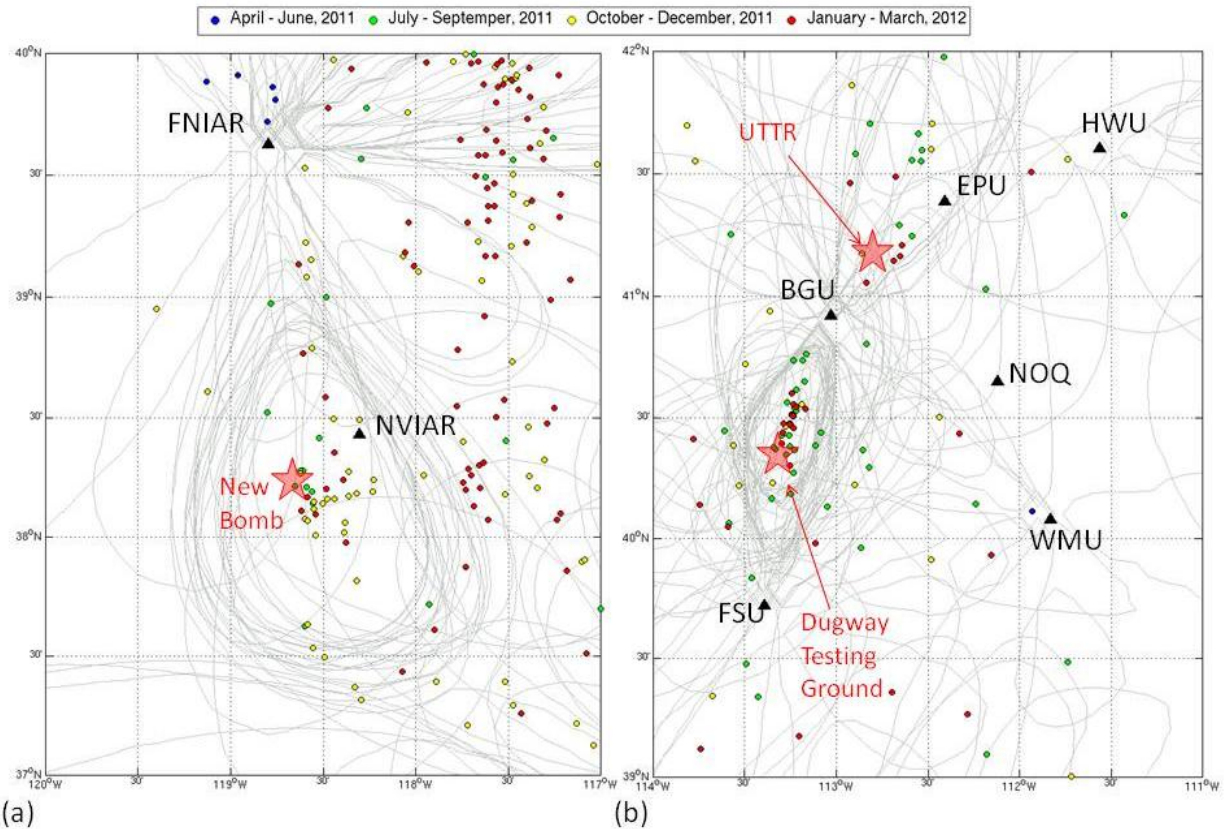
Figure 43 Automatic Event Locations Near the New Bomb Site (a) and the Region Between BGU and FSU (B) from the Time Period of May 2011 to March 2012

In Figure 43, the sites of New Bomb, Dugway Testing Ground and UTTR are presented by red stars in (a) and (b). The events are color-coded by time. Events with uncertainties less than 25,000 km^2 are emphasized by grey error contours.

4.9 Comparison of Korean and Western US Results

Figure 44 compares the number of automated infrasound events found in this study for the region surrounding the Korean Peninsula and the western US. Significantly the western US data have many events during January 2012, while few infrasound events were found from May 2011 to September 2011 (summer time). Since the routinely repeating sources generated by man-made activities such as military exercises, mining, and quarrying are distributed in this area, the origin times of infrasound events are strongly related to human work-related activities. Walker *et al*. (2011) demonstrated that there are detection gaps during the summer of 2008 due to seasonal stratospheric winds in the western U.S consistent with our result.

Number of Infrasound Event Locations
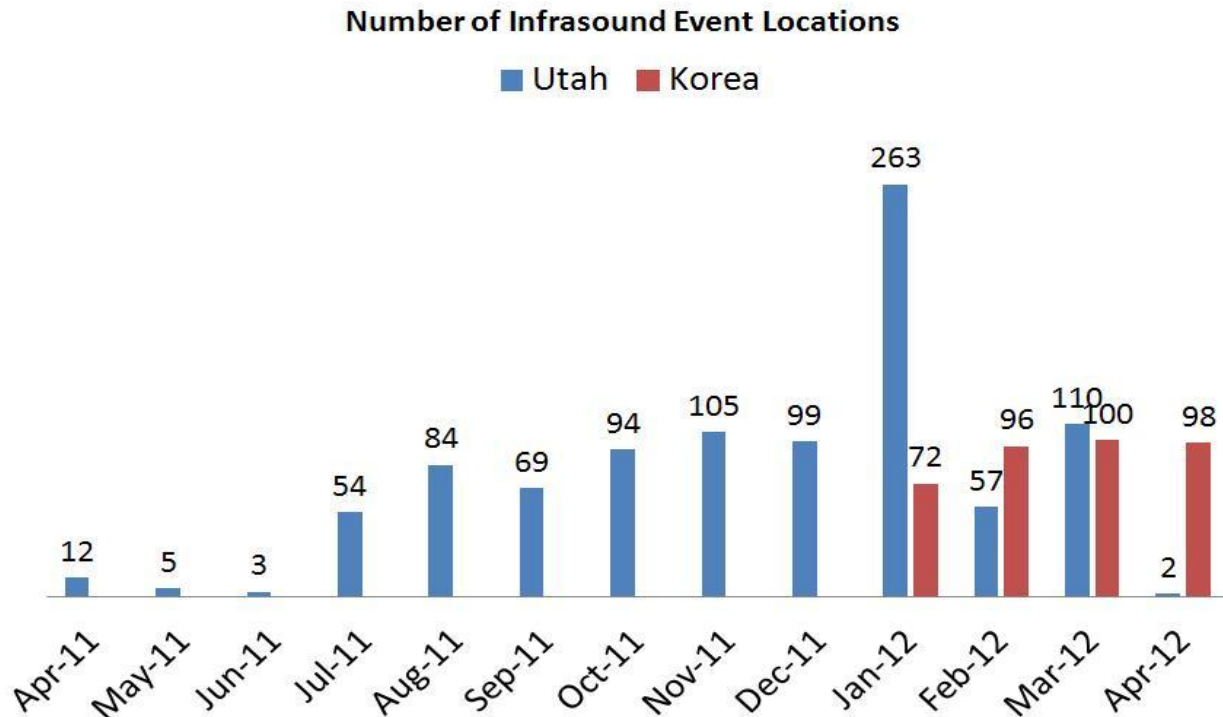
Figure 44: Comparison of the Number of Automatic Infrasound Events Per Month Determined for the Four Month Korean Data Set and the One Year Western US Data Set

Figure 45 shows histograms of source times for all located events for the four-month Korean and the one-year western US data set. The rate-of-occurrence versus weekday and day-hour show that detected events mostly occurred during the work-week day time and this result is consistent with the analysis of Walker *et al*. (2011). Both results of Korea and the western US have a similar trend of occurrence rate with respect to time that indicates that both event sources might be related to human activities. The day-of-week histograms are peaked on Tuesday with the fewest number of events on Sunday in both cases, Korea and the western US. A small difference between the two cases is that the number of events in the case of the western US is significantly increased on Friday while there were few event numbers in Korea on Friday. In comparison, the number of events for the case of Korea is relatively increased on Saturday while those are decreased in the case of the western US. The local time of day histograms have a peak from 8 A.M. for the western US and 9 A.M. for Korea until noon and a noticeable dip between noon and 2 P.M. Both Korea and the western US have two representative peaks 11 A.M. and 4 P.M. This analysis should be further investigated with another one-year dataset to separate seasonal atmospheric and noise effects from the timing of human activities. Similarly the Korea analysis needs to be extended over several years.
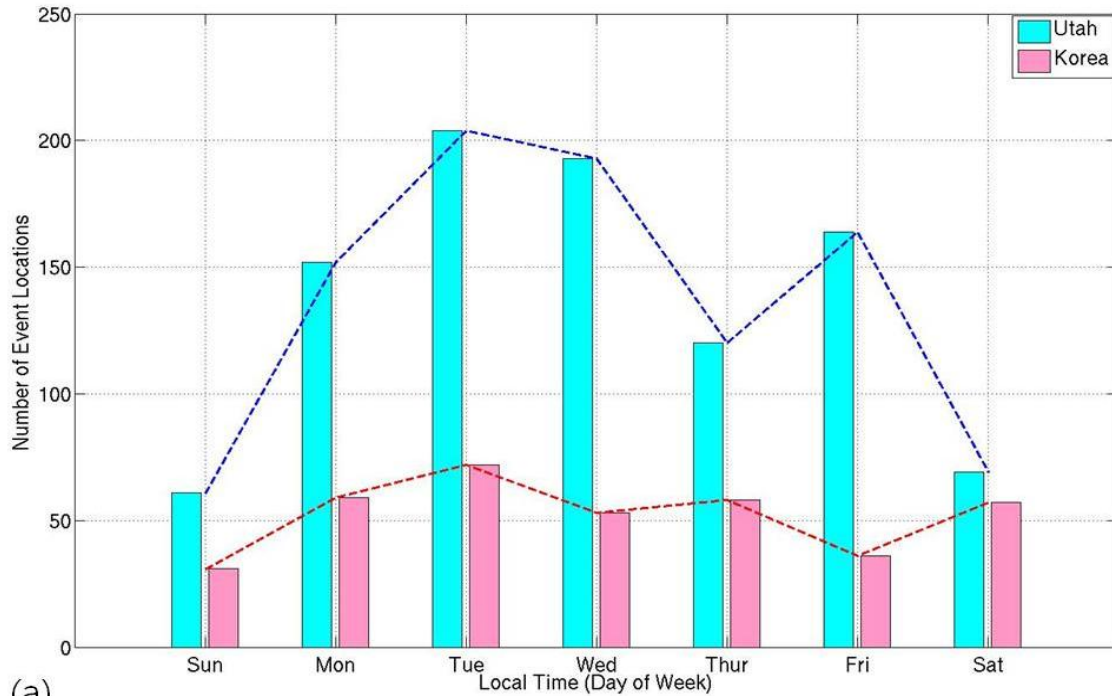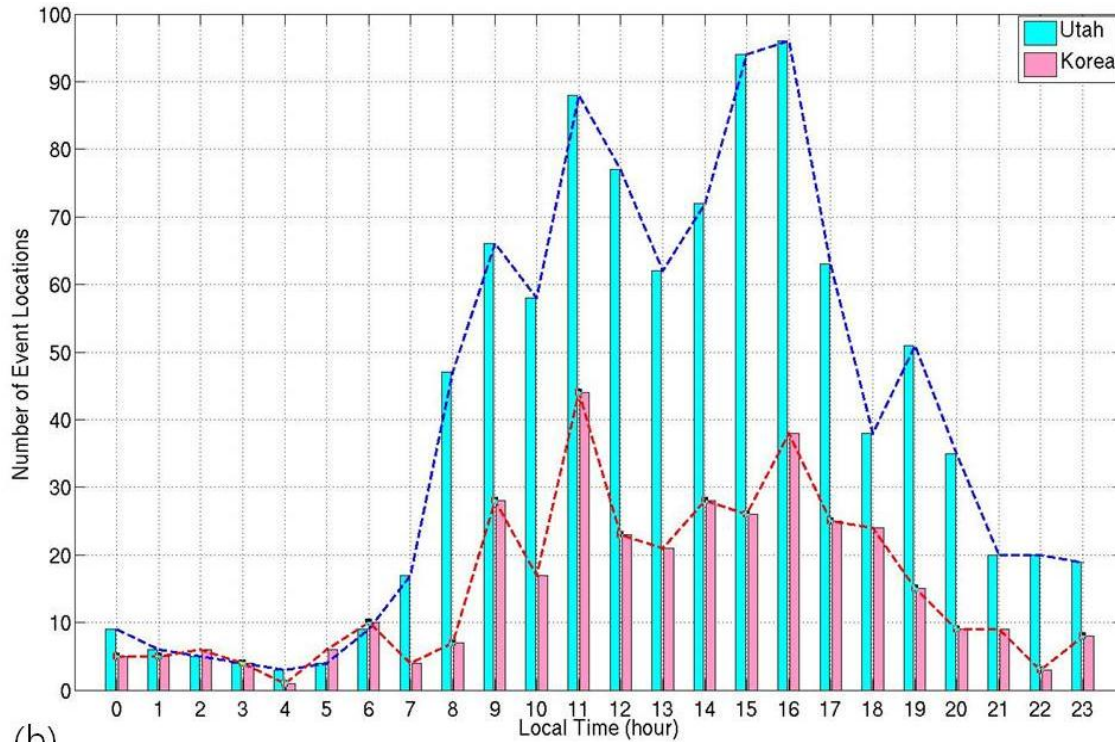
Figure 45: Histograms of Source Times for All Located Events for the Four Month Korean Data Set and the One Year Western US Data Set. Peaks of All Intervals Are Drawn by Red Dot Line for Korea and Blue Dot Line for Utah

Figure 45 shows the rate-of-occurrence versus (a) weekday and (b) day-hour shows that most detected events occurred during the work week daytime.

4.10 Conclusions and Discussion

The generation of automated infrasound event bulletins provides the opportunity to quantify the source distribution in time and space as well as the characteristics of events that can be automatically detected and located by a regional network of infrasound arrays. Such a data set is the starting place for refinement of our understanding of seasonal variations in propagation path effects and noise. Additionally, such automated bulletins can be used to highlight special events of interest and locations of repeated events that might provide some degree of ground truth for more detailed atmospheric studies. Processing of infrasound detection, association, and location were done using InfraMonitor (Arrowsmith *et al.*, 2009) applied the adaptive F-statistic for detection and the Bayesian Infrasonic Source Location (BISL) algorithm for location (Modrak *et al.* 2010).

Based on the local environment and source characteristics, parameters for detection, association, and location were tuned with a common set of parameters applied to all stations in this study. Considering that longer duration signals are observed at the more distant stations, such as the two IMS stations in the Korean data set, it might be necessary to apply station specific tuning parameters. Such station specific values may also be needed to account for the different spatial sizes of the arrays used in the studies. Future work will include the assessment of station centric tuning parameters focusing on not only signal duration but also the frequency content of the signals, the array geometry, as well as local environmental conditions.

Examples of automated infrasound detections and locations using data from Korea and the western US are illustrated in this report. A common propagation path characterization as a function of time and space was assumed in this initial work. Since the infrasonic signal depends on atmospheric conditions that change with respect to time and location, it will be important to assess the affect of time varying models on the detection and location process. The continental arrays, CHN and TJI, and the mountain-surrounded array, KSG, have a relatively smaller number of detections in some directions. The temporal trend in the detections follows a diurnal pattern with many high correlation signals during local daytime. The C-values estimated seem to also follow diurnal patterns but change little for arrays on the continent, some surrounded by mountains. The arrays near the ocean produce greater variation in C-values accompanied by higher wind velocities from the northwest. This analysis suggests that the different noise environments at the arrays can affect the C-value estimates and thus must be quantified with respect to seasonal variation.

An example event from southern Russia with infrasonic signals extending in duration to 30 s was analyzed. Since most Korean arrays are located in the Peninsula, this event from outside the network was shown to have a location with relatively large errors despite the large number of observations. Modrak *et al.* (2010) notes the importance of network coverage in the source location estimate. In this analysis, ULD and I30JP, located outside of the Korean array network, are shown to be crucial to constraining this source, especially when the backazimuth estimates from the different stations cross at large angles. This result emphasizes the importance of array coverage for determination of event location, and that the stations have to be distributed around the source.

Automatic infrasound detections and locations using four-months of Korean data and one-year of western US data were shown as a first step toward producing a regional infrasound event bulletin. In the case of Korea, there are many detections at the arrays BRD and YPD located on islands to the NW of the peninsula and TJI located in the center of the Peninsula. The detections on the two ocean arrays have relatively high correlation with backazimuths indicating propagation from the north during spring. A total of 366 infrasound event locations were produced during the four months. A number of events occurred in February near the capital of North Korea, Pyungyang. Due to the station configuration these events have higher uncertainty. This emphasizes the importance of an evenly distributed array configuration. This analysis of infrasound detection and location will be extended to a full year to assess seasonal patterns of infrasound propagation across the Korean Peninsula.

In the western US study, detections from the arrays during winter produce higher correlation values relative to those from the summer. This result implies that infrasound detections are affected by seasonal variations in atmospheric conditions, and possibly in noise. A total of 963 infrasound event locations were determined for the one-year time period with clusters of events matching the locations of UTTR, Dugway Testing Ground, and New Bomb. Some infrasound events located on the east of the map might be generated from mining regions, since a total of 16 mining events occurred from May 2011 to March 2012 in this area (USGS's mine blasts catalog). The distribution of infrasound events in the western U.S. is well matched by the infrasound hot spots, correlated with military activities, as presented by Walker *et al*. (2011). The number of infrasound events during January is significantly larger, many in Nevada. The rate of occurrence versus weekday and day-hour shows that detected events mostly occurred during the work week day time and these trends of both Korea and the western US are similar. The day-of-week histograms are peaked on Tuesday with the fewest number of events on Sunday for both cases. This result indicates that both event sources are strongly related to human work-related activities. The occurrence of infrasound events should be further investigated with an additional one-year dataset to investigate whether this pattern is due to man-made processes or seasonal propagation and noise effects. Since so much ground truth information such as that from UTTR, Dugway Training Ground, New Bomb, and mining activity exist in the western US, the accuracy of detection and location results can be assessed and possibly improved with the development of time varying models.

REFERENCES

Arabasz, W.J., Nava, S.J., and Phelps, W.T., 1997, Mining Seismicity in the Wasatch Plateau and Book Cliffs Mining Districts, Utah, USA: in Gibowicz, S.J., and Lasocki, S., eds., Rockbursts and Seismicity in Mines, Balkema, Rotterdam, pp. 111-116.

Arrowsmith, S., C. Hayward, B. Stump, R. Burlacu, I. Che and G. Singh, 2008, Multi-Array Detection, Association and Location of Infrasound and Seismo-Acoustic Events in Utah, *Proceedings of the 30th Monitoring Research Review: Ground-based Nuclear Explosion Monitoring Technologies,* September 23-25, 2008, Portsmouth, VA, LA-UR-08-05261, pp. 844-852, Los Alamos National Laboratory, Los Alamos, NM.

Arrowsmith, S., I Che, C. Hayward, J. Park and B. Stump, 2009, Multiple-Array Detection, Association and Location of Infrasound and Seismo-Acoustic Events – Utilization of Ground Truth Information, *Proceedings of the 2009 Monitoring Research Review: Ground-Based Nuclear Explosion Monitoring Technologies,* September 21-23, 2009, Tucson, Arizona, LA-UR-09-05276, pp. 706-713, Los Alamos National Laboratory, Los Alamos, NM.

Arrowsmith, S., I. Che, C. Hayward and B. Stump, 2010, Multiple-Array Detection, Association and Location of Infrasound and Seismo-Acoustic Events – Utilization of Ground Truth Information, *Proceedings of the 2010 Monitoring Research Review: Ground-Based Nuclear Explosion Monitoring Technologies,* September 21-23, 2010, Orlando, Florida, LA-UR-10-05578, pp. 667-677, Los Alamos National Laboratory, Los Alamos, NM.

Arrowsmith, S.J., and M.A.H. Hedlin, 2005, Observations of Infrasound from Surf in Southern California, *Geophys. Res. Lett*., **32**, L09810, doi:10.1029/2005GL022761.

Arrowsmith, S.J., and R. Whitaker, 2008, InfraMonitor: A Tool for Regional Infrasound Monitoring, in *Proceeding of the 2008 Monitoring Research Review: Ground-Based Nuclear Explosion Monitoring Technologies*, LA-UR-08-05261, **2**, pp. 837-843.

Arrowsmith, S.J., R. Whitaker, S.R. Taylor, R. Burlacu, B. Stump, M. Hedlin, G. Randall, C. Hayward, and D. ReVelle, 2008b, Regional Monitoring of Infrasound Events Using Multiple Arrays: Application to Utah and Washington State, *Geophys. J. Int*., **175**, pp. 291-300

Arrowsmith, S.J., R. Whitaker, C. Katz, and C. Hayward, 2009b, The F-Detector Revisited: An Improved Strategy for Signal Detection at Seismic and Infrasound Arrays, *Bull. Seismol. Soc. Am*., **99**, 1, pp. 449-453.

Arrowsmith, S.J., Drob, D., Hedlin, M.A.H., and Edwards, W., 2007, A Joint Seismic and Acoustic Study of the Washington State Bolide, *J. Geophys. Res.*, **112**, doi:10.1029/2006JD008001.

Arrowsmith, S. J., M. A. H. Hedlin, B. W. Stump and M. D. Arrowsmith, 2008b. Infrasonic Signals from Large Mining Explosions, *Bull. Seismo. Soc. Am*., **98**, pp. 768-777.

Arrowsmith, S.J., 2012, Users Guide of InfraMonitor3.1 (beta version).

Arrowsmith, S.J., R. Burlacu, K. Pankow, B. Stump, R. Stead, R. Whitaker and C. Hayward, 2012, A Seismoacoustic Study of the 2011 January 3 Circleville Earthquake, *Geophys. J. Int,* **189**, pp. 1148-1158, doi:10.1111/j.1365-246X.2012.05420.x.

Blandford, R.R., 2002, Detection and Azimuth Estimation by Infrasonic Arrays as a Function of Array Aperture and Signal Coherence, AFTAC-TR-02-005, Air Force Technical Applications Center (AFTAC/TT), Patrick AFB, FL.

Blandford, R.R., 1974, An Automatic Event Detector at the Tonto Forest Seismic Observatory, *Geophysiscs,* **39**, pp. 633-643.

Bowman, J.R., G.E. Baker, and M. Bahavar, 2005, Ambient Infrasound Noise, *Geophys. Res. Lett*., 32, L09803, doi:10.1029/2005GL022486.

Cansi, Y., 1995, An Automated Seismic Event Processing for Detection and Location: The P.M.C.C. Method, *Geophys. Res. Lett*., **22**, pp. 1021-1024.

Cansi, Y., and A. Le Pichon, 2009, Infrasound Event Detection Using the Progressive Multi-Channel Correlation Algorithm, *Handbook of Signal Processing in Acoustics*, PartXIV, pp. 1425-1435, doi:10.1007/978-0-30441-0_77.

Che, I.-Y., B. Stump and H.-I. Lee, 2011, Experimental Characterization of Seasonal Variations in Infrasonic Travel Times on the Korean Peninsula with Implications for Infrasonic Event Location, *Geophys. J. Int.* **185**, pp. 190-200, doi: 10.1111/j.1365-246X.2011.04948.x

Coyne, J., and I. Henson, 1995, Geotool Sourcebook: User's Manual, PL-TR-96-2021, Teledyne Brown Engineering, Huntsville, AL.

Daniels, F.B., 1962, Generation of Infrasound by Ocean Waves, *J. Acoust. Soc. Am.*, **34**, pp. 352-353.

Evers, L.G., and Haak, H.W., 2001, Listening to Sounds from an Exploding Meteor and Oceanic Waves, *Geophys. Res. Lett*., **28,** pp. 41-44.

Freedman, H.W. (1966), The "Little Variable Factor" a Statistical Discussion of the Reading of Seismograms, *Bull. Seismol. Soc. Am*., **56**, pp. 593-604.

Garcés, M., Hansen, R.A., and Lindquist, K.G., 1998, Traveltimes for Infrasonic Waves Propagating in a Stratified Atmosphere*, Geophys. J. Int*., **135**, pp. 255-263.

Garcés, M., and C. Hetzer, 2002, Evaluation of Infrasonic Detection Algorithms, in Proceeding of the *24th Seismic Research Review - Nuclear Explosion Monitoring: Innovation and Integration,* LA-UR-02-5048, **2**, pp.745-754 .

Garcés, M., and C. Hetzer, 2001, Infrasonic Signals Detected by the Kona Array, Hawaii, in Proceeding of the *23rd Seismic Research Review: Worldwide Monitoring of Nuclear Explosions,* LA-UR-01-4454, **2**, pp.101-110 .

Hart, D.H., and Chris J. Young, 2002, MatSeis User Manual version 1.7, https://www.nemre.nnsa.doe.gov/cgi-bin/prod/nemre/matseis.cgi.

Hedlin, M.A.H., J. Berger, and F.L. Vernon, 2002, Surveying Infrasonic Noise on Oceanic Islands, *Pure Appl. Geophys.*, **159**, pp. 1127-1152.

Jacobson, M.,1957, Analysis of a Multiple Receiver Correlation System, *J. Acoust. Soc. Am.*, **29**, pp. 1342-1347.

Johnson, D.H., and D.E. Dudgeon, 1993, *Array Signal Processing: Concepts and Techniques*, Prentice-Hall, Englewood Cliffs.

Keystone, 1997, 1997 Keystone Coal Industry Manual, Intertec, Chicago, 800 pp.

Leonard, M., 2000, Comparison of Manual and Automatic Onset Time Picking, *Bull. Seismol. Soc. Am.*, **90**, pp. 1384-1390.

Le Pichon, A., V. Maurer, D. Raymond, and O. Hyvernaud, 2004, Infrasound from Ocean Waves Observed in Tahiti, *Geophys. Res. Lett.*, **31**, L19103, doi:10.1029/2004GL020676.

Le Pichon, A., J. Vergoz, P. Herry, and L. Ceranna, 2008, Analyzing the Detection Capability of Infrasound Arrays in Central Europe, *J. Geophys. Res.*, **113**, D12115, doi:10.1029/2007JD009509.

McKissic, M., 1996, Infrasound and the Infrasonic Monitoring of Atmospheric Nuclear Explosions: An Annotated Bibliography, PL-TR-96-2282, DOE/Phillips Laboratory.

Mining event catalog of the USGS/NEIC (http://earthquake.usgs.gov/earthquakes/eqarchives/mineblast/).

Modrak, R.T., Arrowsmith, S.J. & Anderson, D.N., 2010, A Bayesian Framework for Infrasound Location, *Geophys. J. Int.*, **181**, pp. 399–405, doi:10.1111/j.1365-246X.2010.04499.x.

Negraru, P.T., P. Golden, and E.T. Herrin, 2010, Infrasound Propagation in the "Zone of Silence", *Seismo. Res. Lett.,* **81**, pp. 614-624, doi:10.1785/gssrl.81.4.614.

Park, J., B.W. Stump, C.T. Hayward, S.J. Arrowsmith, I.-Y. Che, 2011, Multiple-Array Detection, Association, and Location of Infrasound and Seismo-Acoustic Event - Utilization of Ground Truth Information, in Proceeding of the 2011 *Monitoring Research Review: Ground-Based Nuclear Explosion Monitoring Technologies,* **2**, pp. 798-807.

Park, J., B. W. Stump, C. T. Hayward, S. J. Arrowsmith, and I.-Y. Che (2011). Multiple-Array Detection, Association and Location of Infrasound and Seismo-Acoustic Event − Utilization of Ground Truth Information, *Proceedings of the 2011 Monitoring Research Review: Ground-Based Nuclear Explosion Monitoring Technologies,* September 13-15, 2011, Tucson, Arizona, LA-UR-11-04823, pp. 798-807, Los Alamos National Laboratory, Los Alamos, NM.

Posmentier, E., 1967, A Theory of Microbaroms, *Geophys. J. R. Astron. Soc.*, **13**, pp. 487-501.

Richins, W.D., compiler, 1979, Data Processing and Analysis, in Arabasz, W.J., Smith, R.B., and Richins, W.D., eds., Earthquake Studies in Utah 1850 to 1978: Special Publication of the University of Utah Seismographic Stations, Salt Lake City, pp. 79-90.

Rind, D., 1980, Microseisms at Palisades: 3. Microseisms and Microbaroms, *J. Geophys. Res.*, **85**, pp. 4854-4862.

Rost, S., and Thomas, C., 2002, Array Seismology: Methods and Applications, *Rev. Geophys.*, **40**, doi:10.1029/2000RG000100.

Sereno, T.J. 1990 Attenuation of Regional Phases in Fennoscandia, and Estimates of Arrival Time and Azimuth Uncertainty using Data Recorded by Regional Arrays, SAIC-90/1472, Science Applications International Corp., San Diego, California.

Shumway, B.H., 1971, On Detection a Signal in N Stationarily Correlated Noise Series, *Technometrics,* **13**, pp. 499-519.

Shumway, R.H., S. Kim, and R.R. Blandford, 1999, Nonlinear Estimation for Time Series Observed on Arrays, In *Asymptotics, Nonparametrics, and Time Series*, S. Ghosh, Editor, Marcel Dekker, New York.

Sipkin, S.A., W.J. Person, and B.W. Presgrave 2000, Earthquake Bulletins and Catalogs at the USGS National Earthquake Information Center, in *Incorporate Research Institutions for Seismology Newsletter* 2000, **1**, pp. 2-4.

Smart, E., 1971, Erroneous Phase Velocities from Frequency-Wavenumber Spectral Sections, *Geophys. J.R. Astr. Soc.*, **26**, pp. 247-253.

Smart, E., and E.A. Flinn, 1971, Fast Frequency-Wavenumber Analysis and Fisher Signal Detection in Real-Time Infrasonic Array Data Processing, *Geophys. J.R. Astr. Soc.*, **26**, pp. 279-284.

Stump, B., Burlacu, R., Hayward, C., Bonner, J., Pankow, K., Fisher, A., and Nava, S., 2007, Seismic and Infrasound Energy Generation and Propagation at Local and Regional Distances: Phase 1 - Divine Strake Experiment, in *Proceedings of the 29th Monitoring Research Review*, Denver, CO, 25-27 Sept., pp. 674-683.

Tabulevich, V.N., 1993, Microseismic and Infrasound Waves, Res. Rep. Phys., 150 pp., Springer-Verlag, New York.

Walker, K.T., and M.A.H. Hedlin, 2010, A Review of Wind Noise Reduction Methodologies, in *Infrasound Monitoring for Atmospheric Studies*, edited by A. Le Pichon, E. Blanc, and A. Hauchecorne, pp. 141-182, Springer, New York, doi:10.1007/978-1-4020-9508-5.

Walker, K.T., R. Shelby, M.A.H. Hedlin, C. de Groot-Hedlin, and F. Vernon, 2011, Western U.S. Infrasonic Catalog: Illuminating Infrasonic Hot Spots with the USArray, *J. Geophys. Res*., **116**, doi:10.1029/2011JB008579.

Welch, P.D., 1967, The Use of Fast Fourier Transforms for the Estimation of Power Spectra: A Method Based on Time Averaging Over Short Modified Periodograms, *Trans IEEE AU*, pp. 70-73.

Woodward, R., H. Israelsson, I. Bondár, K. McLaughlin, J.R. Bowman, and H. Bass, 2005, Understanding Wind-generated Infrasound Noise, in *Proceedings of the 27th Seismic Research Review: Ground-Based Nuclear Explosion Monitoring Technologies*, LA-UR-05-6407, Vol. 2, pp. 866-875.

Zeiler, C.P., and A.A. Velasco, 2009, Seismogram Picking Error from Analyst Review (SPEAR): Single-Analyst and Institution Analysis, *Bull. Seismol. Soc. Am*., **99**, 5, pp. 2759-2770.

DISTRIBUTION LIST

DTIC/OCP
8725 John J. Kingman Rd, Suite 0944
Ft Belvoir, VA 22060-6218   1 cy

AFRL/RVIL
Kirtland AFB, NM 87117-5776   2 cys

Official Record Copy
AFRL/RVBYE/Robert Raistrick   1 cy